# CHAPTER V

# RESULTS AND DISCUSSION

## 5.1 Preparations of Ferrocenyl Derivatives

### 5.1.1 Ferrocenylamine Derivatives

Ferrocene can be aminomethylated readily to form dimethylaminomethyl ferrocene with high yield. The unreactive ferrocene was recovered and reemployed by recrystallized with hexane. The aminometallation of ferrocene furnishes a new route to the synthesis a number of unavailable ferrocenyl derivatives.

*N, N*-dimethylaminomethylferrocene was methylated with methyl iodide to generate quarternary ammonium salt (*N, N*-dimethylaminomethylferrocene methiodide) with excellent yield. This step is performed to convert a poor leaving group, $-N(CH_3)_2$, into a good leaving group, $^{+}N(CH_3)_3$ and that the methiodide of this tertiary-amine is useful intermediate for the synthesis of monosubstituted ferrocenyl derivatives.[38] It can be seen from Scheme 5.1 that tertiary-amine was converted through its methiodide to the corresponding ferrocenyl derivatives, this involved the displacement of trimethyl amine which was observed to be formed as a by-product. Ferrocenylmethyl anion ($Fc\text{-}CH_2^-$) was reacted with potassium cyanide, methylamine, and diphenylamine to give ferrocenylacetonitrile, α-methylferrocenylmethylamine, *N, N*-diphenylamino methylferrocene, respectively. Ferrocenylethylamine was prepared by reducing ferrocenyl acetonitrile with $LiAlH_4$.

The synthesized ferrocenylamine derivatives were characterized by $^1H$ NMR and FTIR techniques. The results are shown in Table 5.1 and Table 5.2

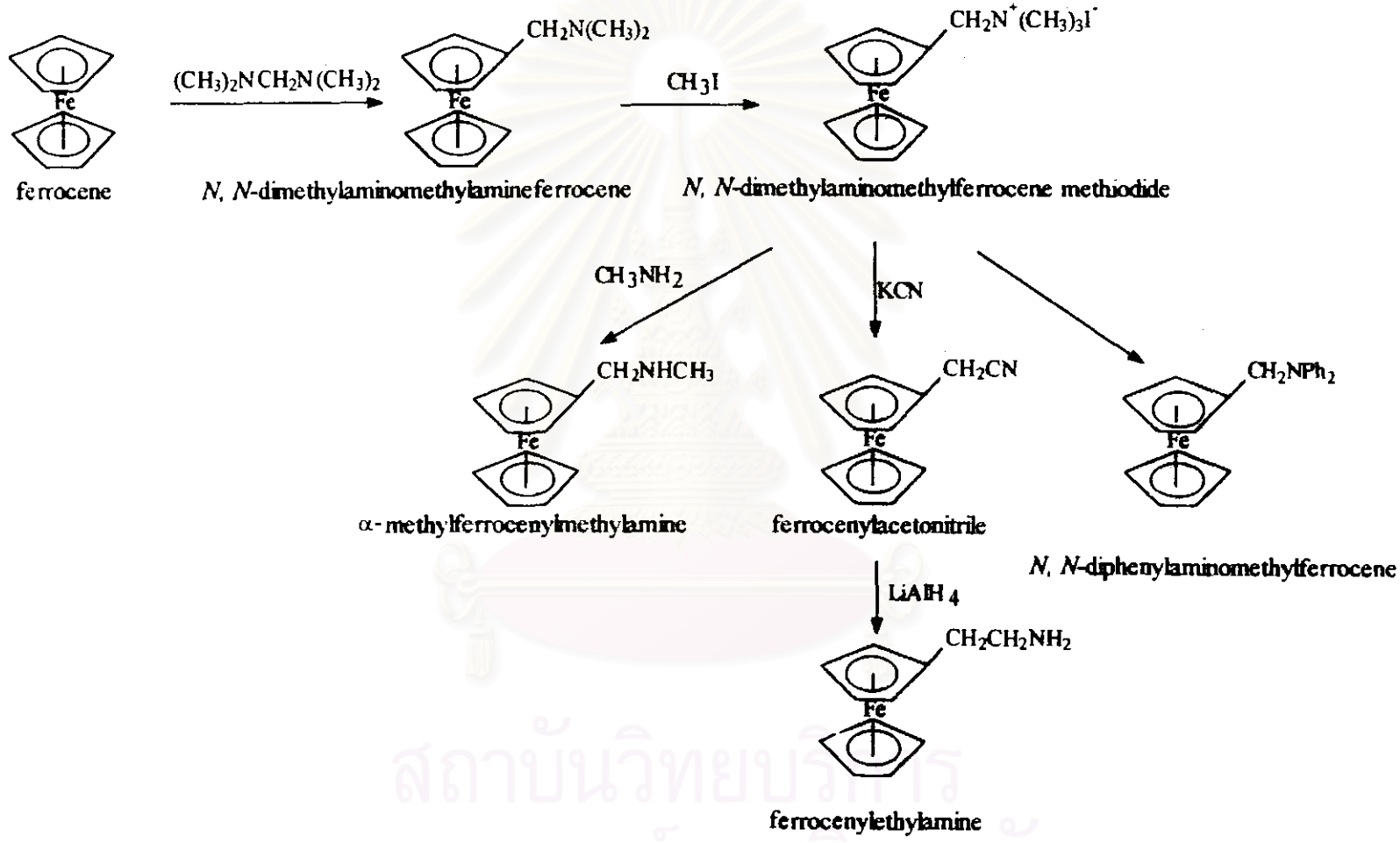


**Scheme 5.1** Preparation of ferrocenylamine derivatives

**Table 5.1** $^{1}$H NMR data of ferrocenylamine derivatives

| Compounds | Amino moiety | | | | | | Cp ring protons | | |
|---|---|---|---|---|---|---|---|---|---|
| | $NCH_3$ | NH | $CH_2N$ | $CH_2CH_2N$ | $NH_2$ | $NPh_2$ | $C_5H_5$ | αH | βH |
| Fc-$CH_2N(CH_3)_2$ | 2.15(s) | - | 3.27(s) | - | - | - | 4.09(s) | 4.14(s) | 4.09(s) |
| Fc-$CH_2N(CH_3)_3I$ | 3.33(s) | - | 2.90(s) | - | - | - | 4.24(s) | 4.38(d) J = 5 Hz | 4.48(s) |
| $FcCH_2NHCH_3$ | 2.43(s) | 2.80(br) | 3.46(s) | - | - | - | 4.11(s) | 4.09(m) | 4.18(t) J = 3 Hz |
| Fc-$CH_2CH_2NH_2$ | - | - | 2.75(t) J = 6 Hz | 2.44(t) J = 6 Hz | 3.50 (br) | | 4.08(s) | 4.10(m) | 4.10(m) |
| Fc-$CH_2NPh_2$ | - | - | 4.70(s) | - | - | 7.0(m) | 3.90(s) | 4.15(s) | 4.05(s) |

**Table 5.2** FTIR data of ferrocenylamine derivatives

| Compounds | -NH stretching | =CH stretching | -CH stretching | C=C stretching | -NH bending | $-CH_2$ | $CH_3$ | -CH out of plane bending |
|---|---|---|---|---|---|---|---|---|
| $Fc\text{-}CH_2N(CH_3)_2$ | - | 3092, 2938 | 2858, 2768 | 1637 | - | 1460 | 1350 | 818 |
| $Fc\text{-}CH_2N(CH_3)_3I$ | - | 3052 | 2993 | 1655 | - | 1483 | 1408, 1387 | 886 |
| $FcCH_2NHCH_3$ | 3439 | 2920 | 2748 | 1638 | 1510 | 1465 | 1392 | 817 |
| $Fc\text{-}CH_2CH_2NH_2$ | 3751, 3312 | 2967 | 2859 | 1651 | 1541 | 1452 | - | 814 |
| $Fc\text{-}CH_2NPh_2$ | 3093 | 3093 | 3047 | 1600 | - | 1465 | - | 692 |

### 5.1.2 Schiff Base and Reduced Derivatives

1, 2 Bis (ferrocen-1-ylmethyleneamino)ethane (Schiff base) was prepared by condensation of ferrocenylaldehyde with ethylenediamine. Hydrogenation of Schiff base with $LiAlH_4$ resulted in the corresponding amine as shown in Scheme 5.2.

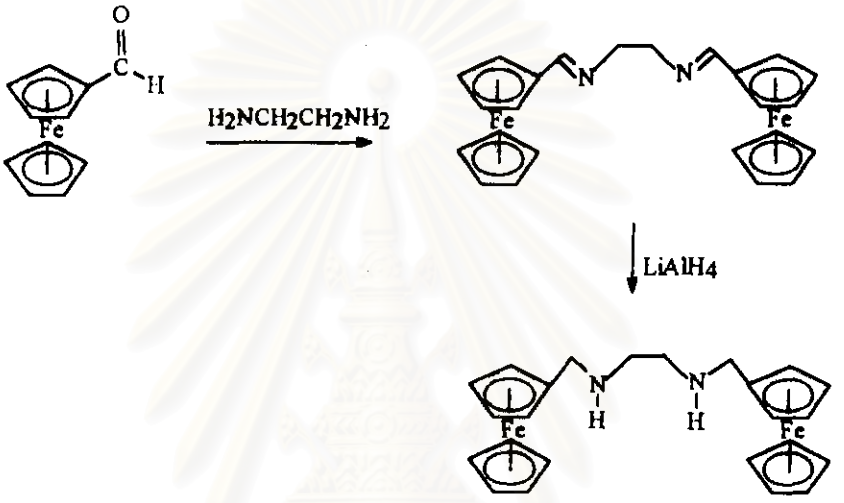


**Scheme 5.2** Condensation of ferrocenylaldehyde with ethylenediamine and reduction with $LiAlH_4$

Ferrocenylaldehyde was reacted with ethylenediamine (2:1 mole ratio) to produce orange solution from which Schiff base was isolated in a good yield. Hydrogenation of Schiff base with $LiAlH_4$ gave yellow solids of reduced Schiff base. $^1H$ NMR spectra and the data of both complexes were shown in Figures 5.1-5.2 and Tables 5.3 -5.4. The spectrum of Schiff base showed HC=N chemical shift at 8.15 ppm while the spectrum of reduced form showed the disappearance of this group but showed NH-$CH_2$ chemical shift at 2.75 ppm.

FTIR data of Schiff base and reduced Schiff base were shown in Tables 5.5 and 5.6 respectively. Schiff base showed a strong C=N stretching vibration at 1642 $cm^{-1}$ while reduced Schiff base showed secondary amine group at 1543 $cm^{-1}$.

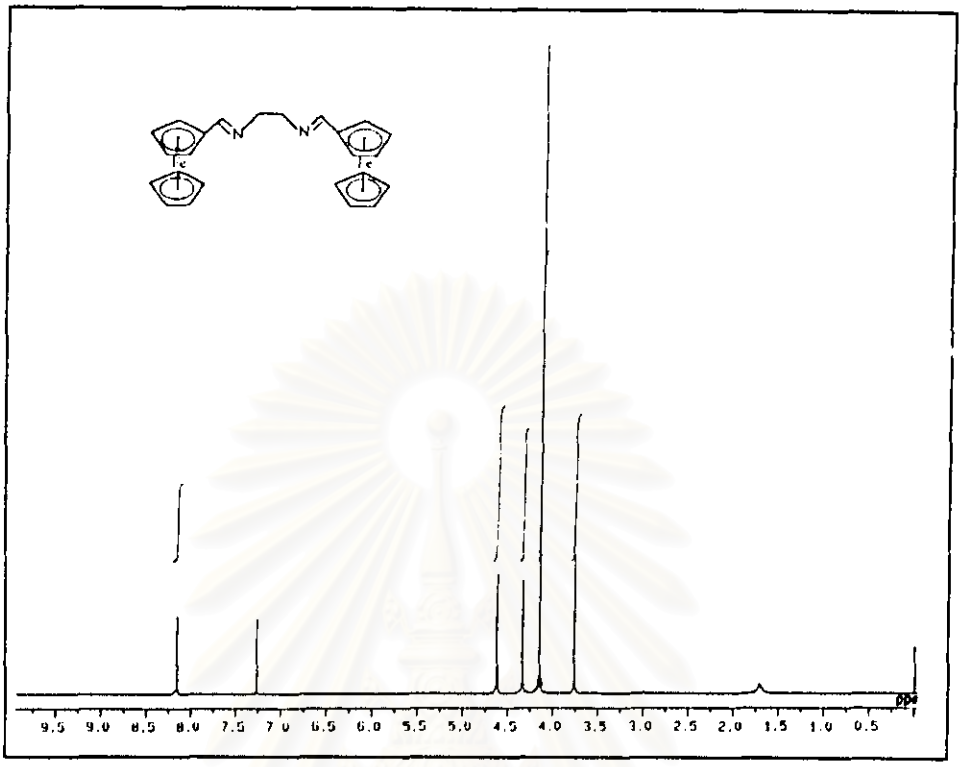

**Figure 5.1** $^{1}$H NMR spectrum of Schiff base derivative

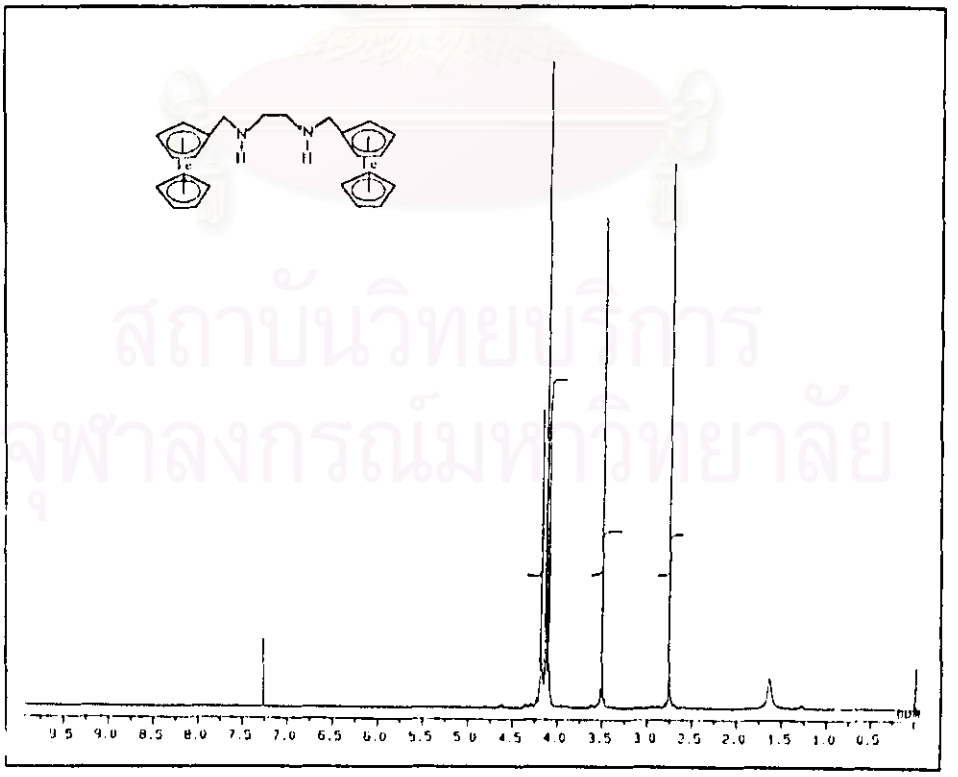

**Figure 5.2** $^{1}$H NMR spectrum of reduced Schiff base derivative

**Table 5.3** $^{1}H$ NMR data of Schiff base derivative

| Chemical shift (ppm) | Multiplicity | Number of protons | Assignment |
|---|---|---|---|
| 8.15 | singlet | 2H | HC=N |
| 4.60 | triplet | 4H | α-$C_5H_4$ (J = 1.5 Hz) |
| 4.31 | triplet | 4H | β-$C_5H_4$ (J = 1.5 Hz) |
| 4.13 | singlet | 10H | $C_5H_5$ |
| 3.75 | singlet | 4H | =N–$CH_2$ |

**Table 5.4** $^{1}H$ NMR data of reduced Schiff base derivative

| Chemical shift (ppm) | Multiplicity | Number of protons | Assignment |
|---|---|---|---|
| 4.20 | singlet | 4H | α-$C_5H_4$ |
| 4.15 | singlet | 10H | $C_5H_5$ |
| 4.12 | singlet | 4H | β-$C_5H_4$ |
| 3.50 | singlet | 4H | –$CH_2$-$CH_2$ |
| 2.75 | singlet | 4H | –NH-C$H_2$ |

**Table 5.5** FTIR data of Schiff base derivative

| Wavenumber ($cm^{-1}$) | Assignment |
|---|---|
| 3111, 3072 | =CH stretching |
| 2895, 2830 | –CH stretching |
| 1642 | C=N stretching |
| 1470 | $-CH_2$ stretching |
| 1106, 1012 | –CN stretching |
| 820 | =CH out of plane |

**Table 5.6** FTIR data of reduced Schiff base derivative

| Wavenumber ($cm^{-1}$) | Assignment |
|---|---|
| 3435 | –NH stretching |
| 3092 | =CH stretching |
| 2927, 2833 | –CH stretching |
| 1636 | C=C stretching |
| 1543 | –NH bending |
| 1456 | $-CH_2$ stretching |
| 1116, 1025 | –CN stretching |
| 817 | =CH out of plane |

### 5.1.3 Lithiation of Ferrocene

Ferrocenylbipyridine was synthesized by the reaction of lithioferrocene with 2, 2′-bipyridine. The intermediate complex gave the product after elimination of lithium hydride. The position of the substituent is governed by the inherent reactivity of the ortho position towards nucleophiles.[39] In the reaction, a suspension of the lithioferrocence in diethyl ether under nitrogen was reacted over a period of 3 days with 2, 2′-bipyridine, followed by a standard work-up in air to achieve oxidation of the expected dihydrointermediate into the desired aromatic product as shown in Scheme 5.3.

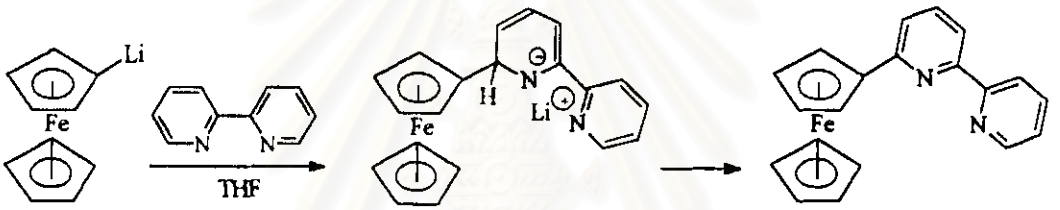


**Scheme 5.3** Preparation of 6-ferrocenyl-2, 2′-bipyridine

2, 2′-Bipyridine is used as a ligand with a transition metal.[39] There is a propensity towards cyclometallation since the nitrogen atom is β-to ferrocenyl ring and thus can coordinate effectively and stabilize a metal sigma bonded to the cyclopentadienyl ring (Figure 5.3). This may be a desirable effect in the case of new catalyst design for alkylation with diethylzinc.

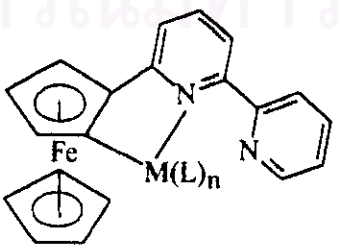


**Figure 5.3** Coordination of ferrocenylbipyridine and a metal

The $^1$H NMR data and spectrum of 6-ferrocenyl-2, 2′-bipyridine are shown in Table 5.7 and Figure 5.4.

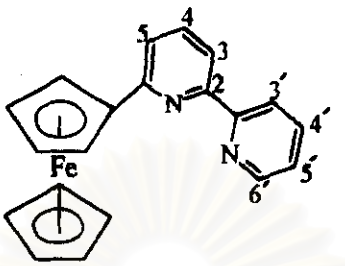


**Table 5.7** $^1$H NMR data of 6-ferrocenyl-2, 2′-bipyridine

| Chemical shift (ppm) | Multiplicity | Number of protons | Assignment |
|---|---|---|---|
| 8.68 | doublets of doublet5 of doublets | 1H | H6′ ( J = 1.0, 1.8 and 5.0 Hz ) |
| 8.57 | triplets of doublet | 1H | H3′ ( J = 1.0 and 7.0 Hz ) |
| 8.21 | doublets of doublet | 1H | H3 (J = 1.0 and 7.0 Hz) |
| 7.85 | doublets of doublets of doublet | 1H | H4′ ( J = 1.0, 5.0 and 7.0 Hz ) |
| 7.74 | multiplet | 1H | H4 |
| 7.43 | doublets of doublets of doublet | 1H | H5 ( J = 1.0, 1.8 and 7.0 Hz ) |
| 7.31 | doublets of doublets of doublet | 1H | H5′ ( J = 1.0, 5.0 and 7.0 Hz) |
| 5.03 | triplets of doublet | 2H | αH-$C_5H_4$ ( J = 1.8 and 6.0 Hz ) |
| 4.42 | triplet | 2H | βH-$C_5H_4$ ( J = 1.8 Hz) |
| 4.07 | singlet | 5H | $C_5H_5$ |

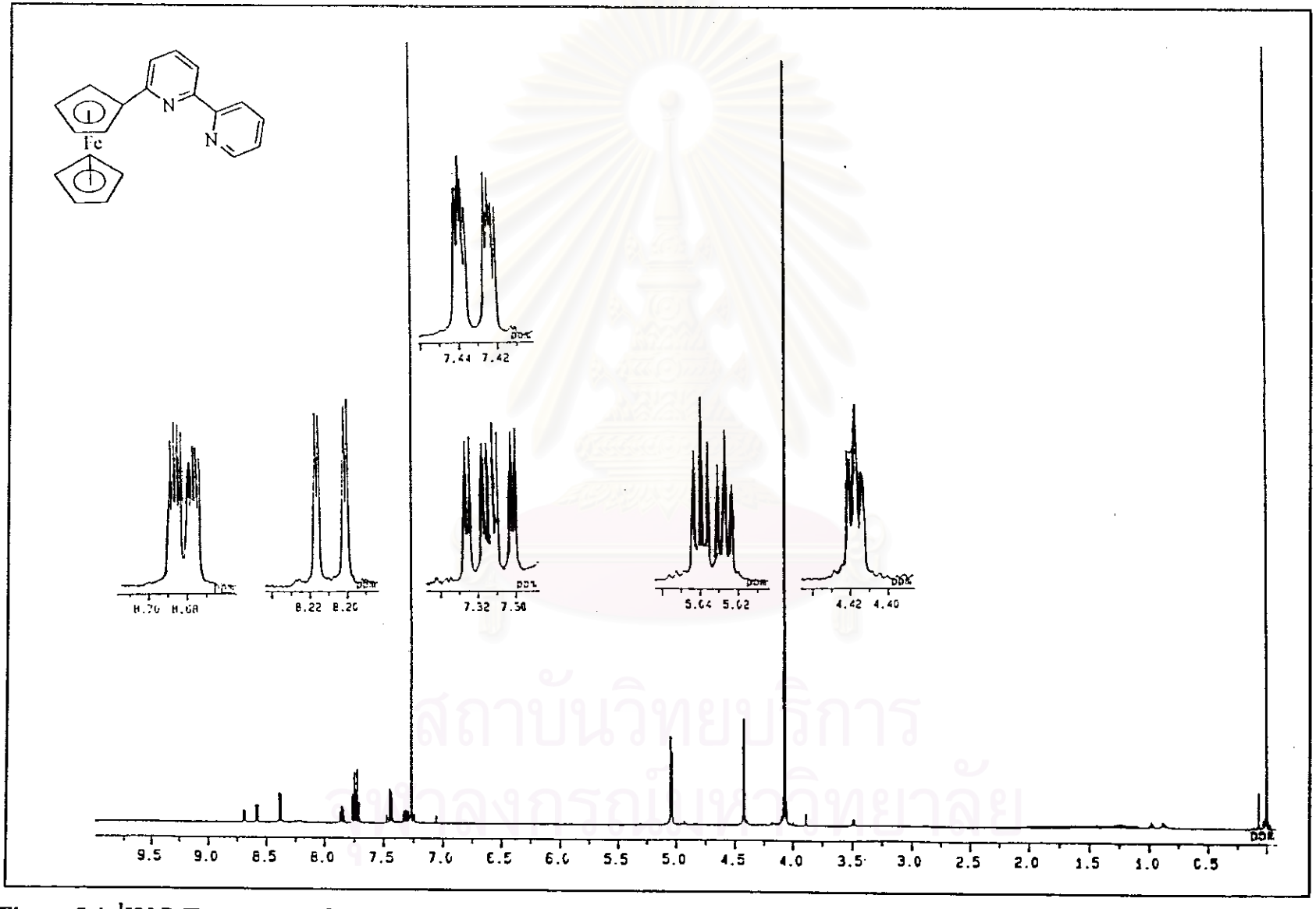


**Figure 5.4** $^{1}$H NMR spectrum of 6-ferrocenyl-2, 2′-bipyridine

The FTIR spectrum of 6-ferrocenyl-2, 2′-bipyridine in Figure 5.5 shows strong peak at 1635 $cm^{-1}$. The data of other vibrations are shown in Table 5.8.

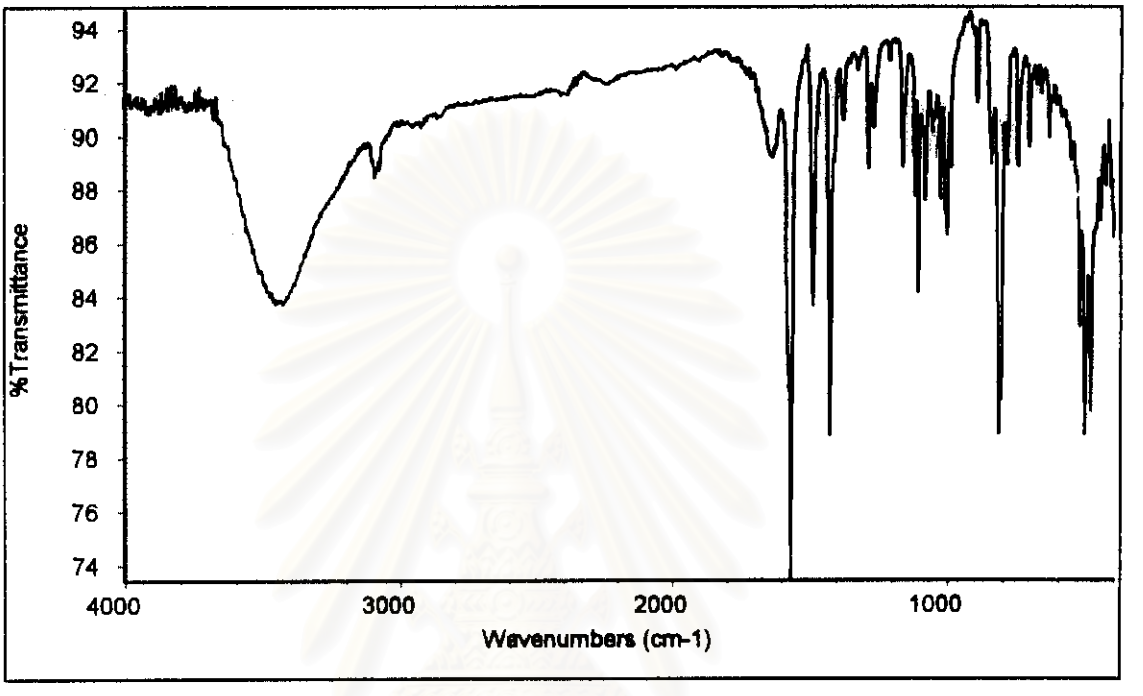


**Figure 5.5** FTIR spectrum of 6-ferrocenyl-2, 2′-bipyridine

**Table 5.8** FTIR data of 6-ferrocenyl-2, 2′-bipyridine

| Wavenumber ($cm^{-1}$) | Assignment |
|---|---|
| 3098 | =C-H stertching |
| 1635 | C=N stretching |
| 1572, 1489 | C=C stretching |
| 1111 | C–N stretching |
| 813 | =CH out of plane |

*N, N*-Dimethylaminomethylferrocene was metalated with *n*-butyllithium in diethyl ether-hexane, and the resulting monolithioamine was condensed with benzophenone, to form 1, 2-disubstituted ferrocene as shown in Scheme 5.4

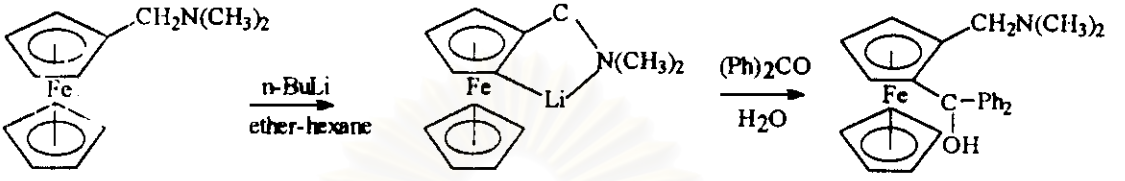


**Scheme 5.4** Preparation of 2-(α, α-diphenylhydroxylmethyl)dimethylaminomethyl ferrocene

2-Lithiation of *N* ,*N*-dimethylaminomethylferrocene was thought to proceed by preliminary abstraction of a proton by the *n*-butyl anion, it might at first be thought that the position adjacent to the dimethylaminomethyl group, being perhaps highest in electron density due to effect of the substituent, would be the least acidic proton and hence undergo lithiation least readily. In the structure of 2-lithio intermediate, the lithium ion was locked in a five-membered chelate ring, bound by the ferrocene ring on one side and by the free electron pair of the amine nitrogen on the other.[4]

The structure of 1, 2-disubstituted ferrocene was supported by spectroscopic techniques. The infrared spectrum in Figure 5.6 indicates the broad peak of hydroxyl group of disubstituted ferrocene at 3450 $cm^{-1}$ (Table 5.9). The $^1H$ NMR spectrum (Figure 5.7) and data (Table 5.10) showed hydroxyl group at 7.55 ppm, phenyl ring at 7.15 ppm and tertiary amine at 1.95 ppm.

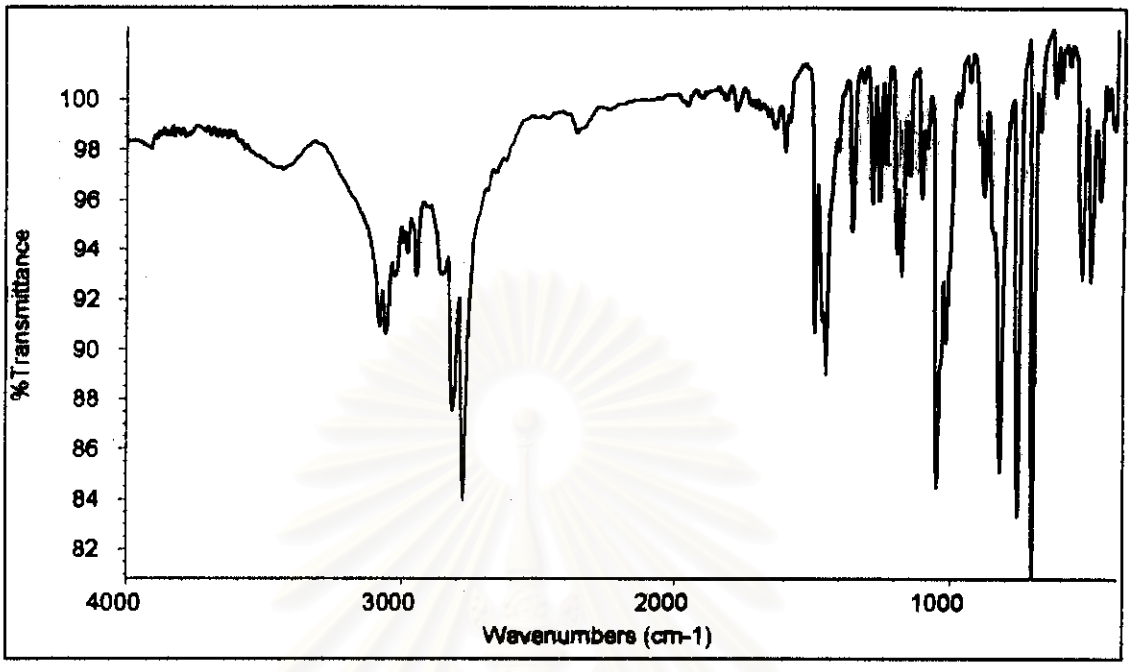


**Figure 5.6** FTIR spectrum of 2-(α, α-diphenylhydroxymethyl)dimethylaminomethyl ferrocene

**Table 5.9** FTIR data of 2-(α, α-diphenylhydroxymethyl)dimethylaminomethyl ferrocene

| **Wavenumber ($cm^{-1}$)** | **Assignment** |
|---|---|
| 3450 | –OH stretching |
| 3088, 3067 | =CH stretching |
| 2817, 2781 | –CH stretching |
| 1603,1495 | C=C stretching |
| 1460 | $-CH_2$ |
| 1357 | $-CH_3$ |
| 1055 | –CN stretching |
| 707 | =CH out of plane |

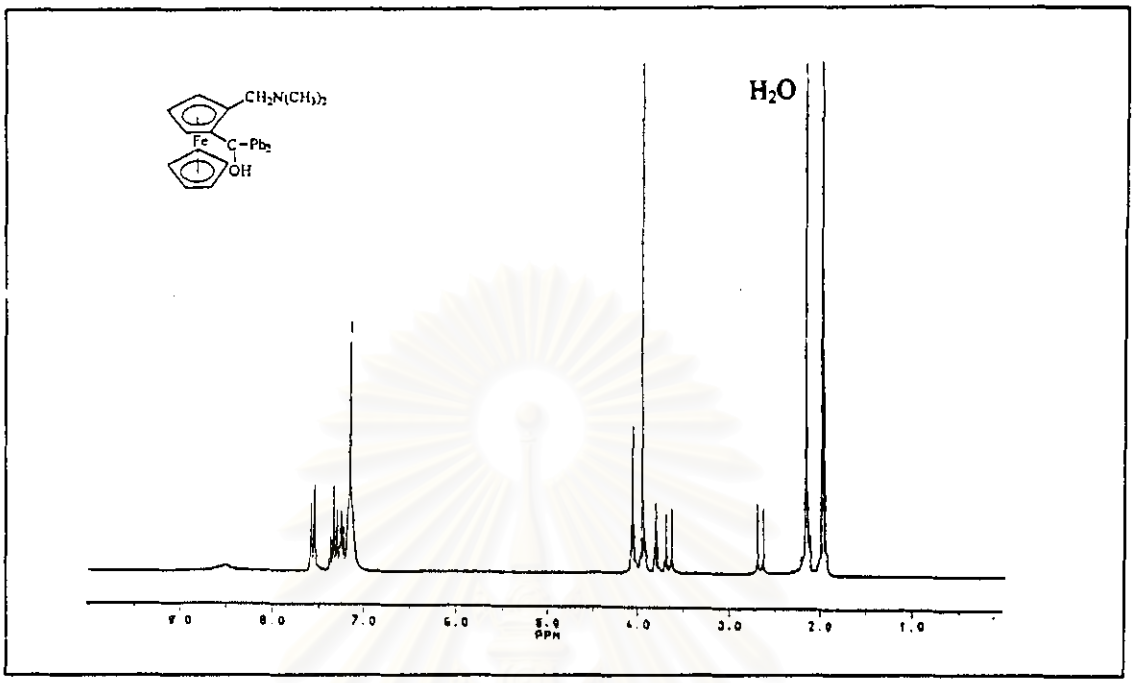


**Figure 5.7** $^1$H NMR spectrum of 2-(α, α-diphenylhydroxymethyl)dimethylamino methylferrocene

**Table 5.10** $^1$H NMR data of 2-(α, α-diphenylhydroxymethyl)dimethylaminomethyl ferrocene

| Chemical shift (ppm) | Multiplicity | Number of protons | Assignment |
|---|---|---|---|
| 7.55 | doublet | 1H | –OH ( J = 6 Hz) |
| 7.15 | multiplet | 5H | $C_6H_5$ |
| 4.05 | doublet | 2H | α-$C_5H_4$ ( J = 2 Hz) |
| 3.95 | singlet | 5H | $C_5H_5$ |
| 3.15 | multiplet | 2H | –$CH_2$ |
| 3.79 | triplet | 1H | β-$C_5H_4$ ( J = 2 Hz) |
| 1.95 | singlet | 6H | –$N(CH_3)_2$ |

### 5.1.4 Other Ferrocenyl Derivatives

#### 5.1.4.1 Acetylferrocene

Acetylferrocene was prepared by Friedel-Crafts reaction of ferrocene with acetyl chloride in the presence of aluminium chloride as shown in Scheme 5.5. Monosubstituted acetylferrocene was separated and characterized by $^1$H NMR and FTIR, the data are shown in Tables 5.10 and 5.11.


**Scheme 5.5** Preparation of acetylferrocene

#### 5.1.4.2 Ferrocenylmethylalcohol

$N(CH_3)_3$ which is a good leaving group was easily substituted with $OH^-$, as shown in Scheme 5.6. The complex was characterized by $^1$H NMR and FTIR, the data are shown in Tables 5.10 and 5.11

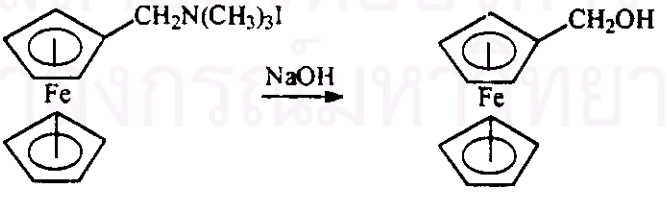


**Scheme 5.6** Preparation of ferrocenylmethylalcohol

### 5.1.4.3 α-Hydroxyethylferrocene

α-Hydroxyethylferrocene was produced by the reduction of acetylferrocene with lithium aluminium hydride as shown in Scheme 5.7 The structure was confirmed by $^{1}H$ NMR and FTIR, the data agreed well with those in the literature[37] as shown in Tables 5.10 and 5.11

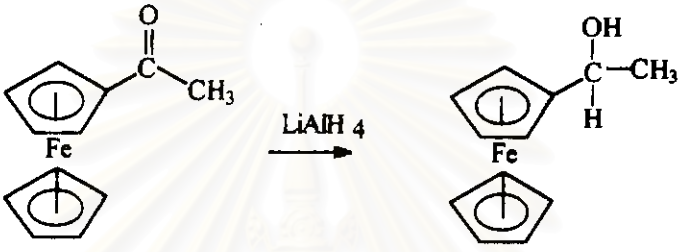


**Scheme 5.7** Preparation of α-hydroxyethylferrocene

**Table 5.11** $^1$H NMR data of ferrocenyl derivatives

| Compounds | Ferrocene moiety | | | | Cp ring protons | | |
|---|---|---|---|---|---|---|---|
| | **CH** | **$CH_2$** | **$CH_3$** | **OH** | **$C_5H_5$** | **αH** | **βH** |
| Fc-$COCH_3$ | - | - | 2.37(s) | - | 4.18(s) | 4.88(t)<br>J = 2 Hz | 4.76(t)<br>J = 2 Hz |
| $FcCH_2OH$ | - | 4.32(s) | - | 4.32(s) | 4.15(s) | 4.20(t)<br>J = 3 Hz | 4.10(s) |
| Fc-CHOH<br>\|<br>$CH_3$ | 1.87(d)<br>J = 4 Hz | - | 1.44(d)<br>J = 6 Hz | 4.52(m) | 4.21(s) | 4.25(m) | 4.25(m) |

**Table 5.12** FTIR data of ferrocenyl derivatives

| **Compounds** | **OH stretching** | **=CH stretching** | **-CH stretching** | **C=C stretching** | **C=O** | **$-CH_2$** | **$CH_3$** | **-CH out of plane bending** |
|---|---|---|---|---|---|---|---|---|
| Fc-$COCH_3$ | - | 3116 | 3094 | 1654 | 1662 | - | 1377 | 1005 |
| $FcCH_2OH$ | 3236 | 3088 | 2956 | 1646 | - | 1378 | - | 987 |
| Fc-CHOH<br>\|<br>$CH_3$ | 3217 | 3097 | 2975 | 1637 | - | - | 1308 | 1002 |

## 5.2 Properties of Inclusion Compounds

Ferrocene and its derivatives are excellent substrate for inclusion compound in cyclodextrin hosts. They can be included in β-cyclodextrin with high yields and a simple method as shown in Scheme 5.8. A 2-fold molar excess of ferrocene derivatives was added to aqueous solution of cyclodextrin at 60 °C with stirring. The products were washed with water to remove any remaining cyclodextrin and nonincluded ferrocenyl derivatives were removed by washing with tetrahydrofuran. The included guests were not liberated from the β-cyclodextrin cavity.

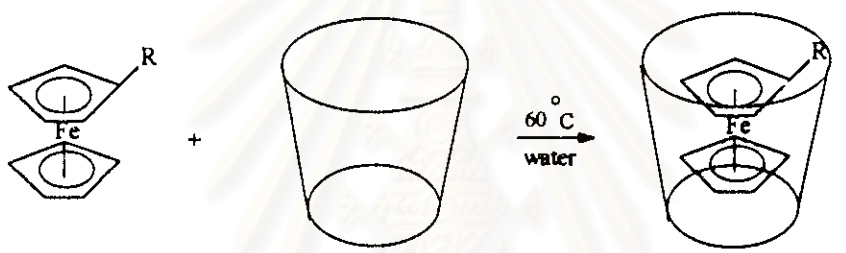


Ferrocenyl derivatives β-Cyclodextrin Inclusion compounds

R = amino, acyl or hydroxyl group

**Scheme 5.8** Inclusion compound of β-cyclodextrin-ferrocenyl derivatives

### 5.2.1 Thermogravimetric Analysis

The inclusion compounds are obtained thermally stable, did not liberate the guest when heated at 150 °C while the nonincluded melted under the same condition. Figure 5.8 shows the results of the thermogravimetric analyses of a) β-cyclodextrin, b) α-methylferrocenylmethylamine, c) mixture and d) β-cyclodextrin-α-methylferrocenylmethylamine inclusion compound. In the case of mixture each component behaved independently, α-methylferrocenylmethylamine melts below 200 °C and β-cyclodextrin decomposed around 250 °C. In the case of inclusion compound there was no change around 200 °C except the loss of hydrated water. It was stable up to 220 °C and decomposed above 250 °C. The results indicated that the α-methylferrocenyl

methylamine was included tightly in the β-cyclodextrin cavity. The decomposing point of the inclusion compound is lower than that of β-cyclodextrin. This may be due to the promoting effects of the guest.

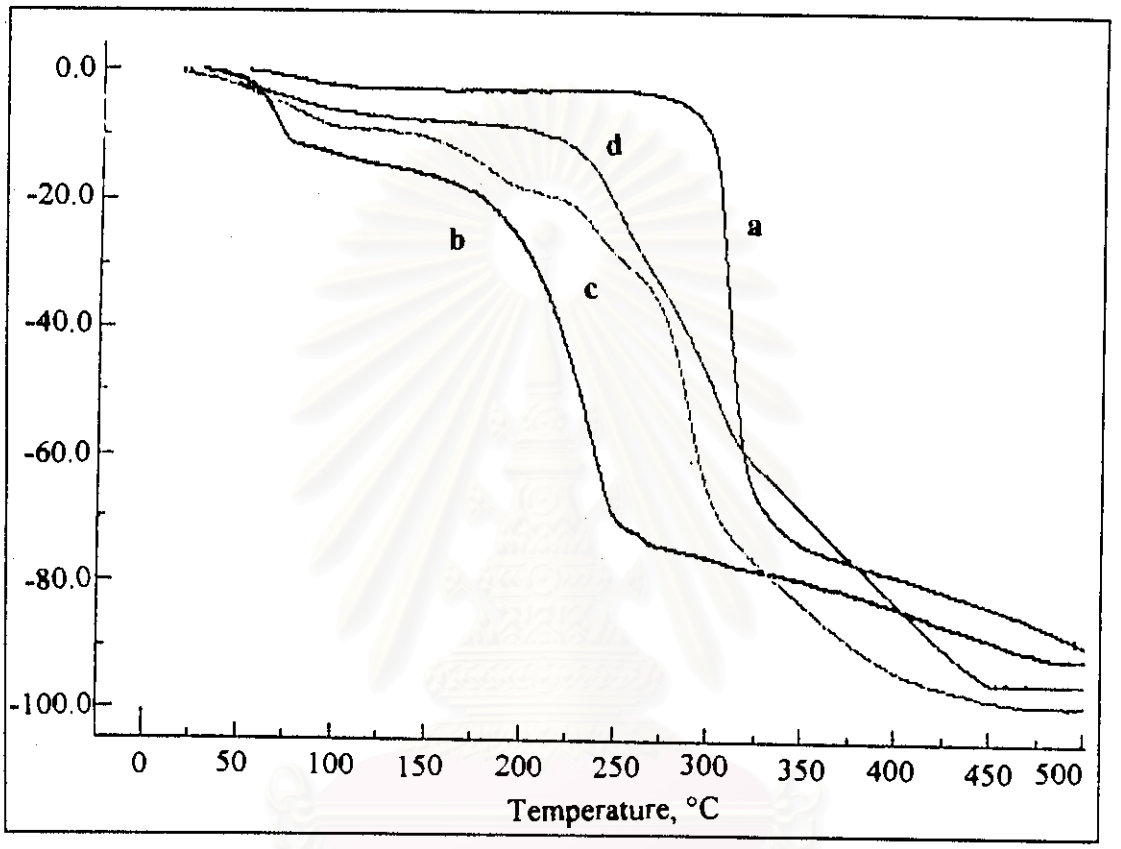


**Figure 5.8** Thermogravimetric analysis of

a) β-cyclodextrin
b) α-methylferrocenylmethylamine
c) mixture
d) β-cyclodextrin-α-methylferrocenylmethylamine inclusion compound

### 5.2.2 Elemental Analysis

Stoichiometries were determined by elemental analyses. These results show that ferrocenyl derivative can form inclusion compound with β-cyclodextrin with a 1:1 stoichiometry, regardless of the molar ratio of the host to guest in the reaction.

In addition, elemental analyses reveal number of water in cavity. It was found that about 3-6 molecules of water were included in β-cyclodextrin inclusion compound. From X-ray crystal structure of β-cyclodextrin at ambient condition, there were about 12 molecules of water.[40]

Characterization data of ferrocenyl derivative-β-cyclodextrin inclusion compounds are shown in Tables 5.13 and 5.14.

**Table 5.13** Characterization data of ferrocenylamine inclusion compounds

| Inclusion compound | Formula | % yield | mp[a] (°C) | Analysis[b] (%) | |
|---|---|---|---|---|---|
| | | | | C | H |
| Fc-$CH_2$-N($CH_3$)$_2$-CD | $C_{55}H_{97}O_{35}NFe.4H_2O$ | 65 | 207-208 | 44.75 (44.55) | 6.38 (6.60) |
| Fc-$CH_2$-N($CH_3$)$_3$I-CD | $C_{56}H_{90}NIO_{35}Fe.4H_2O$ | 62 | 218-220 | 42.39 (42.25) | 6.38 (6.20) |
| Fc-$CH_2$-NH-$CH_3$-CD | $C_{54}H_{85}NO_{35}Fe.4H_2O$ | 60 | 208-210 | 45.19 (45.16) | 6.50 (6.53) |
| Fc-$CH_2$-$CH_2NH_2$-CD | $C_{54}H_{85}NO_{35}Fe.4H_2O$ | 65 | 235-237 | 44.95 (45.16) | 6.62 (6.53) |
| CD-Fc-CH=N-($CH_2$)$_2$-N=CH-Fc-CD | $C_{108}H_{164}N_2O_{76}Fe_2.6H_2O$ | 58 | 258-260 | 44.21 (44.33) | 6.27 (6.06) |
| CD-Fc-$CH_2$-NH-($CH_2$)$_2$-NH-$CH_2$-Fc-CD | $C_{108}H_{168}N_2O_{76}Fe_2.6H_2O$ | 62 | 245-247 | 44.10 (44.27) | 6.30 (6.19) |

[a] With decomposition.

[b] Required values are given in parentheses

**Table 5.14** Characterization data of ferrocenyl derivative inclusion compounds

| Inclusion Compound | Formula | % yield | mp[a] (°C) | Analysis[b] (%) | |
|---|---|---|---|---|---|
| | | | | C | H |
| Fc-$COCH_3$-CD | $C_{54}H_{82}O_{36}Fe.3H_2O$ | 70 | 244-247 | 45.58 (45.77) | 6.30 (6.26) |
| Fc-COH-CD | $C_{53}H_{80}O_{36}Fe.3H_2O$ | 75 | 228-230 | 45.38 (45.57) | 5.80 (6.18) |
| Fc-$CH_2$-OH-CD | $C_{53}H_{82}O_{36}Fe.4H_2O$ | 63 | 221-222 | 44.38 (44.73) | 6.29 (6.37) |
| FC-CH(CH3)-OH-CD | $C_{54}H_{84}O_{36}Fe.4H_2O$ | 65 | 222-223 | 45.13 (45.13) | 6.30 (6.45) |
| Fc-$CH_2$-CN | $C_{54}H_{81}O_{35}NFe.4H_2O$ | 61 | 198-199 | 45.00 (45.29) | 6.29 (6.26) |

[a] With decomposition.

[b] Required values are given in parentheses

## 5.3 Characterization of β-Cyclodextrin by NMR Technique

Cyclodextrin is insoluble in most common organic solvents but soluble in water and dimethylsulfoxide. Solvent has a profound influence on $^1$H NMR spectra, in water there is a fast exchange of OH protons. To avoid this, dimethylsulfoxide was frequently used. In such medium one can obtain detailed insight into the intramolecular cyclodextrin hydrogen-bond network and often observes better resolved signals for other protons. Another way to reach a higher dispersion of overlapping cyclodextrin signal is to use a 500 MHz NMR instrument. So in this work, structural characterization of β-cyclodextrin was done, using 500 MHz NMR instrument and DMSO-$d_6$ solvent. Proton positions of β-cyclodextrin are shown below. $^1$H NMR data and spectrum are given in Table 5.15 and Figure 5.9, respectively. The result agrees well with that in the literature.[41]

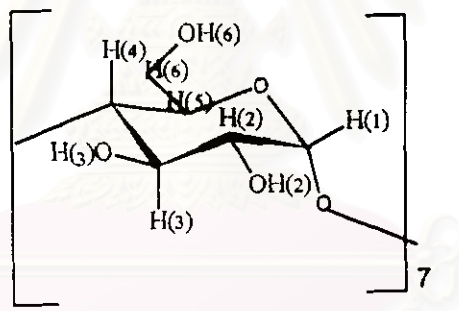


**Table 5.15** $^1$H NMR data of β-cyclodextrin

| Chemical shift (ppm) | Multiplicity | Number of protons | Assignment | Coupling constant (Hz) |
|---|---|---|---|---|
| 5.73 | doublet | 7H | OH(2) | J = 6.7 |
| 5.68 | doublet | 7H | OH(3) | J = 2.0 |
| 4.83 | doublet | 7H | H(1) | J = 3.4 |
| 4.45 | triplet | 7H | OH(6) | J = 5.5 |
| 3.64 | multiplet | 21H | H(3), H(6) | |
| 3.59 | multiplet | 7H | H(5) | |
| 3.35 | multiplet | 7H | H(4) | |
| 3.30 | multiplet | 7H | H(2) | |

Cyclodextrin has primary and secondary hydroxyl groups crowding opposite ends of its torus, H(3) and H(5) directed toward its interior H(1), H(2) and H(4) located on its exterior. The secondary hydroxyl groups, at the wider rim of the cyclodextrin, form intramolecular bonds in which the OH(3) group of one glucose is interacting with the OH(2) group of the neighboring glucose unit. This leads to a belt of hydrogen bonds around the secondary cyclodextrin side that gives the whole molecule a rather rigid structure. The primary hydroxyl groups OH(6) placed at the smaller rim are not participating in intramolecular hydrogen bonds and therefore can rotate the C(5)-C(6) bond.[41]

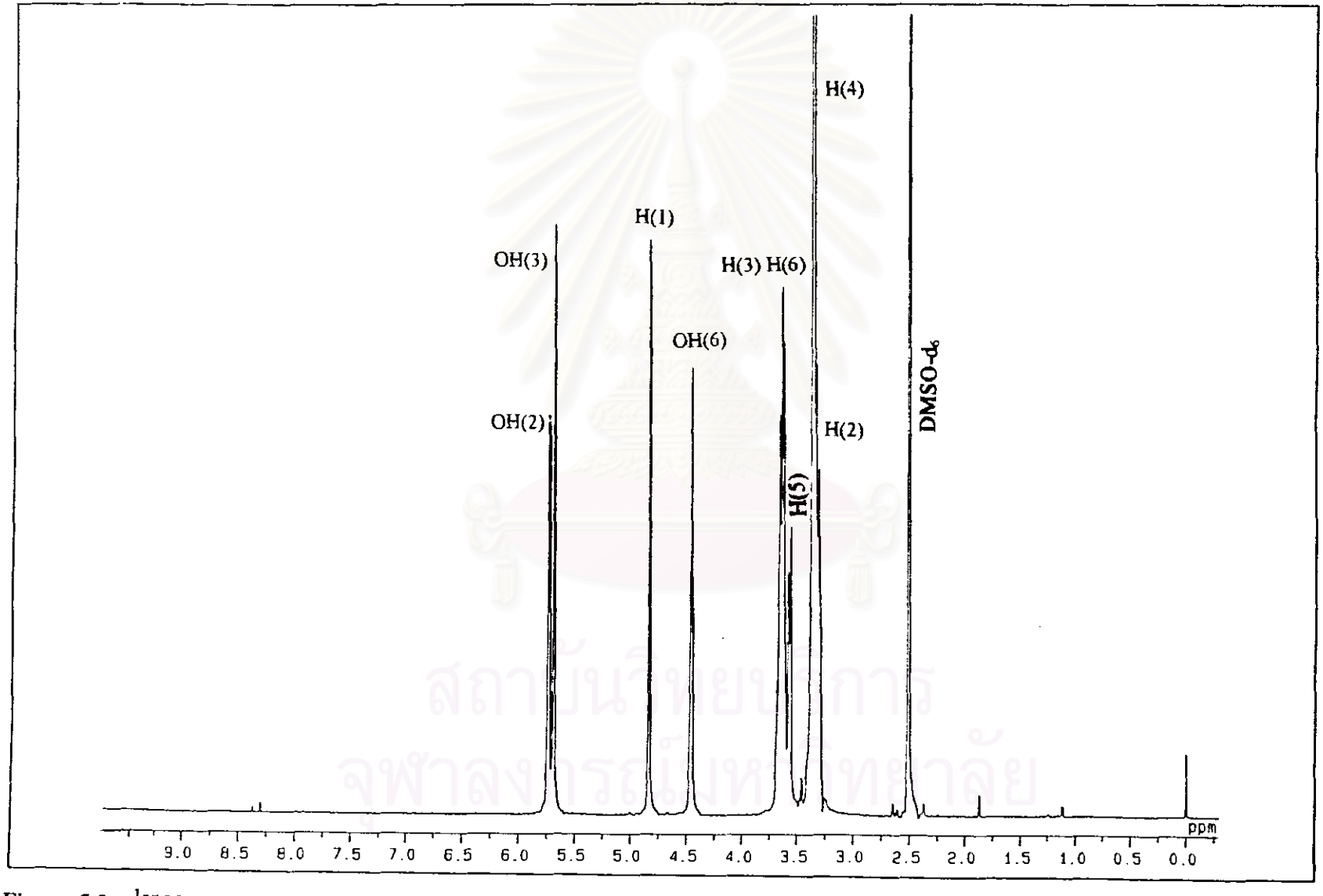


**Figure 5.9** $^{1}$H NMR spectrum of β-cyclodextrin

## 5.4 Characterization of Inclusion Compounds by NMR Technique

Cyclopentadienyl ring of ferrocene, the delocalized π electrons give rise to a ring current when field is perpendicular to the molecular plane, as shown in Figure 5.10. The induced field opposes Bo at the middle of the molecule but reinforces it at the periphery. As a result, protons in the molecular plane and outside the ring are deshielded. Conversely, protons in the regions above or below the plane to the ring are strongly shielded.

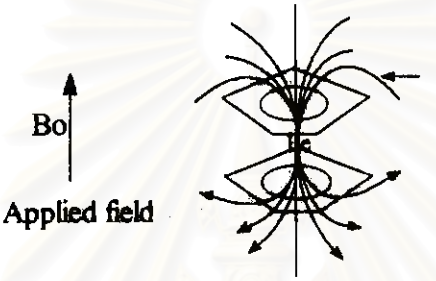


**Figure 5.10** Anisotropic effect of cyclopentadienyl ring

In the β-cyclodextrin-ferrocene inclusion compound, a ferrocene molecule could fit well into a β-cyclodextrin cavity by axial inclusion.[21] The delocalized π electrons of cyclopentadienyl rings affected H(3) and H(5) at the interior wall of cyclodextrin. H(3) and H(5) are directed to molecular plane of cyclopentadienyl ring (Figure 5.11) so they show downfield shifts. The chemical shifts of H(1), H(2 ) and H(4) which are on the outer surface of the β-cyclodextrin torus are unaffected.

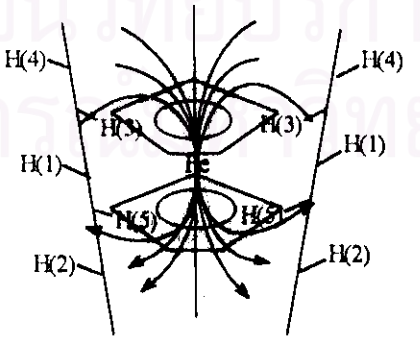


**Figure 5.11** Anisotropic effect of cyclopentadienyl rings to H(3) and H(5) of β-cyclodextrin

It was indicated that if only H(3) underwent a shift in the presence of substrate then the cavity penetration was shallow, whereas if H(5) also shifted the penetration was deep[41] as shown in Figure 5.12.

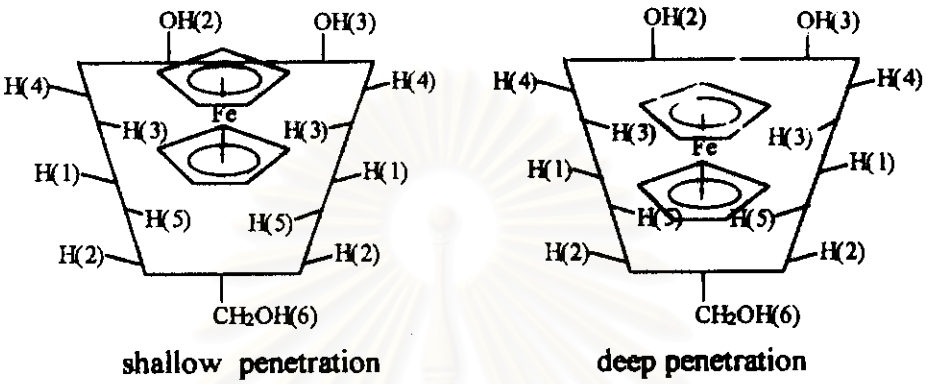


**Figure 5.12** Ferrocene in cyclodextrin with interaction sites of proton observable by $^1$H NMR

## 5.5 Characterization of β-Cyclodextrin-Ferrocenyl Derivative Inclusion Compounds by NMR Technique

### 5.5.1 β-Cyclodextrin-*N*, *N*-Dimethylaminomethylferrocene Inclusion Compound ($FcCH_2N(CH_3)_2$-CD)

The $^1$H NMR spectrum and the data of inclusion compound of β-cyclodextrin with $FcCH_2N(CH_3)_2$ are shown in Figure 5.12 and Table 5.16. The resonance at 4.13 ppm was assigned to unsubstituted cyclopentadienyl ring, the two doublet peaks at 4.10 and 4.14 ppm resulted from four protons in the substituted cyclopentadienyl ring. The splitting of the $^1$H NMR resonances for the substituted cyclopentadienyl ring upon inclusion of $FcCH_2N(CH_3)_2$ in β-cyclodextrin cavity suggests that rotation of the bond between the ring and the methylene substituent is hindered by the cyclodextrin.[42] H(3) and H(5) of β-cyclodextrin located in the cavity were 0.03 and 0.02 ppm downfield shifted but H(1), H(2) and H(4) which located in the exterior of the cavity were unaffected. Secondary hydroxyl groups, OH(3) was downfield shifted and became

singlet because of moderate hydrogen bond between N of amino group (acceptor) and H of hydroxyl group (donor). OH(2) was 0.02 ppm downfield shifted because of ferrocene moiety. Primary hydroxyl OH(6) became singlet, this can be explained from partially block in the cyclodextrin cavity by hydrogen bonding with cyclopentadienyl ring. The two conformers of β-cyclodextrin reported,[43] as shown below are the (-) gauche form with OH(6) pointing away and the (+) gauche form with OH(6) toward the cavity. The latter form is observed if certain packing requirements are met or if a hydrogen bond is formed with an included guest molecule.

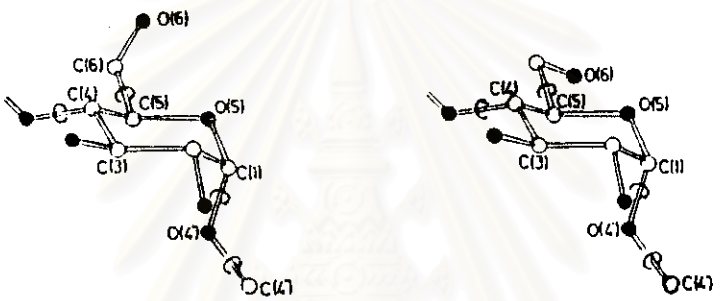


(-) gauche (+) gauche

From these results, it indicates that $FcCH_2N(CH_3)_2$ was included in the hydrophobic cavity of β-cyclodextrin and a possible geometry was proposed as shown below.

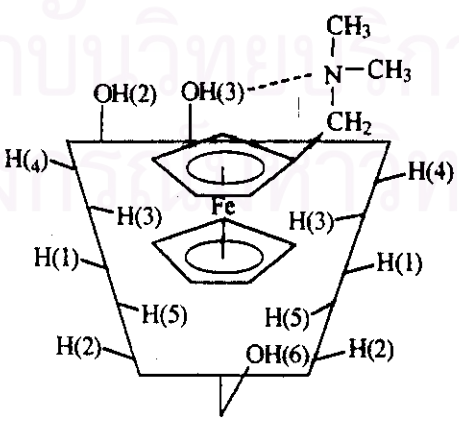

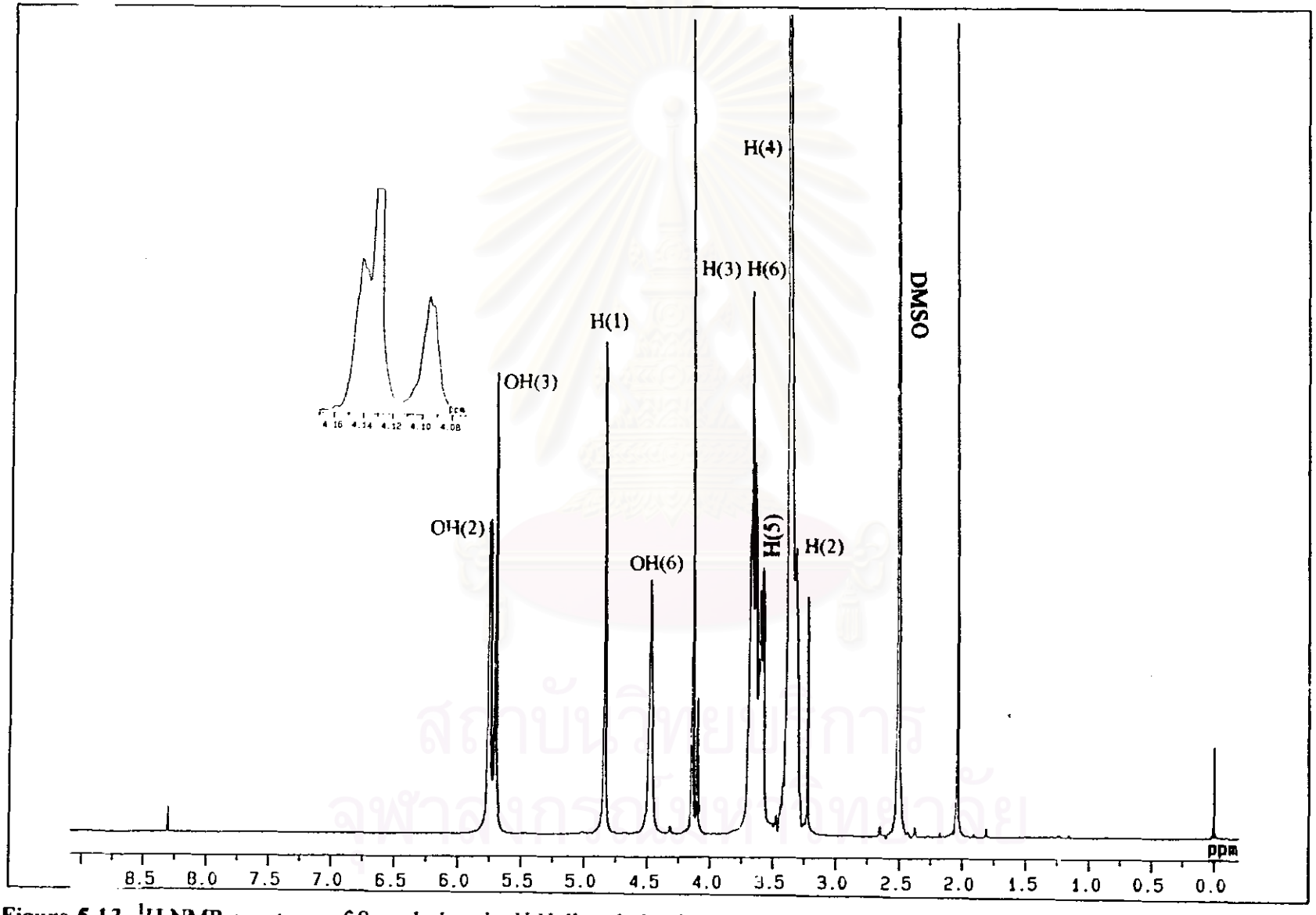


**Figure 5.13** $^{1}$H NMR spectrum of β-cyclodextrin-*N,N*-dimethylaminomethylferrocenene inclusion compound

**Table 5.16** $^1$H NMR data of β-cyclodextrin-*N*, *N*-dimethylaminomethylferrocene inclusion compound

| Chemical shift (ppm) | Multiplicity | Number of protons | Assignment | Coupling constant (Hz) |
|---|---|---|---|---|
| 5.75 | doublet | 7H | OH(2) | J = 6.5 |
| 5.70 | singlet | 7H | OH(3) | |
| 4.83 | doublet | 7H | H(1) | J = 3.0 |
| 4.47 | singlet | 7H | OH(6) | |
| 4.14 | doublet | 2H | αH-$C_5H_4$ | J = 2.0 |
| 4.13 | singlet | 5H | $C_5H_5$ | |
| 4.10 | doublet | 2H | βH-$C_5H_4$ | J = 2.0 |
| 3.67 | multiplet | 21H | H(3), H(6) | |
| 3.61 | multiplet | 7H | H(5) | |
| 3.35 | multiplet | 7H | H(4) | |
| 3.30 | multiplet | 7H | H(2) | |
| 3.21 | singlet | 2H | $CH_2$ | |
| 2.04 | singlet | 6H | $N(CH_3)_2$ | |

### 5.5.2 β-Cyclodextrin-*N*, *N*-Dimethylaminomethylferrocene Methiodide Inclusion Compound ($FcCH_2N(CH_3)_3I$-CD)

The $^1H$ NMR spectrum and the data of inclusion compound of β-cyclodextrin with $FcCH_2N(CH_3)_3I$ were shown in Figure 5.14 and Table 5.17. The quaternary salt of $FcCH_2N(CH_3)_3I$ was hindered and polar. The inclusion compound with β-cyclodextrin showed the resonance at 4.13 ppm that corresponded to the unsubstituted cyclopentadienyl ring. The two triplet peaks at 4.18 and 4.25 ppm result from the substituted cyclopentadienyl ring. The peak from the unsubstituted cyclopentadinyl ring was observed to split into two peaks due to the interaction with β-cyclodextrin.

For β-cyclodextrin resonance, 0.02 ppm downfield shifts with spitting was observed for the H(3) and H(5), which are located within the cavity of β-cyclodextrin. The chemical shifts of H(1), H(2) and H(4) were unaffected. Splittings of H(3) and H (5) were resulted from H of cyclopentadienyl ring and $-CH_2$ of ferrocenyl moiety. OH (6) was unchanged. A possible geometry was proposed as shown below.

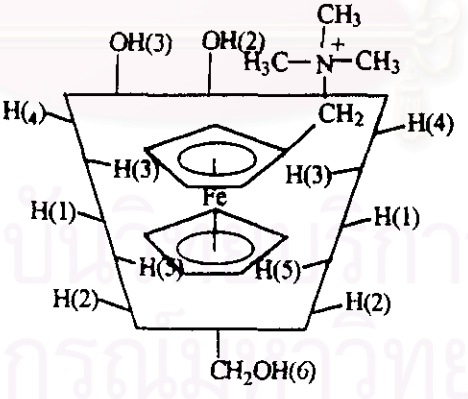

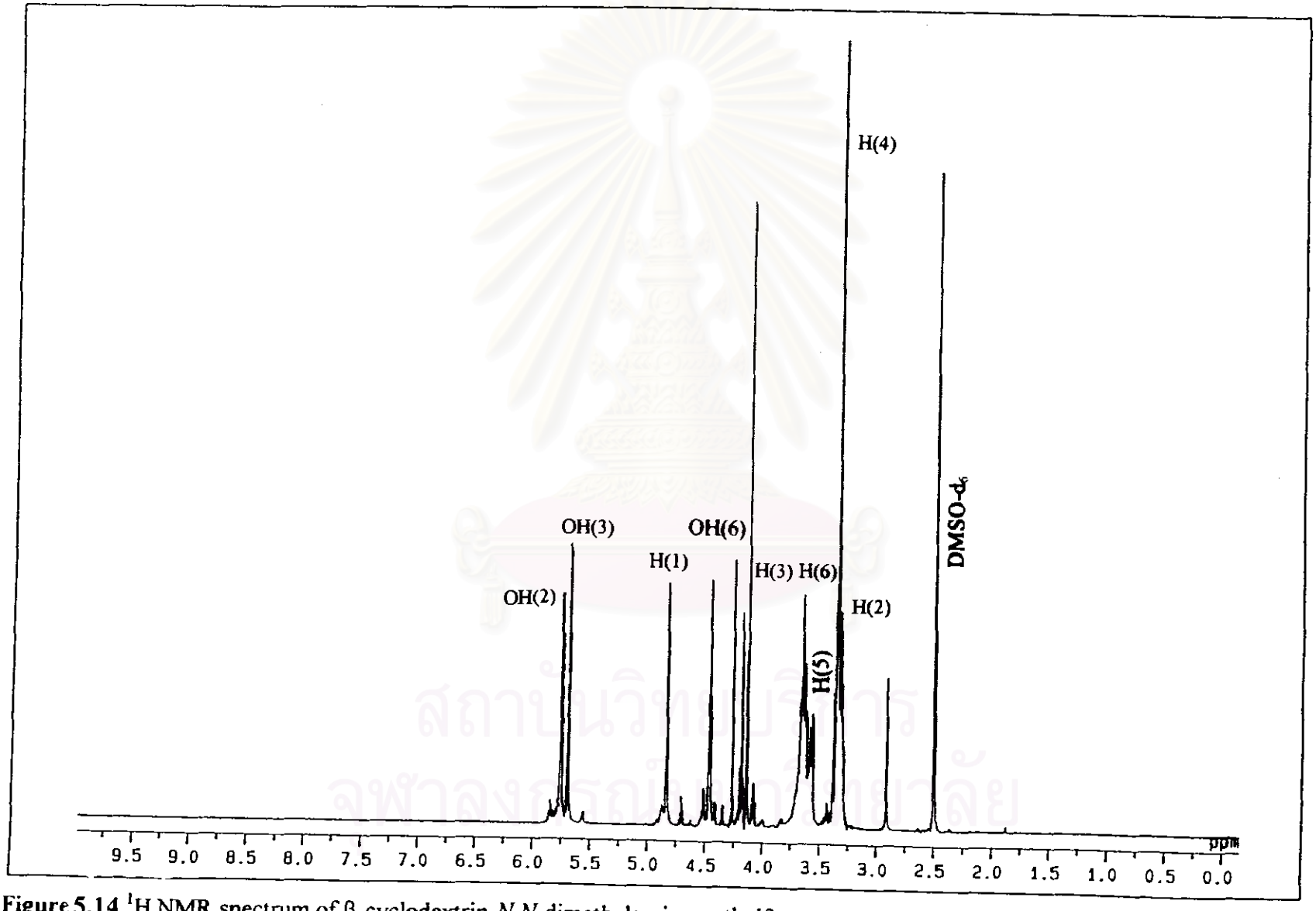


**Figure 5.14** $^1$H NMR spectrum of β-cyclodextrin-*N,N*-dimethylaminomethylferrocene methiodide inclusion compound

**Table 5.17** $^1$H NMR data of β-cyclodextrin- *N, N*-dimethylaminomethylferrocene methiodide inclusion compound

| Chemical shift(ppm) | Multiplicity | Number of protons | Assignment | Coupling constant (Hz) |
|---|---|---|---|---|
| 5.75 | doublet | 7H | OH(2) | J = 7.0 |
| 5.68 | doublet | 7H | OH(3) | J = 2.0 |
| 4.83 | doublet | 7H | H(1) | J = 4.0 |
| 4.45 | triplet | 7H | OH(6) | J = 5.5 |
| 4.25 | singlet | 2H | αH-$C_5H_4$ | |
| 4.18 | triplet | 2H | βH-$C_5H_4$ | J = 7.0 |
| 4.13 | doublet | 5H | $C_5H_5$ | J = 3.0 |
| 3.66 | multiplet | 21H | H(3), H(6) | |
| 3.61 | multiplet | 7H | H(5) | |
| 3.37 | singlet | 2H | $CH_2$ | |
| 3.35 | multiplet | 7H | H(4) | |
| 3.30 | multiplet | 7H | H(2) | |
| 2.91 | singlet | 9H | $N(CH_3)_3$ | |

### 5.5.3 β-Cyclodextrin-α-Methylferrocenylmethylamine Inclusion Compound ($FcCH_2NHCH_3$-CD)

$^1H$ NMR spectrum and the data of inclusion compound of α-methyl ferrocenylmethylamine with β-cyclodextrin are shown in Figure 5.15 and Table 5.18. Broad peaks of OH(2), OH(3) and OH(6) appeared at 5.75, 5.71 and 4.47 ppm, respectively. These results indicate that hydrogen bonding between OH of cyclodextrin and -NH of ferrocene moiety was formed. Chemical shifts of H(3) and H(5) were 0.02 ppm downfield shifted while H(1), H(2) and H(4) were unaffected. H(6) was deshielded due to amino group. These results indicated that $FcCH_2NHCH_3$ was included in cyclodextrin cavity. Possible geometries were proposed as shown below.

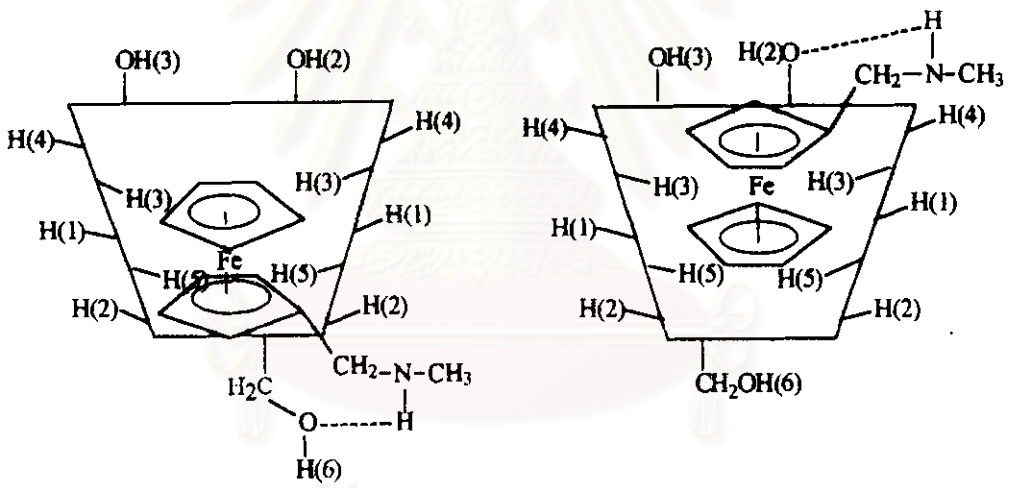

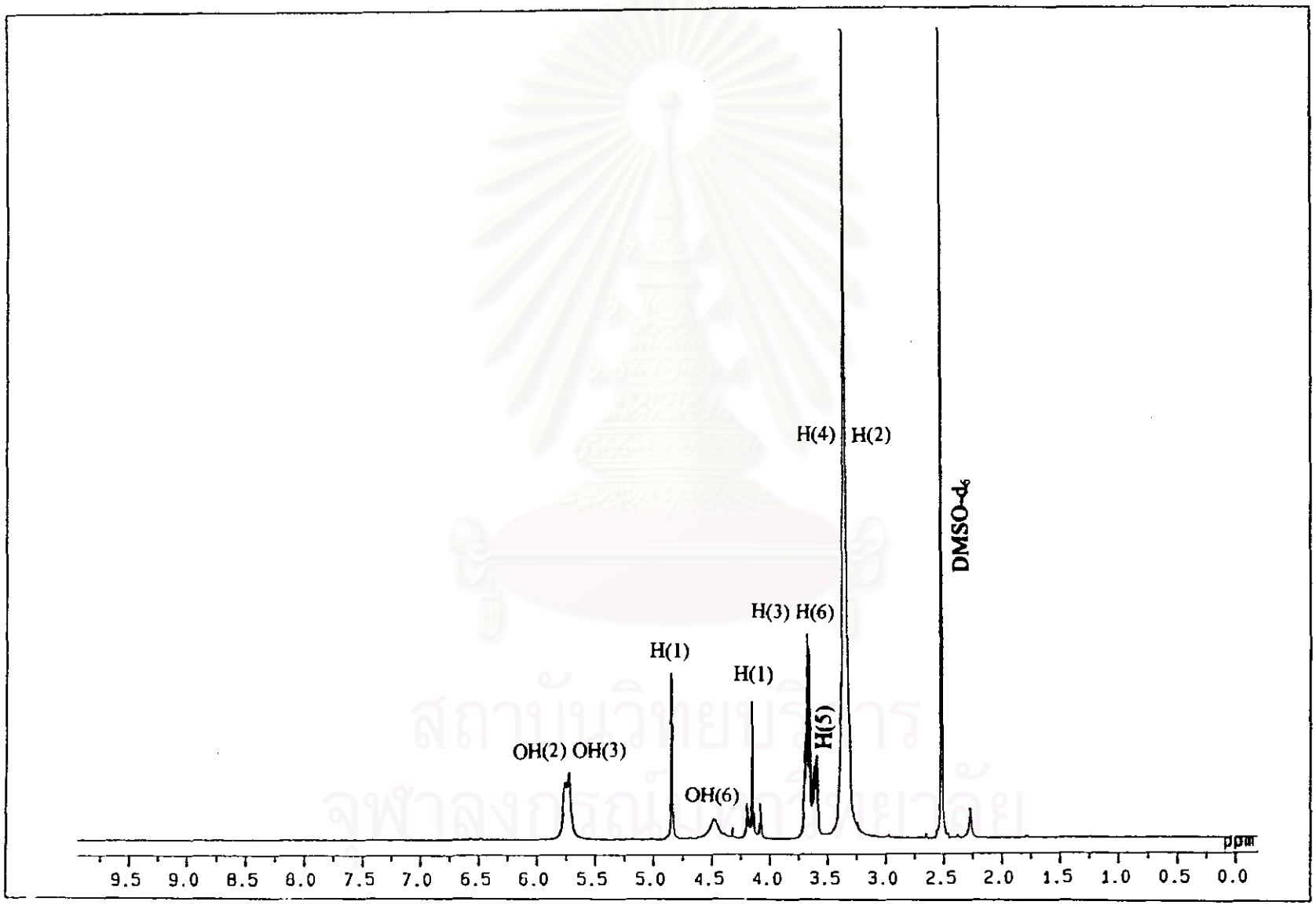


**Figure 5.15** $^{1}$H NMR spectrum of β-cyclodextrin-α-methylferrocenylmethylamine inclusion compound

**Table 5.18** $^1H$ NMR data of α-methylferrocenylmethylamine-β-cyclodextrin inclusion compound

| Chemical shift (ppm) | Multiplicity | Number of protons | Assignment | Coupling constant (Hz) |
|---|---|---|---|---|
| 5.75 | broad | 7H | OH(2) | |
| 5.71 | broad | 7H | OH(3) | |
| 4.83 | doublet | 7H | H(1) | J = 3.5 |
| 4.47 | broad | 7H | OH(6) | |
| 4.19 | singlet | 2H | αH-$C_5H_4$ | |
| 4.14 | singlet | 5H | $C_5H_5$ | |
| 4.07 | singlet | 2H | βH-$C_5H_4$ | |
| 3.66 | multiplet | 21H | H(3), H(6) | |
| 3.62 | singlet | 2H | $NCH_2$ | |
| 3.61 | multiplet | 7H | H(5) | |
| 3.35 | multiplet | 7H | H(4) | |
| 3.30 | multiplet | 7H | H(2) | |
| 2.85 | singlet | 1H | NH | |
| 2.25 | singlet | 3H | $NCH_3$ | |

### 5.5.4 β-Cyclodextrin-Ferrocenylethylamine Inclusion Compound ($Fc\text{-}CH_2CH_2NH_2\text{-}CD$)

$^1H$ NMR spectrum and the data of ferrocenylethylamine-β-cyclodextrin inclusion compound are shown in Figure 5.16 and Table 5.19. A singlet peak at 4.22 ppm is assigned to the unsubstituted cyclopentadienyl ring. Two multiplet peaks at 4.14 and 4.18 ppm are assigned to the substituted cyclopentadienyl ring protons. $^1H$ NMR data showed strong upfield shift with splitting (0.07 ppm) of H(5) which located in the interior of smaller cavity but H(3) was unchanged. H(1) and H(6) were also unchanged. H(4) was 0.11 ppm downfield shifted because of amino moiety. OH(6) was strongly downfield shifted (0.09 ppm) which might be from rotation of C(5)-C(6) into the cavity and perhaps from hydrogen bond with guest molecule or water in cavity. Upfield shift of H(5) revealed deep inclusion of guest and also resulted from a slight tipping of guest. A possible geometry was proposed as shown below.

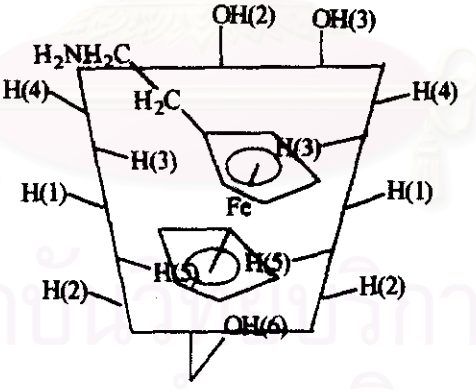

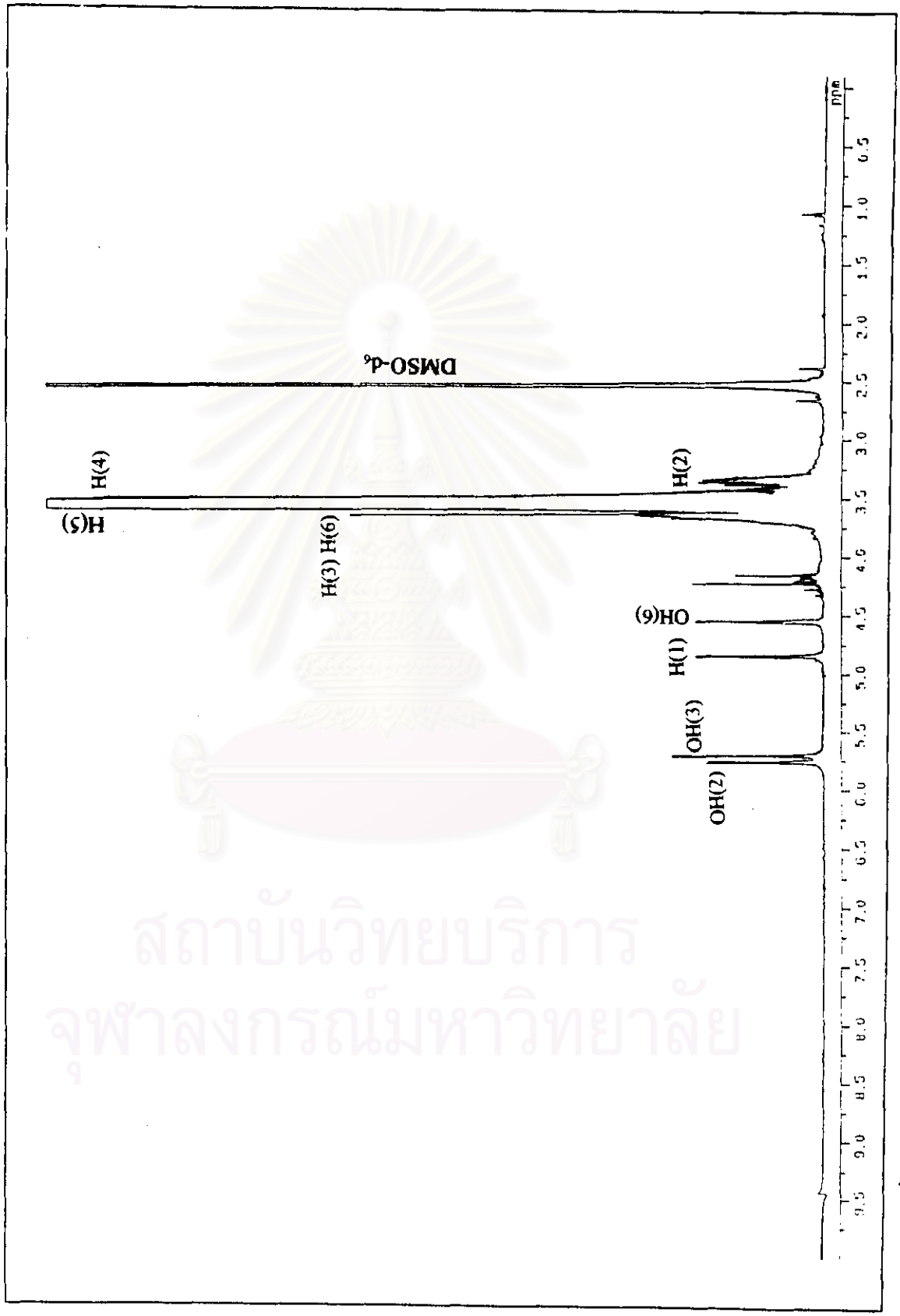


**Figure 5.16** $^{1}$H NMR spectrum of β-cyclodextrin-ferrocenylethylamine inclusion compound

**Table 5.19** $^1$H NMR data of β-cyclodextrin-ferrocenylethylamine inclusion compound.

| Chemical shift (ppm) | Multiplicity | Number of protons | Assignment | Coupling constant (Hz) |
|---|---|---|---|---|
| 5.75 | doublet | 7H | OH(2) | J = 7.0 |
| 5.70 | doublet | 7H | OH(3) | J = 2.0 |
| 4.83 | doublet | 7H | H(1) | J = 3.5 |
| 4.54 | triplet | 7H | OH(6) | J = 6.0 |
| 4.22 | singlet | 5H | $C_5H_5$ | |
| 4.18 | multiplet | 2H | β$H$-$C_5H_4$ | |
| 4.14 | multiplet | 2H | α$H$-$C_5H_4$ | |
| 3.64 | multiplet | 21H | H(3), H(6) | |
| 3.62 | singlet | 2H | $NH_2$ | |
| 3.52 | multiplet | 7H | H(5) | |
| 3.46 | multiplet | 7H | H(4) | |
| 3.35 | multiplet | 7H | H(2) | |

### 5.5.5 β-Cyclodextrin-Schiff Base Derivative Inclusion Compound (CD-Fc-CH=N-$CH_2$-$CH_2$-N=CH-Fc-CD)

$^1$H NMR spectrum and the data of β-cyclodextrin-Schiff base inclusion compound are shown in Figure 5.17 and Table 5.20. Chemical shift of HC=N was seen at 8.30 ppm. Resonances of H(3) and H(5) which located in the cavity showed 0.02 ppm downfield shift but H(1), H(2) and H(4) were unaffected. OH(3) was downfield shifted and became singlet because of moderate hydrogen bond formation between of =N-$CH_2$ of gust and H of cyclodextrin. OH(2) downfield shifts can be influenced by amino groups. OH(6) became singlet because of partial block in the cyclodextrin cavity. Possible inclusion geometries were proposed as shown below.

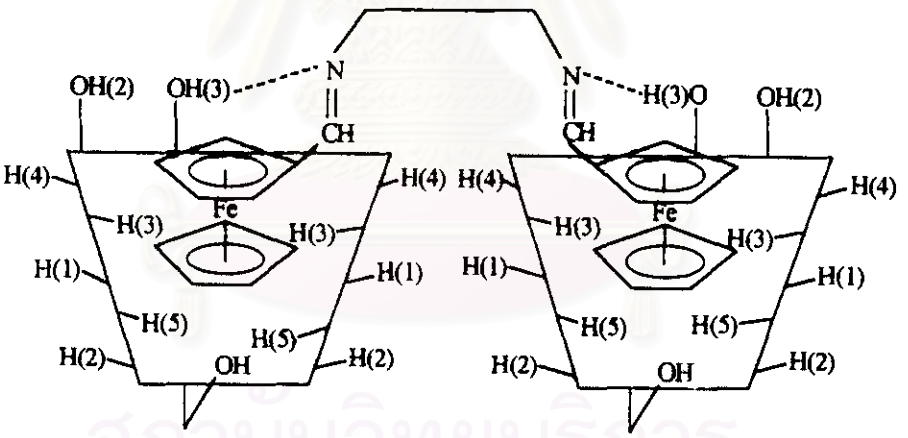

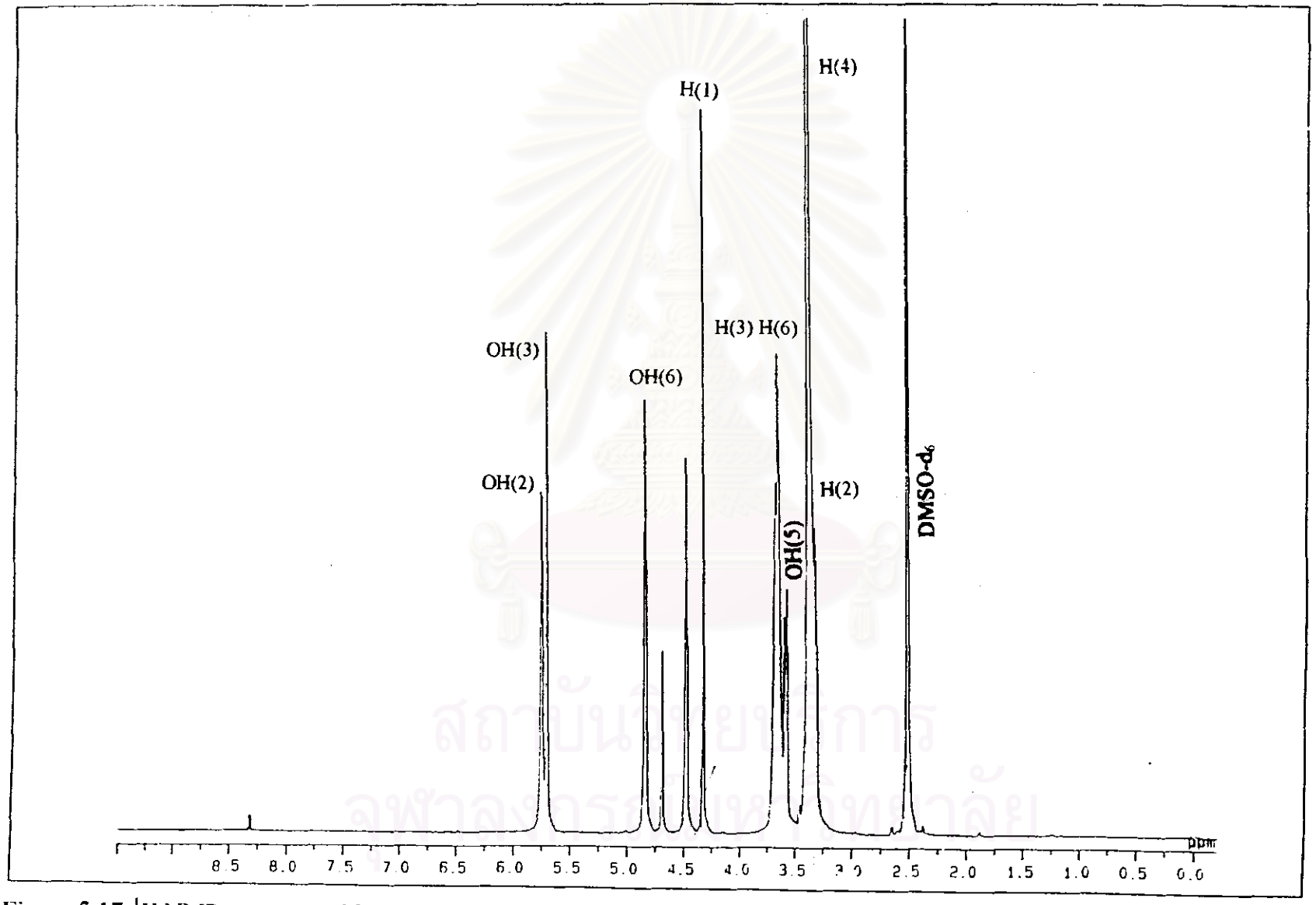


Figure 5.17 $^{1}$H NMR spectrum of β-cyclodextrin-Schiff base inclusion compound

**Table 5.20** $^{1}H$ NMR data of β-cyclodextrin-Schiff base derivative inclusion compound

| Chemical shift (ppm) | Multiplicity | Number of protons | Assignment | Coupling constant(Hz) |
|---|---|---|---|---|
| 8.30 | singlet | 2H | HC=N | |
| 5.74 | doublet | 14H | OH(2) | J = 6.5 |
| 5.70 | singlet | 14H | OH(3) | |
| 4.83 | doublet | 14H | H(1) | J = 2.5 |
| 4.82 | singlet | 4H | αH-$C_5H_4$ | |
| 4.68 | singlet | 4H | βH-$C_5H_4$ | |
| 4.47 | singlet | 14H | OH(6) | |
| 4.31 | singlet | 10H | $C_5H_5$ | |
| 3.75 | singlet | 4H | $CH_2$-$CH_2$ | |
| 3.66 | multiplet | 42H | H(3), H(6) | |
| 3.58 | multiplet | 14H | H(5) | |
| 3.35 | multiplet | 14H | H(4) | |
| 3.30 | multiplet | 14H | H(2) | |

### 5.5.6 β-Cyclodextrin-Reduced Schiff Base Derivative Inclusion Compound (CD-Fc-CHN-$(CH_2)_2$-NCH-Fc-CD)

The $^1H$ NMR spectrum and data of β-cyclodextrin-reduced Schiff base inclusion compound are shown in Figure 5.18 and Table 5.21. The spectrum showed a broad peak of OH(2) and OH(3) around 5.72 ppm and a broad peak of OH(6) at 4.45 ppm. It indicates hydrogen bond formation between –NH of guest and –OH of cyclodextrin. Chemical shifts at 4.05, 4.17 and 4.13 ppm belong to the unsubstituted and substituted cyclopentadienyl rings, respectively. Resonances of H(3) and H(5) of β-cyclodextrin, which are located in the interior of the cavity shifted 0.02 and 0.01 ppm downfield, respectively while H(1), H(2) and H(4) remained unchanged. These indicate inclusion in the cyclodextrin cavity. Possible geometries were proposed as shown below.

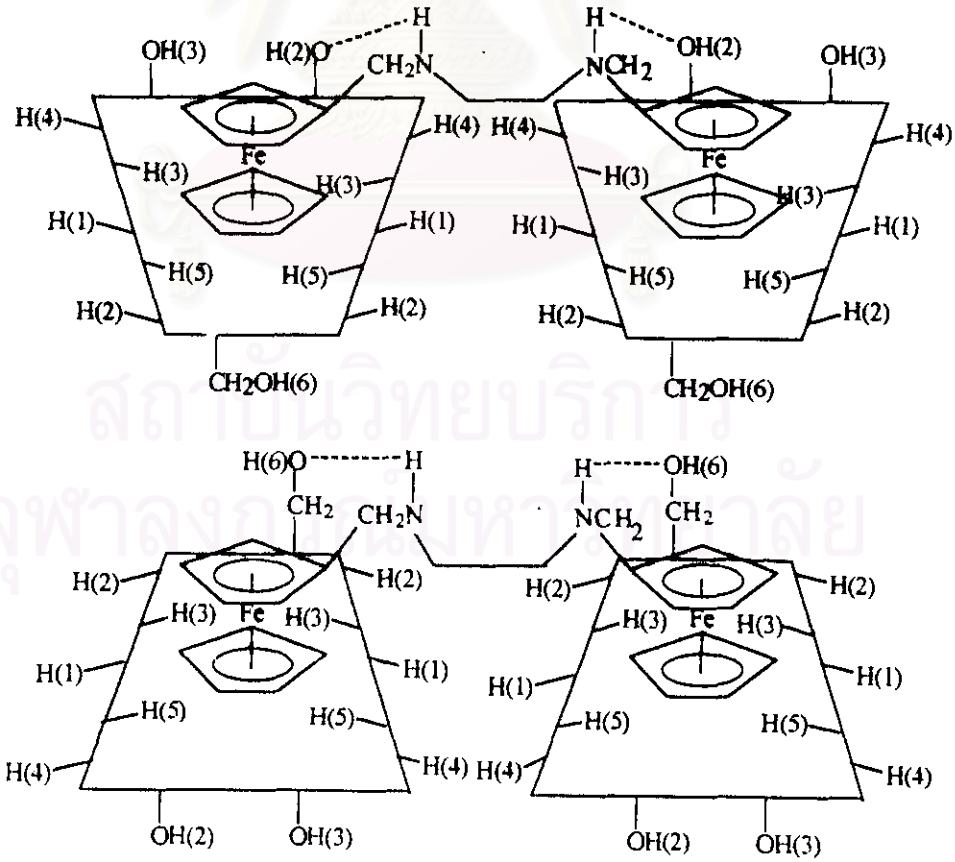

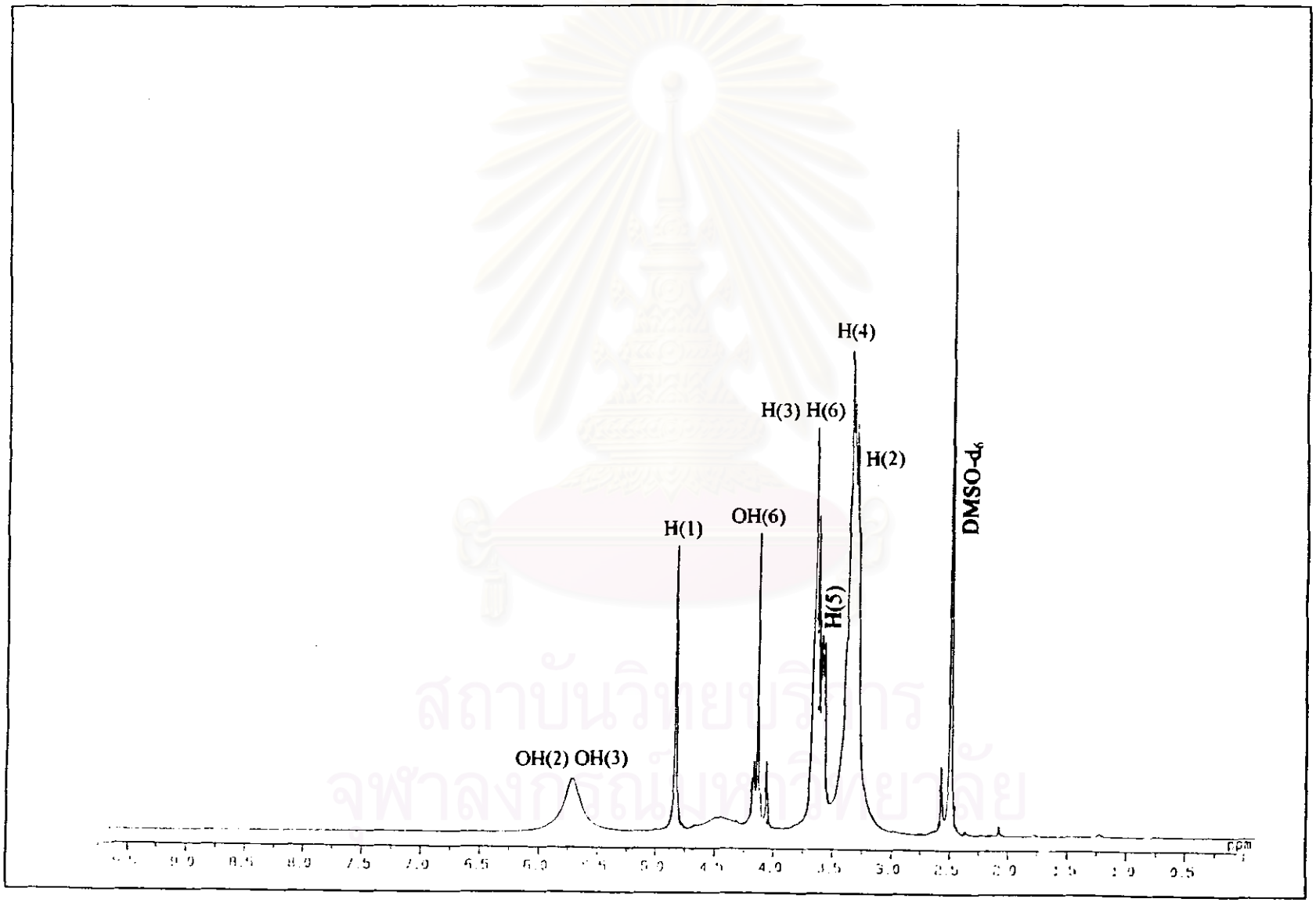


**Figure 5.18** $^{1}$H NMR spectrum of β-cyclodextrin-reduced Schiff base derivative inclusion compound

**Table 5.21** $^{1}H$ NMR data of β-cyclodextrin-reduced Schiff base derivative inclusion compound.

| Chemical shift (ppm) | Multiplicity | Number of protons | Assignment | Coupling constant (Hz) |
|---|---|---|---|---|
| 5.72 | broad | 28H | OH(2), OH(3) | |
| 4.83 | doublet | 14H | H(1) | J = 2.0 |
| 4.45 | broad | 14H | OH(6) | |
| 4.17 | doublet | 4H | αH-$C_5H_4$ | J = 8.5 |
| 4.13 | singlet | 10H | $C_5H_5$ | |
| 4.05 | singlet | 4H | βH-$C_5H_4$ | |
| 3.65 | multiplet | 42H | H(3), H(6) | |
| 3.61 | multiplet | 14H | H(5) | |
| 3.35 | multiplet | 14H | H(4) | |
| 3.49 | singlet | 4H | -$CH_2$ | |
| 3.30 | multiplet | 14H | H(2) | |
| 2.75 | singlet | 4H | -NHC$H_2$ | |

### 5.5.7 β-Cyclodextrin-Acetylferrocene (Fc-$COCH_3$-CD) and β-Cyclodextrin-Ferrocenylaldehyde (Fc-COH-CD) Inclusion Compounds

Inclusion compounds of acetylferrocene and ferrocenylaldehyde with β-cyclodextrin gave similar results. For acetylferrocene, $^1H$ NMR spectrum (Figure 5.19) showed chemical shift of $COCH_3$ at 2.35 ppm while the COH of ferrocenylaldehyde appeared at 9.90 ppm (Figure 5.20). The substituted cyclopentadienyl ring gave rise to two triplets. The splitting suggests that rotation of the ring is not free because of hydrogen bond between carbonyl and secondary alcohol. The data of both inclusion compounds in Table 5.22 and Table 5.23, respectively shows downfield shift with splitting of H(3) and H(5) because of the influence of anisotropic and acyl group. H(1), H(2), H(4) and OH(6) were remain unchanged. Possible geometries were proposed as shown below.

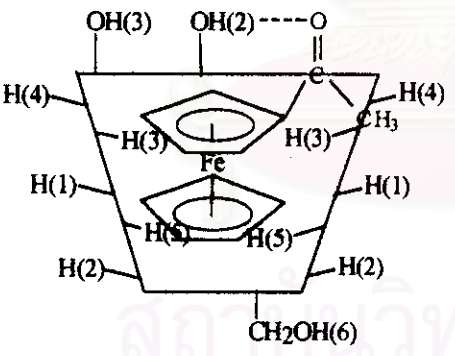


β-cyclodextrin-acetylferrocene

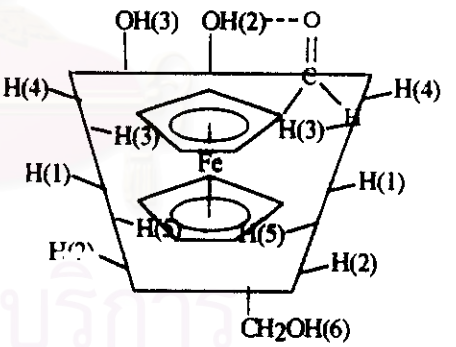


β-cyclodextrin-ferrocenylaldehyde

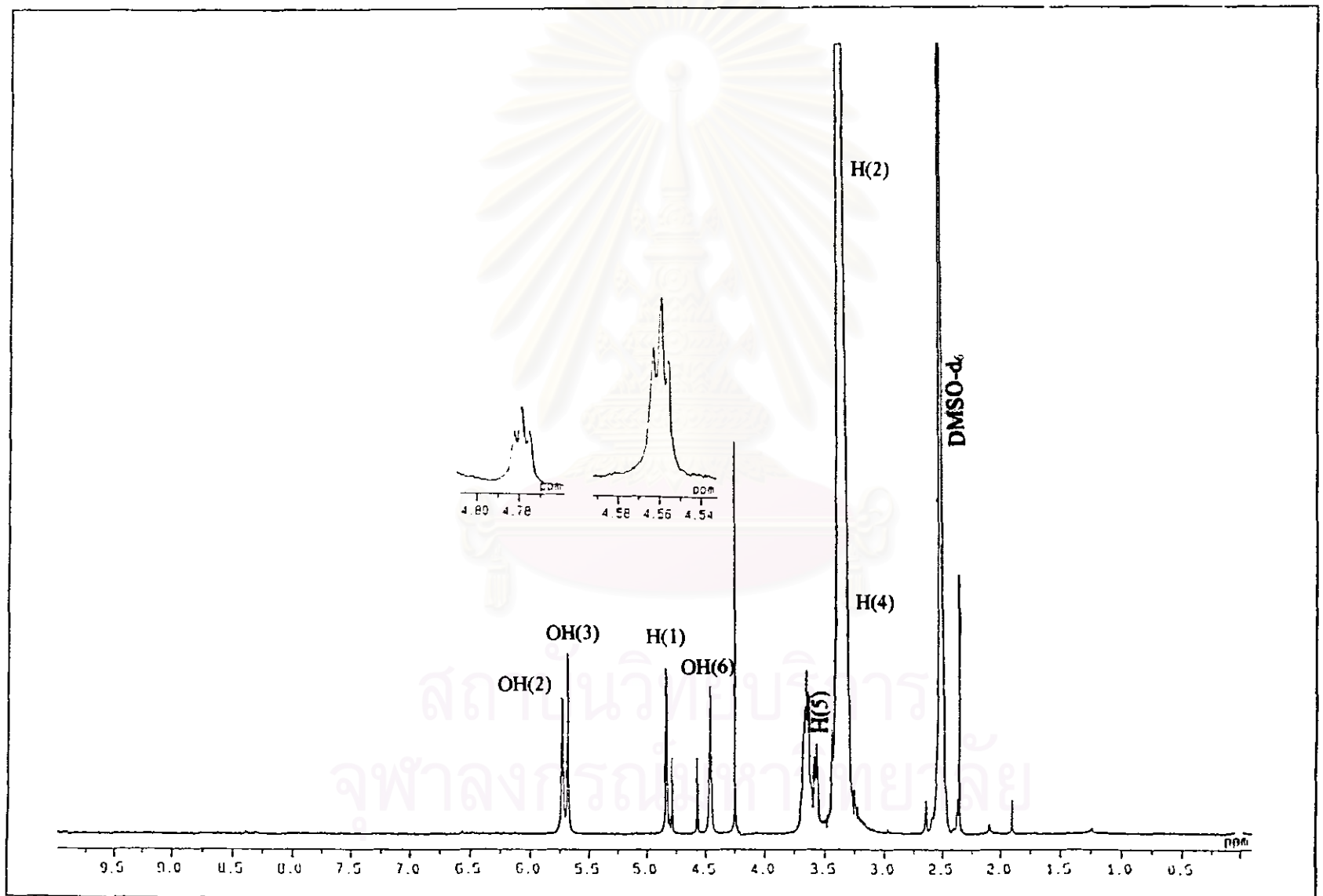


**Figure 5.19** $^1$H NMR spectrum of β-cyclodextrin-acetylferrocene inclusion compound

**Table 5.22** $^{1}H$ NMR data of β-cyclodextrin-acetylferrocene inclusion compound

| Chemical shift (ppm) | Multiplicity | Number of protons | Assignment | Coupling constant (Hz) |
|---|---|---|---|---|
| 5.72 | doublet | 7H | OH(2) | J = 6.5 |
| 5.67 | doublet | 7H | OH(3) | J = 2.0 |
| 4.83 | doublet | 7H | H(1) | J = 3.5 |
| 4.78 | triplet | 2H | αH-$C_5H_4$ | J = 2.0 |
| 4.56 | triplet | 2H | βH-$C_5H_4$ | J = 2.0 |
| 4.45 | triplet | 7H | OH(6) | J = 5.5 |
| 4.24 | singlet | 5H | $C_5H_5$ | |
| 3.65 | multiplet | 21H | H(3), H(6) | |
| 3.60 | multiplet | 7H | H(5) | |
| 3.35 | multiplet | 7H | H(4) | |
| 3.30 | multiplet | 7H | H(2) | |
| 2.35 | singlet | 3H | $CH_3$ | |

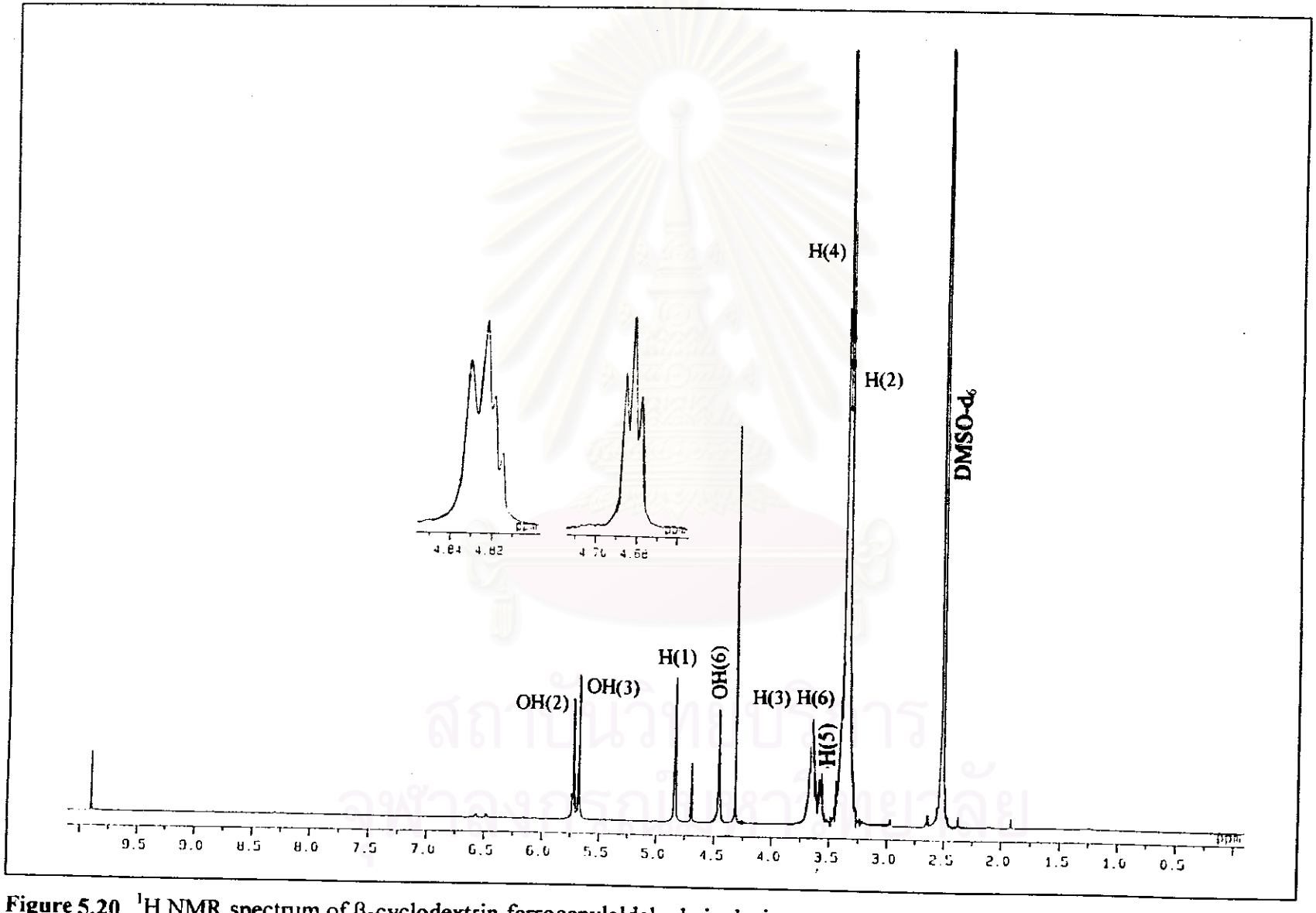


**Figure 5.20** $^{1}$H NMR spectrum of β-cyclodextrin-ferrocenylaldehyde inclusion compound

**Table 5.23** $^{1}H$ NMR data of β-cyclodextrin-ferrocenylaldehyde inclusion compound

| Chemical shift (ppm) | Multiplicity | Number of proton | Assignment | Coupling constant (Hz) |
|---|---|---|---|---|
| 9.90 | singlet | 1H | COH | |
| 5.71 | doublet | 7H | OH(2) | J = 7.0 |
| 5.67 | doublet | 7H | OH(3) | J = 2.5 |
| 4.83 | doublet | 7H | H(1) | J = 4.0 |
| 4.82 | doublet | 2H | αH-$C_5H_4$ | J = 2.0 |
| 4.68 | triplet | 2H | βH-$C_5H_4$ | J = 2.0 |
| 4.45 | triplet | 7H | OH(6) | J = 5.5 |
| 4.31 | singlet | 5H | $C_5H_5$ | |
| 3.65 | multiplet | 21H | H(3), H(6) | |
| 3.60 | multiplet | 7H | H(5) | |
| 3.35 | multiplet | 7H | H(4) | |
| 3.30 | multiplet | 7H | H(2) | |

### 5.5.8 β-Cyclodextrin-Ferrocenylmethylalcohol (Fc-$CH_2OH$-CD) and β-Cyclodextrin α-Hydroxyethylferrocenyl(Fc-CH(-OH)-$CH_3$-CD) Inclusion Compounds

$^1$H NMR spectrum of β-cyclodextrin-ferrocenylmethylalcohol was shown in Figure 5.21. Unsubstituted cyclopentadienyl ring showed doublet peak at 4.14 ppm while resonance of substituted cyclopentadienyl ring appeared as a multiplet around 4.18-4.22 ppm and a triplet at 4.09 ppm. The spectrum of β-cyclodextrin-α-hydroxy ethylferrocene in Figure 5.22 is similar. The $^1$H NMR data of inclusion compound of ferrocenylalcohol and α-hydroxyethylferrocene are shown in Table 5.24 and Table 5.25, respectively.

OH(2) of ferrocenylmethylalcohol and α-hydroxyethylferrocene appeared as a broad peak at 5.74 and 5.76 ppm, respectively. It indicates hydrogen bond. OH(6) was strongly downfield shifted. H(5) proton, located in the smaller interior cavity of cyclodextrin showed 0.05-0.06 ppm upfield shift with splitting. Strong downfield shift (0.13 ppm) of H(4) resulted from substituted group on ferrocene. Upfield shift of H(5) was presumably affected from anisotropic effect below the plane of ring current, resulting from tipping of guest as shown below.

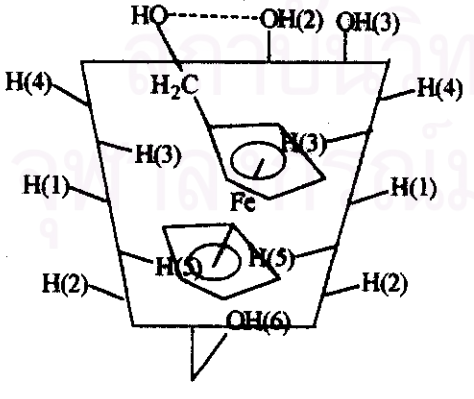


β-cyclodextrin-ferrocenylmethylalcohol

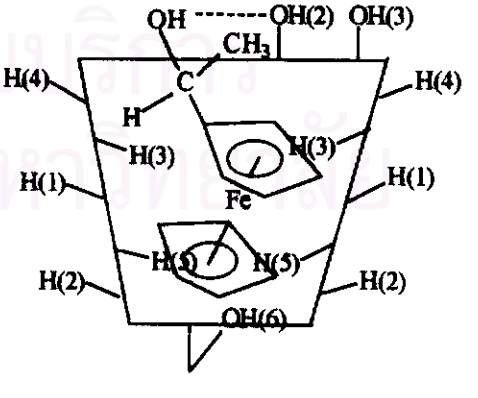


β-cyclodextrin-α-hydroxyethylferrocene

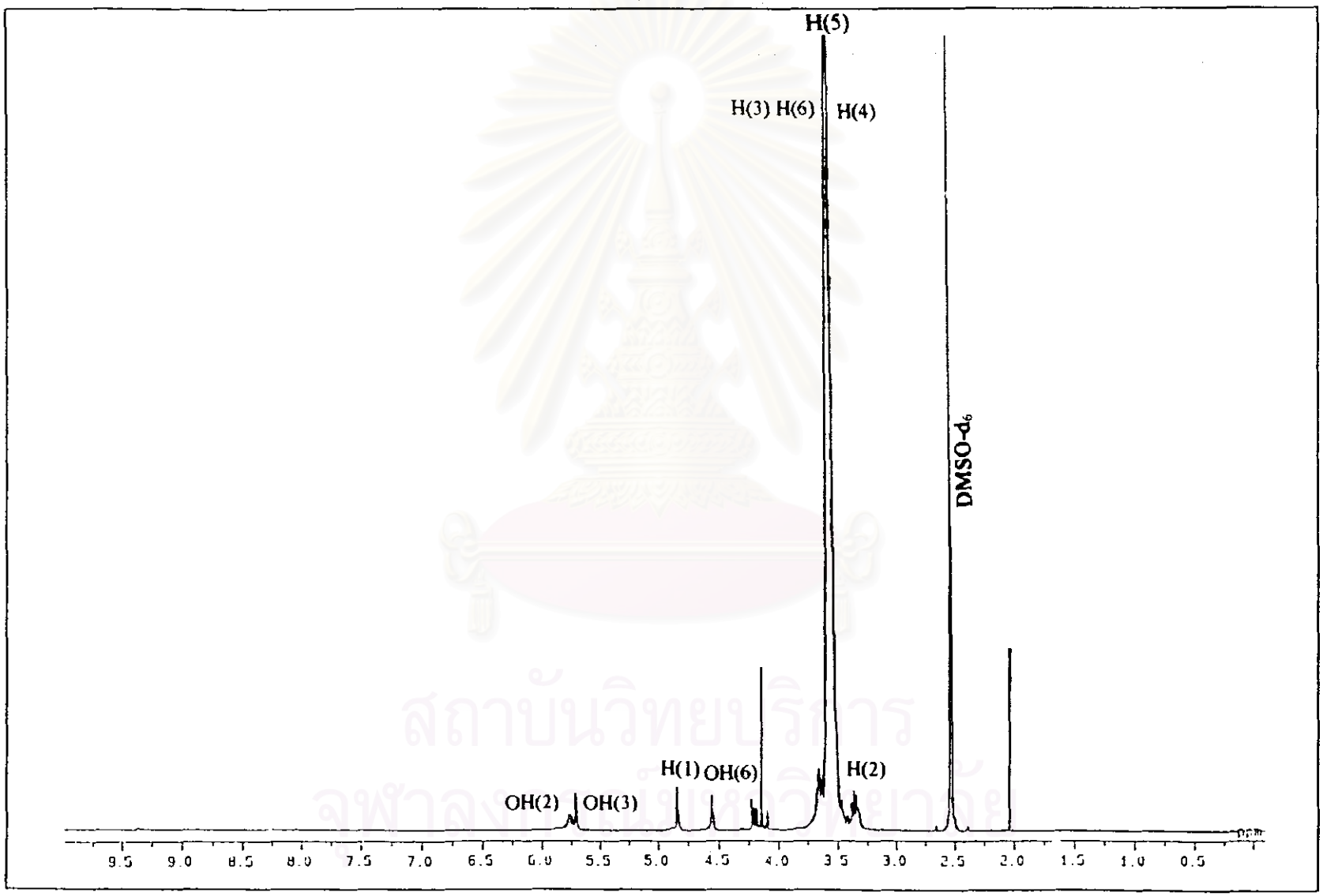


**Figure 5.21** $^{1}$H NMR spectrum of β-cyclodextrin-ferrocenylmethylalcohol inclusion compound

**Table 5.24** $^{1}H$ NMR data of ferrocenylmethylalcohol-β-cyclodextrin inclusion compound

| Chemical shift(ppm) | Multiplicity | Number of proton | Assignment | Coupling constant (Hz) |
|---|---|---|---|---|
| 5.76 | broad | 7H | OH(2) | |
| 5.71 | doublet | 7H | OH(3) | J = 2.0 |
| 4.83 | doublet | 7H | H(1) | J = 3.5 |
| 4.55 | triplet | 7H | OH(6) | J = 5.5 |
| 4.20 | multiplet | 2H | αH-$C_5H_4$ | |
| 4.14 | doublet | 5H | $C_5H_5$ | J = 2.5 |
| 4.09 | triplet | 2H | βH-$C_5H_4$ | J = 2.0 |
| 3.65 | multiplet | 21H | H(3), H(6) | |
| 3.54 | multiplet | 7H | H(5) | |
| 3.49 | multiplet | 7H | H(4) | |
| 3.35 | multiplet | 7H | H(2) | |
| 2.09 | singlet | 3H | $CH_2OH$ | |

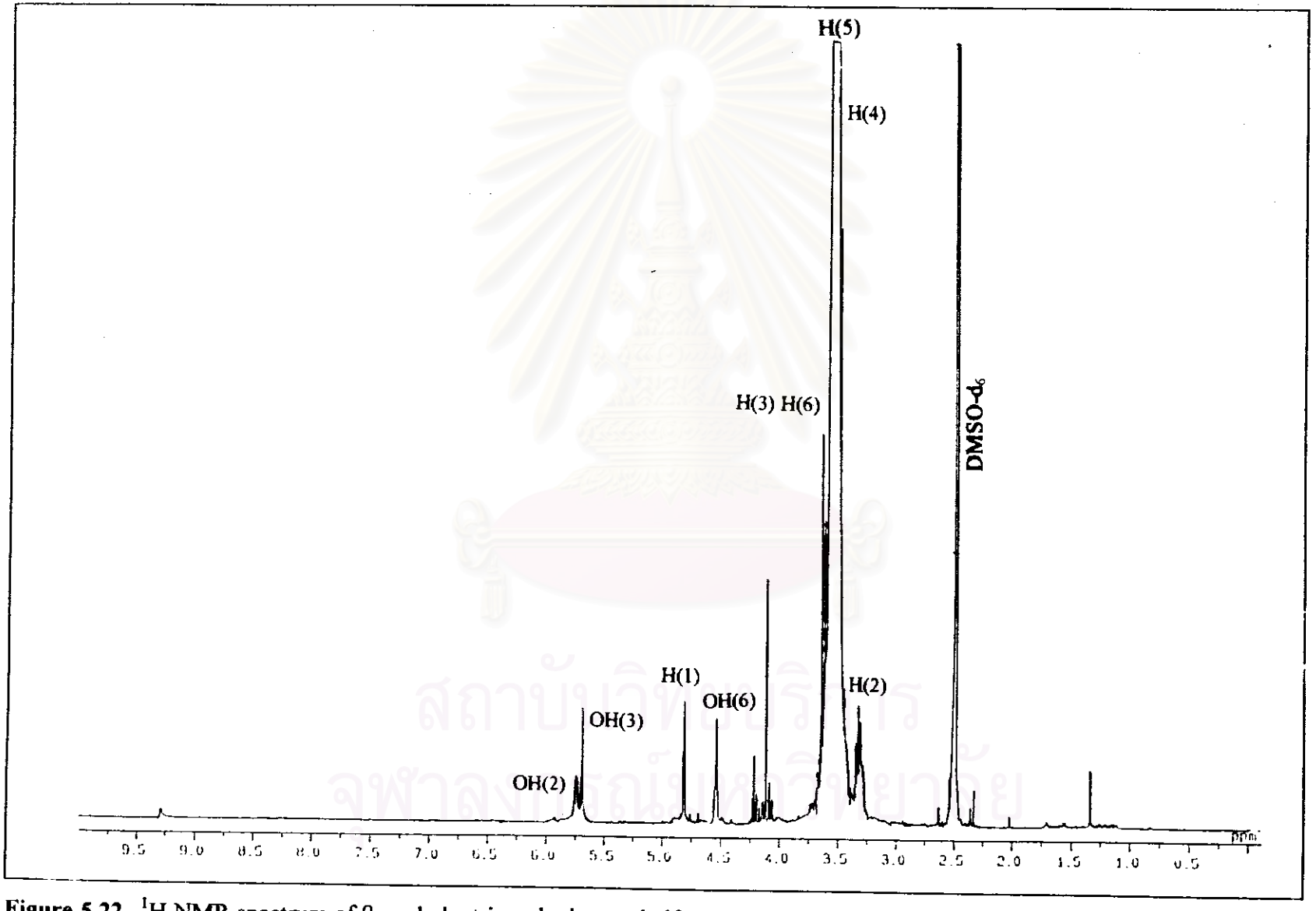


**Figure 5.22** $^{1}$H NMR spectrum of β-cyclodextrin-α-hydroxyethylferrocene inclusion compound

**Table 5.25** $^{1}H$ NMR data of β-cyclodextrin-α-hydroxyethylferrocene inclusion compound

| Chemical shift (ppm) | Multiplicity | Number of protons | Assignment | Coupling constant (Hz) |
|---|---|---|---|---|
| 5.74 | broad | 7H | OH(2) | |
| 5.69 | doublet | 7H | OH(3) | J = 1.5 |
| 4.81 | doublet | 7H | H(1) | J = 3.5 |
| 4.55 | singlet | 1H | CH | |
| 4.53 | triplet | 7H | OH(6) | J = 5.5 |
| 4.23-4.13 | multiplet | 2H | αH-$C_5H_4$ | |
| 4.11 | singlet | 5H | $C_5H_5$ | |
| 4.08-4.04 | multiplet | 2H | βH-$C_5H_4$ | |
| 3.64 | multiplet | 21H | H(3), H(6) | |
| 3.53 | multiplet | 7H | H(5) | |
| 3.48 | multiplet | 7H | H(4) | |
| 3.32 | multiplet | 7H | H(2) | |
| 2.30 | singlet | 1H | OH | |
| 1.30 | doublet | 3H | $CH_3$ | J = 2.0 |

## 5.6 Characterization of β-Cyclodextrin by FTIR Technique

Cyclodextrin has many hydroxyl groups, the FTIR spectrum in Figure 5.23 show strong broad peak of OH stretching and other vibrations. The data are shown in Table 5.26

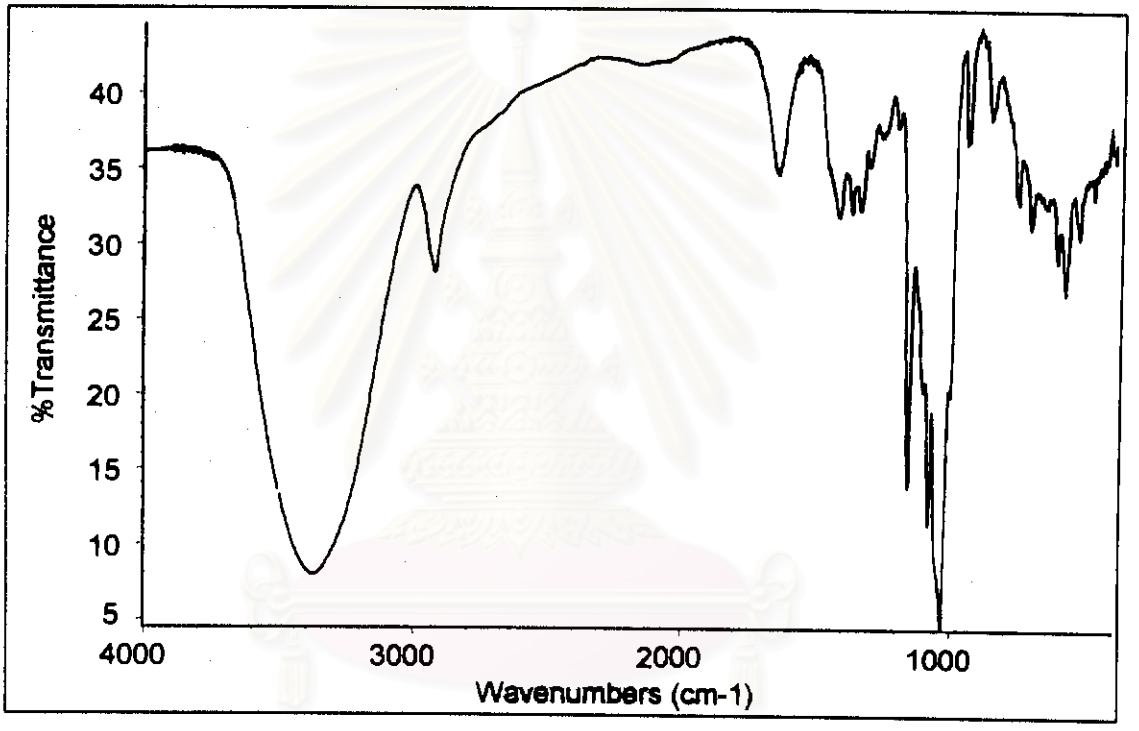


**Figure 5.23** FTIR spectrum of β-cyclodextrin

**Table 5.26** FTIR data of β-cyclodextrin

| Wavenumber ($cm^{-1}$) | Assignment |
|---|---|
| 3375 | –OH stretching |
| 2923 | –CH stretching |
| 1637 | –OH bending |
| 1415, 1367, 1335 | $-CH_2$ |
| 1157, 1081, 1031 | C–O stretching |

## 5.7 Characterization of Inclusion Compounds by FTIR Technique

Inclusion compounds of ferrocenyl derivatives with β-cyclodextrin were characterized by FTIR to study the vibrational variation of functional groups. The data of the complexes and inclusion compounds were shown in Tables 5.27 to 5.36.

When inclusion compound was formed, $CH_2$ group of cyclodextrin show vibrational frequency change. In addition, some characteristic peaks from guest appeared in the FTIR spectrum. FTIR spectrum of ferrocenyl derivatives and its inclusions were shown in Figures 5.24-5.43.

**Table 5.27** FTIR data of β-cyclodextrin-*N*, *N*-dimethylaminomethylferrocene inclusion compound

| Wavenumber ($cm^{-1}$) | Assignment |
|---|---|
| 3358 | –OH stretching |
| 2923 | –CH stretching(CD) |
| 2895 | –CH stretching |
| 1637 | –OH bending |
| 1451 | $-CH_2$ |
| 1419, 1370, 1333 | $-CH_2$ (CD) |
| 1157, 1081, 1031 | C–O stretching |

**Table 5.28** FTIR data of β-cyclodextrin-*N*, *N*-dimethylaminomethylferrocene methiodide inclusion compound

| Wavenumber ($cm^{-1}$) | Assignment |
|---|---|
| 3388 | –OH stretching |
| 2928 | –CH stretching(CD) |
| 2900 | –CH stretching |
| 1637 | –OH bending |
| 1482 | $-CH_2$ |
| 1414, 1368, 1333 | $-CH_2$(CD) |
| 1386 | $-CH_3$ |
| 1157, 1081, 1031 | C–O stretching |

**Table 5.29** FTIR data of β-cyclodextrin-α-methylferrocenylmethylamine inclusion compound

| Wavenumber ($cm^{-1}$) | Assignment |
|---|---|
| 3375 | –OH stretching |
| 2923 | –CH stretching(CD) |
| 2898 | –CH stretching |
| 1637 | –OH bending |
| 1488 | –NH bending |
| 1473 | $-CH_2$ |
| 1413, 1368, 1333 | $-CH_2$(CD) |
| 1381 | $-CH_3$ |
| 1157, 1081, 1031 | C–O stretching |

**Table 5.30** FTIR data of β-cyclodextrin-ferrocenylethylamine inclusion compound

| Wavenumber ($cm^{-1}$) | Assignment |
|---|---|
| 3375 | –OH stretching |
| 2923 | –CH stretching(CD) |
| 2894 | –CH stretching |
| 1637 | –OH bending |
| 1544 | –NH bending |
| 1460 | $–CH_2$ |
| 1413, 1370,1337 | $–CH_2$ (CD) |
| 1157, 1081, 1031 | C–O stretching |

**Table 5.31** FTIR data of β-cyclodextrin-Schiff base derivative inclusion compound

| Wavenumber ($cm^{-1}$) | Assignment |
|---|---|
| 3390 | –OH stretching |
| 2923 | –CH stretching (CD) |
| 2892 | –CH stretching |
| 1685 | C=C stretching |
| 1657 | C=N stretching |
| 1637 | –OH bending |
| 1457 | $–CH_2$ |
| 1412, 1371, 1333 | $–CH_2$ (CD) |
| 1157, 1086, 1031 | C–O stretching |

**Table 5.32** FTIR data of β-cyclodextrin-reduced Schiff base derivative inclusion compound

| Wavenumber ($cm^{-1}$) | Assignment |
|---|---|
| 3375 | –OH stretching |
| 2923 | –CH stretching (CD) |
| 2895 | –CH stretching |
| 1637 | –OH bending |
| 1546 | –NH bending |
| 1488 | $-CH_2$ |
| 1414, 1370, 1332 | $-CH_2$ (CD) |
| 1157, 1081, 1031 | C–O stretching |

**Table 5.33** FTIR data of β-cyclodextrin-acetylferrocene inclusion compound

| Wavenumber ($cm^{-1}$) | Assignment |
|---|---|
| 3356 | –OH stretching |
| 2923 | –CH stretching (CD) |
| 2895 | –CH stretching |
| 1672 | C=O stretching |
| 1655 | C=C stretching |
| 1637 | –OH bending |
| 1413, 1371, 1332 | $-CH_2$ (CD) |
| 1382, 1275 | $-CH_3$ |
| 1157, 1081, 1031 | C–O stretching |

**Table 5.34** FTIR data of β-cyclodextrin-ferrocenylaldehyde inclusion compound

| Wavenumber ($cm^{-1}$) | Assignment |
|---|---|
| 3375 | –OH stretching |
| 2923 | –CH stretching(CD) |
| 2900 | –CH stretching(CD) |
| 1683 | C=O stretching |
| 1659 | C=C stretching |
| 1637 | –OH bending |
| 1414, 1372, 1333 | $-CH_2$ (CD) |
| 1157, 1081, 1031 | C–O stretching |

**Table 5.35** FTIR data of β-cyclodextrin-ferrocenylmethylalcohol inclusion compound

| Wavenumber ($cm^{-1}$) | Assignment |
|---|---|
| 3365 | –OH stretching |
| 2925 | –CH stretching(CD) |
| 2896 | –CH stretching |
| 1637 | –OH bending |
| 1462 | $-CH_2$ |
| 1414, 1374, 1332 | $-CH_2$(CD) |
| 1157, 1081, 1031 | C–O stretching |

**Table 5.36** FTIR data of β-cyclodextrin-α-hydroxyethylferrocene inclusion compound

| Wavenumber ($cm^{-1}$) | Assignment |
|---|---|
| 3375 | –OH stretching |
| 2929 | –CH stretching(CD) |
| 2899 | –CH stretching |
| 1644 | –OH bending |
| 1419, 1367, 1337 | $-CH_2$(CD) |
| 1157, 1086, 1031 | C–O stretching |

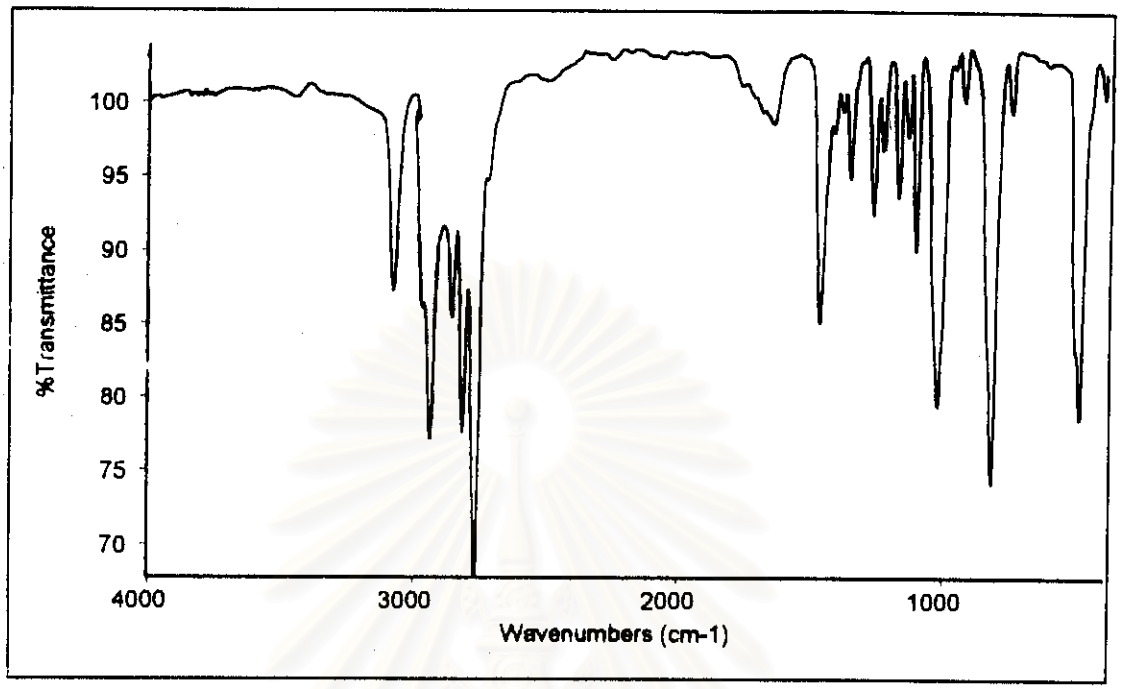


**Figure 5.24** FTIR spectrum of *N, N*-dimethylaminomethylferrocene

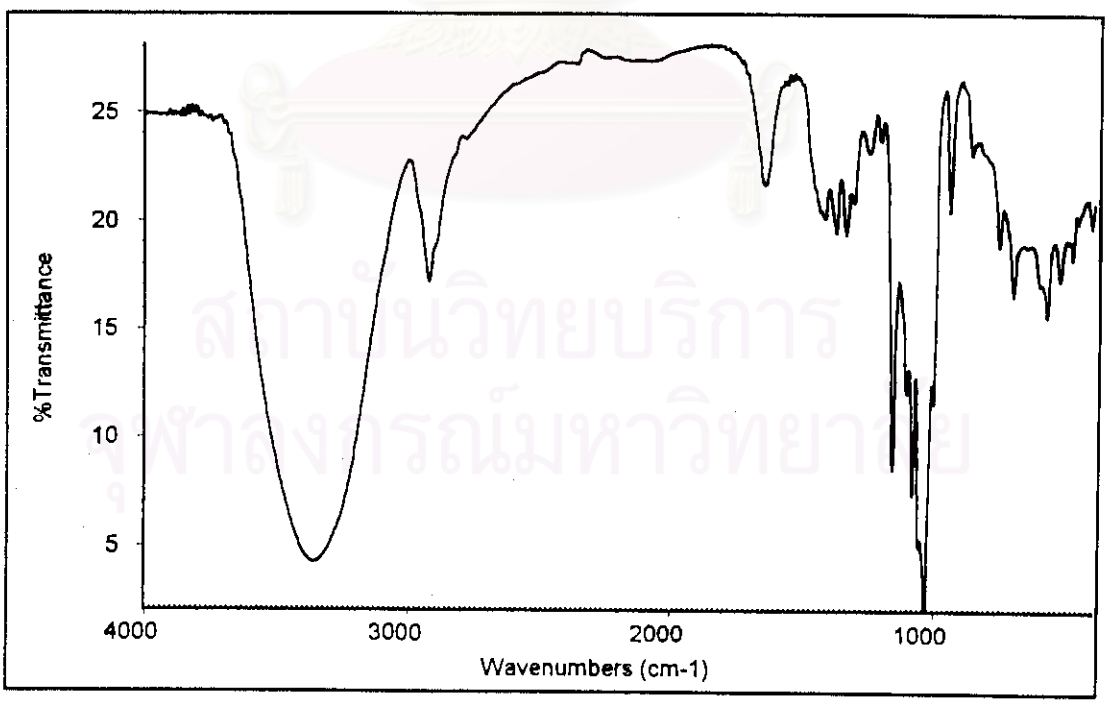


**Figure 5.25** FTIR spectrum of β-cyclodextrin-*N, N*–dimethylaminomethylferrocene Inclusion compound

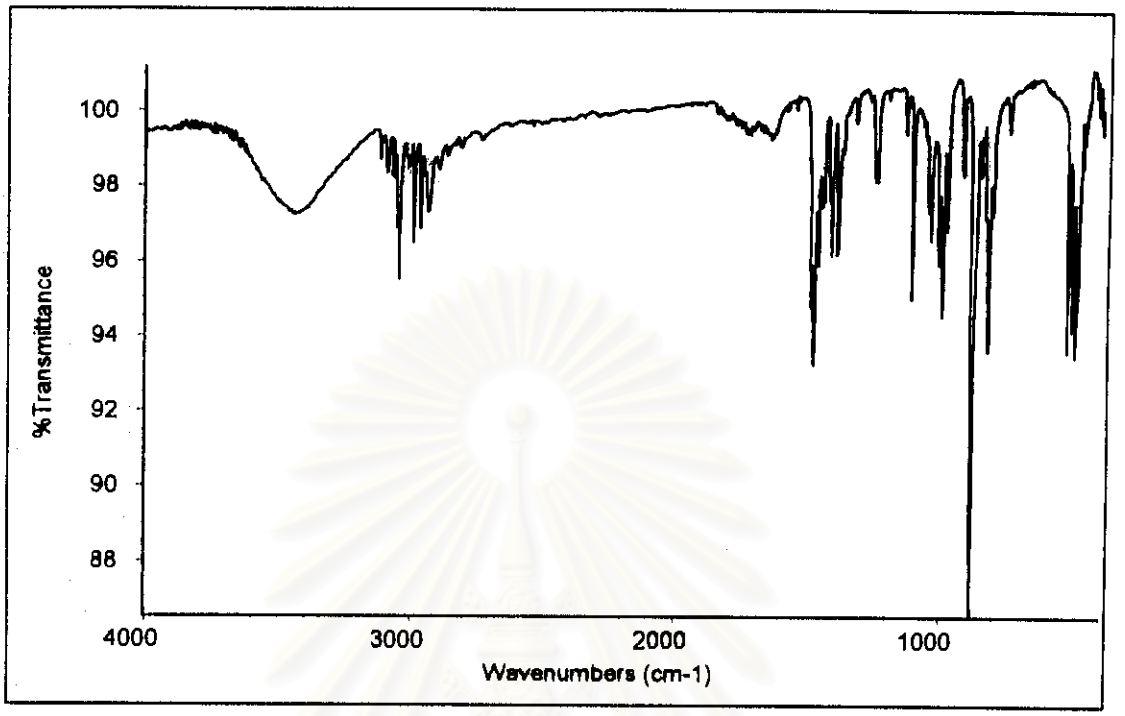


**Figure 5.26** FTIR spectrum of *N, N*- dimethylaminomethylferrocene methiodide

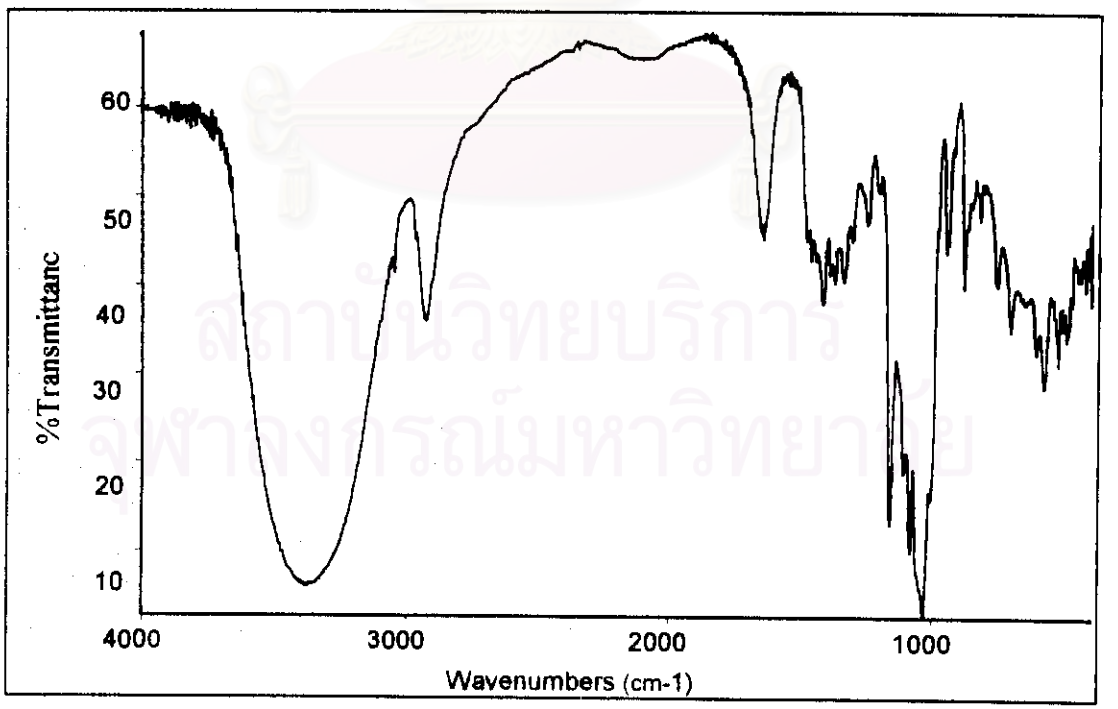


**Figure 5.27** FTIR spectrum of β-cyclodextrin-*N, N*-dimethylaminomethylferrocene methiodide inclusion compound

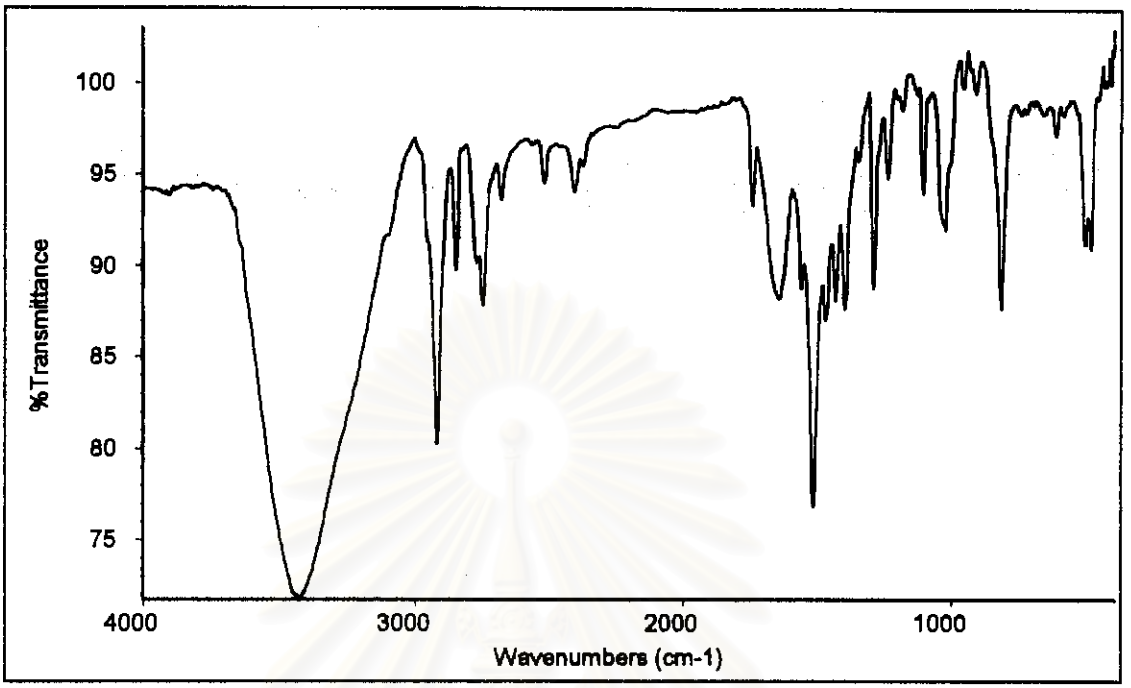


**Figure 5.28** FTIR spectrum of α-methylferrocenylmethylamine

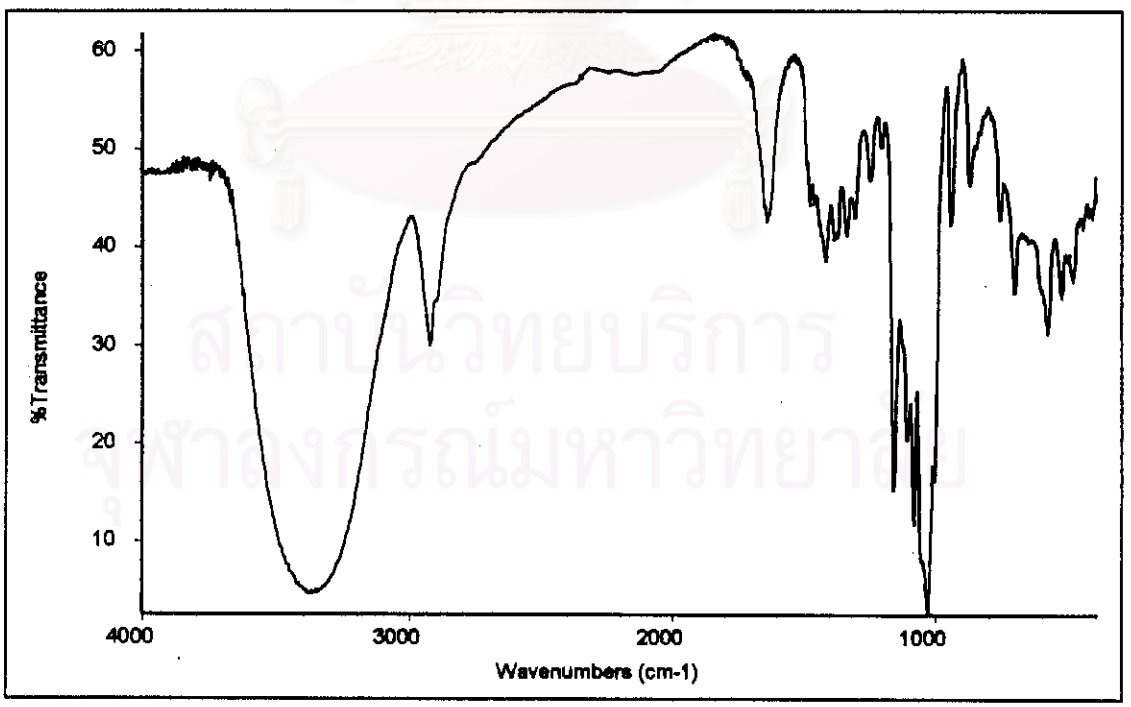


**Figure 5.29** FTIR spectrum of β-cyclodextrin-α-methylferrocenylmethylamine inclusion compound

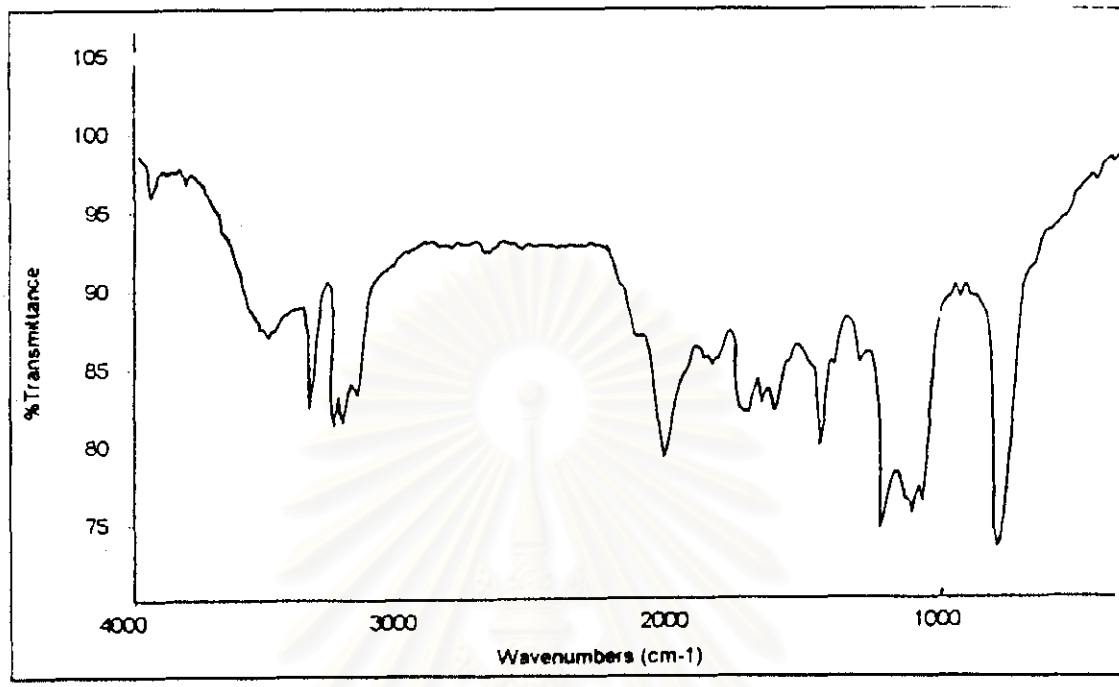


**Figure 5.30** FTIR spectrum of ferrocenylethylamine

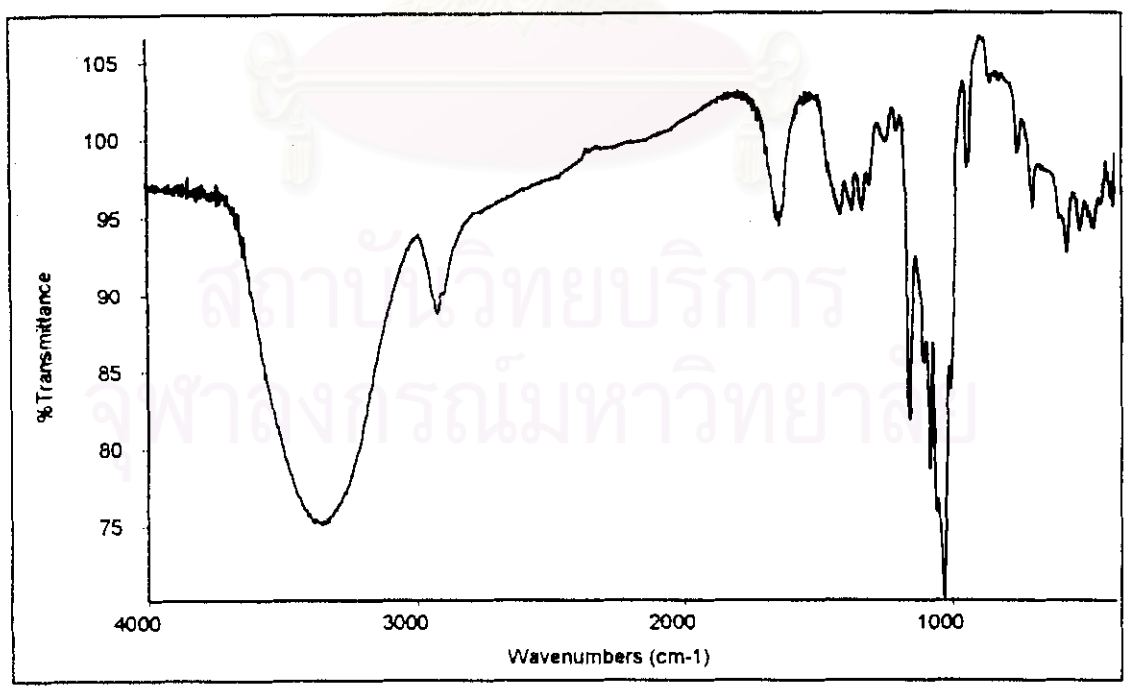


**Figure 5.31** FTIR spectrum of β-cyclodextrin-ferrocenylethylamine inclusion compound

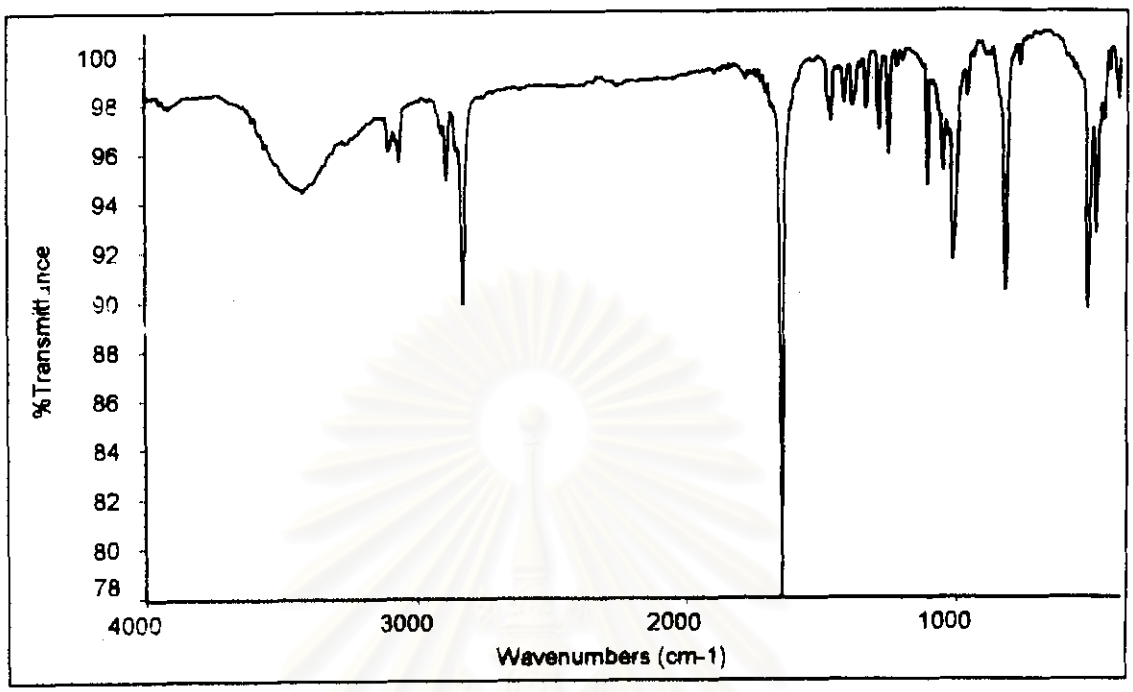


**Figure 5.32** FTIR spectrum of Schiff base derivative

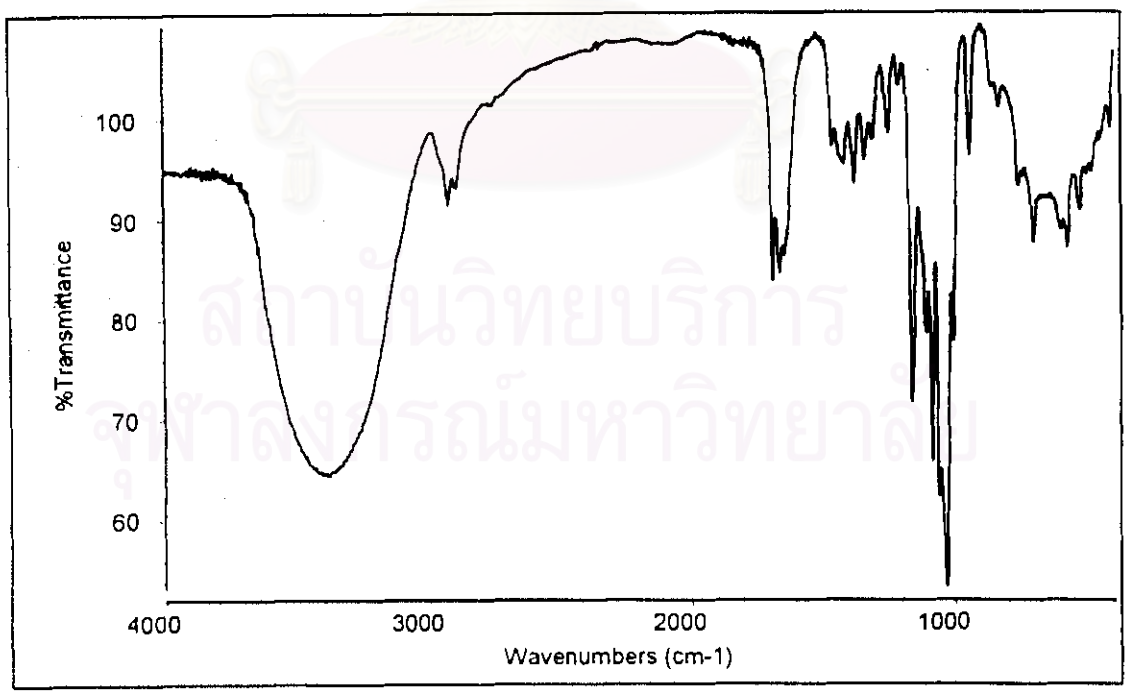


**Figure 5.33** FTIR spectrum of β-cyclodextrin-Schiff base derivative inclusion compound

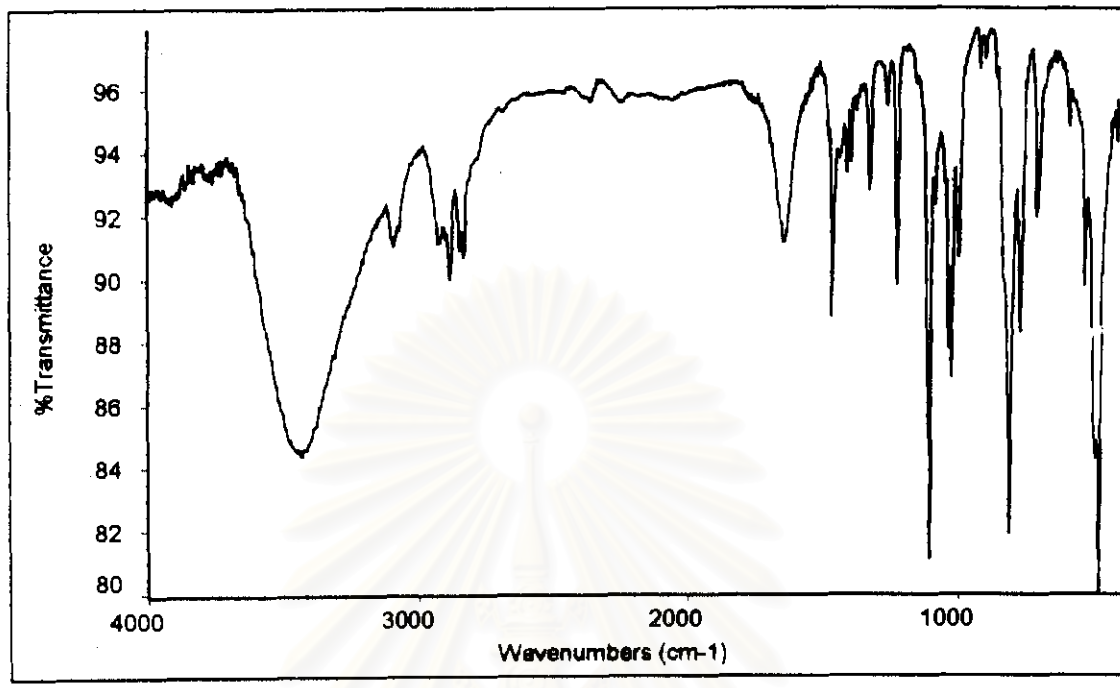


**Figure 5.34** FTIR spectrum of reduced Schiff base derivative

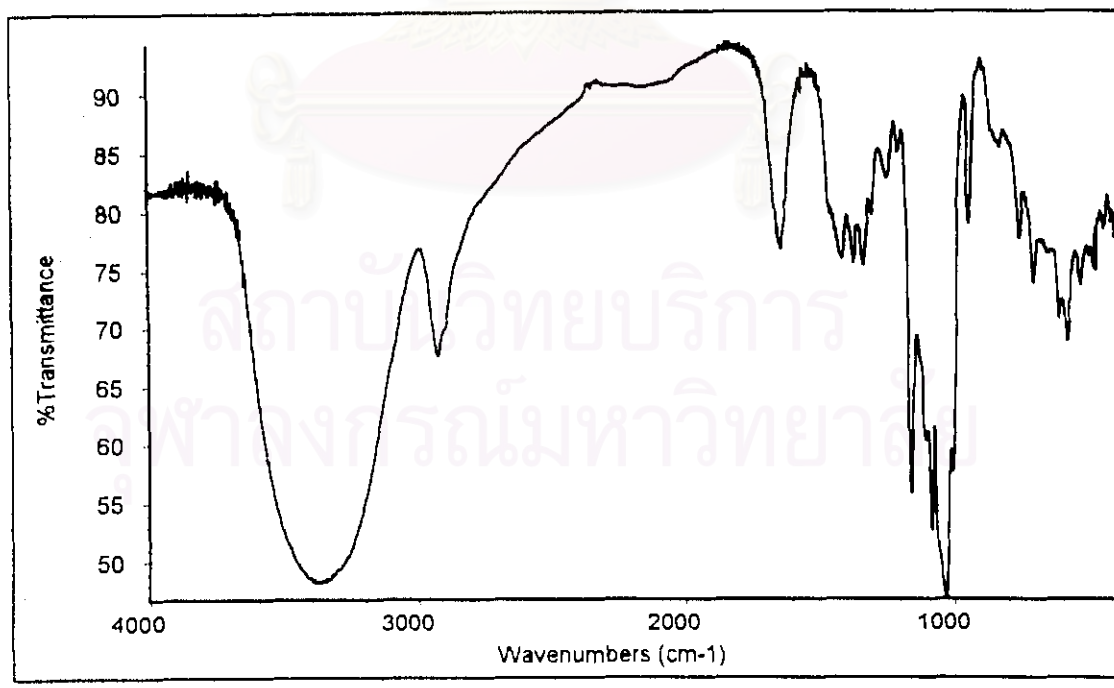


**Figure 5.35** FTIR spectrum of β-cyclodextrin-reduced Schiff base derivative

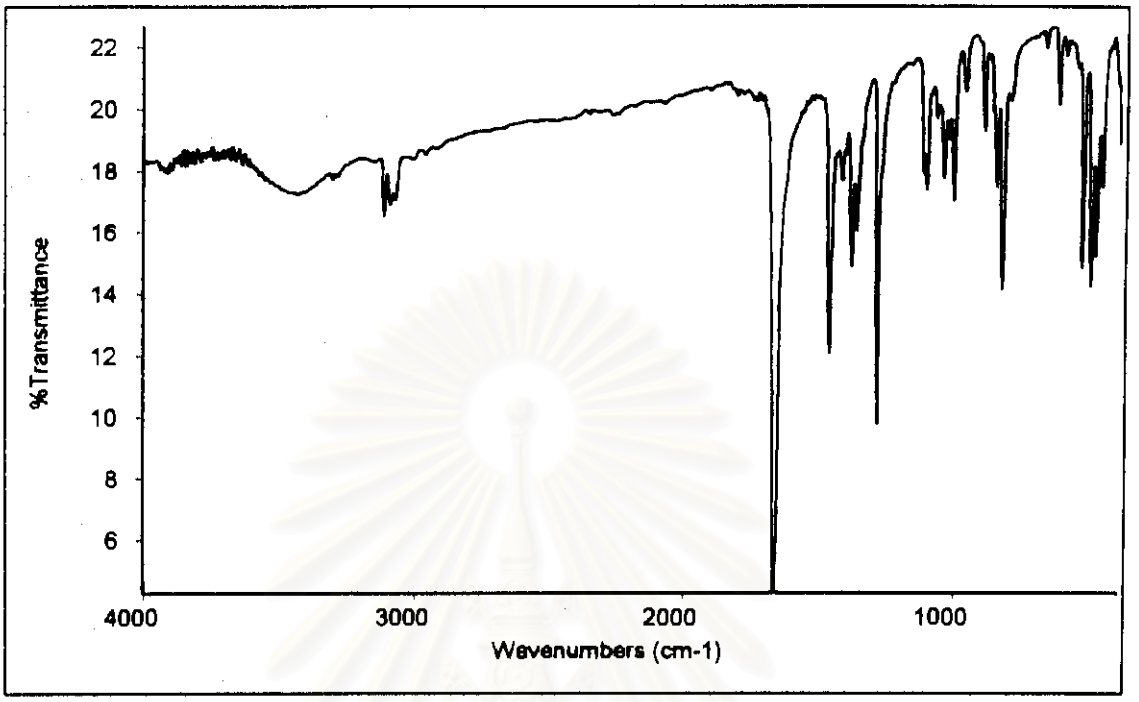


**Figure 5.36** FTIR spectrum of acetylferrocene

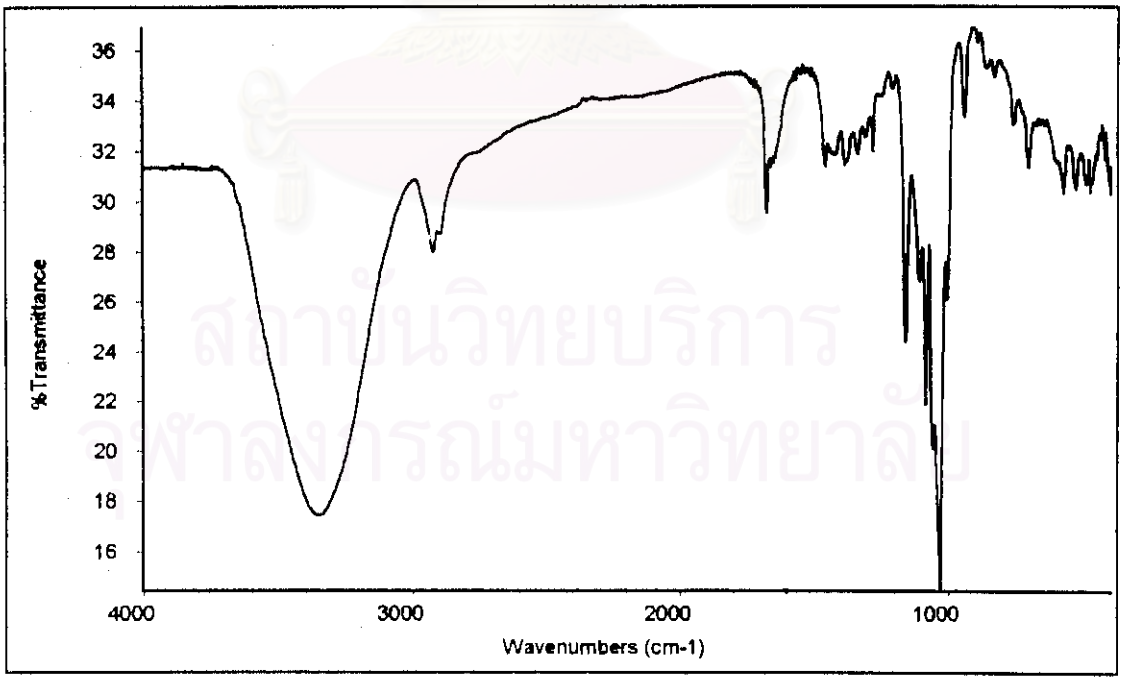


**Figure 5.37** FTIR spectrum of β-cyclodextrin-acetylferrocene inclusion compound

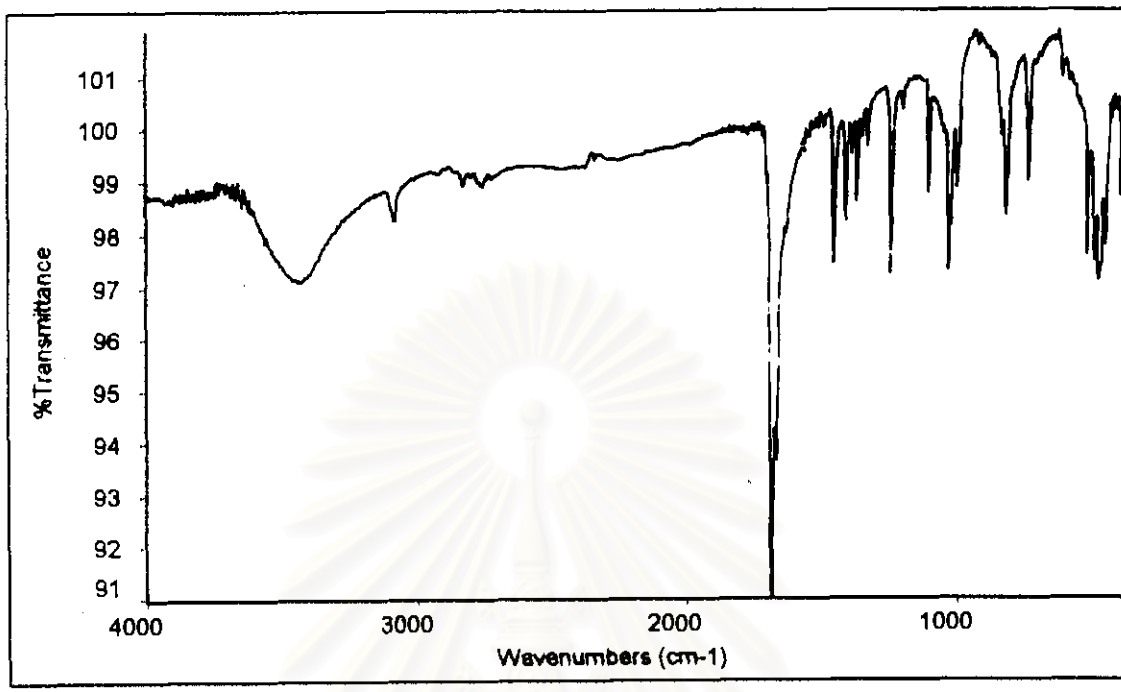


**Figure 5.38** FTIR spectrum of ferrocenylaldehyde

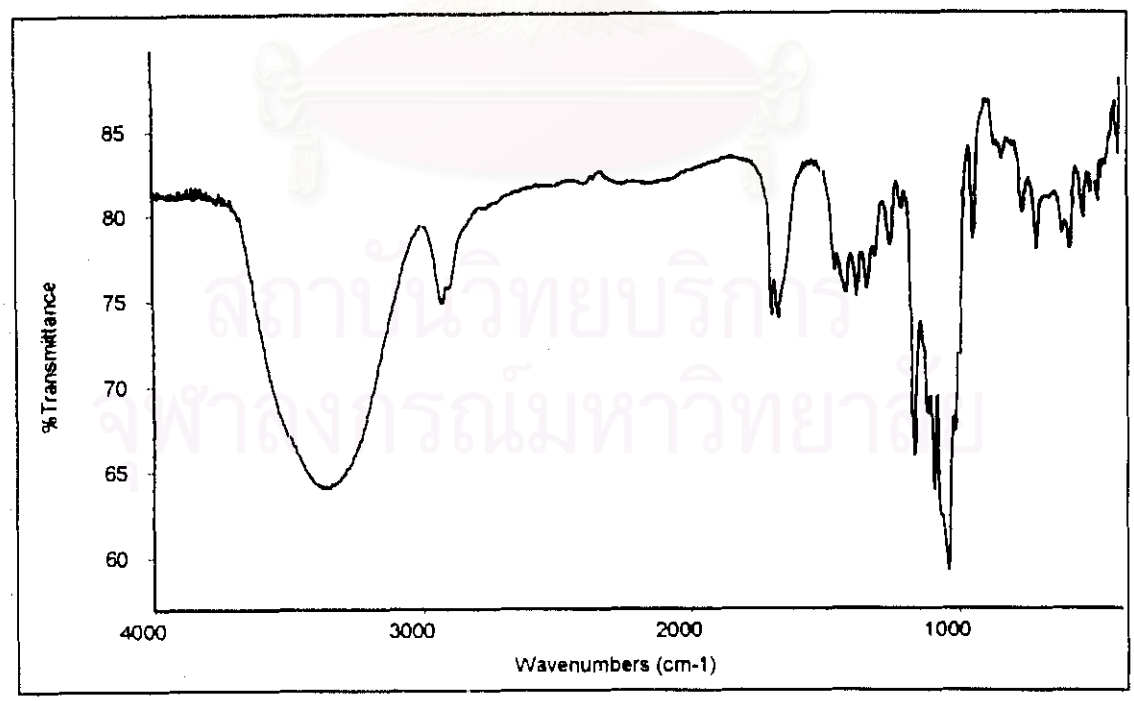


**Figure 5.39** FTIR spectrum of β-cyclodextrin-ferrocenylaldehyde inclusion compound

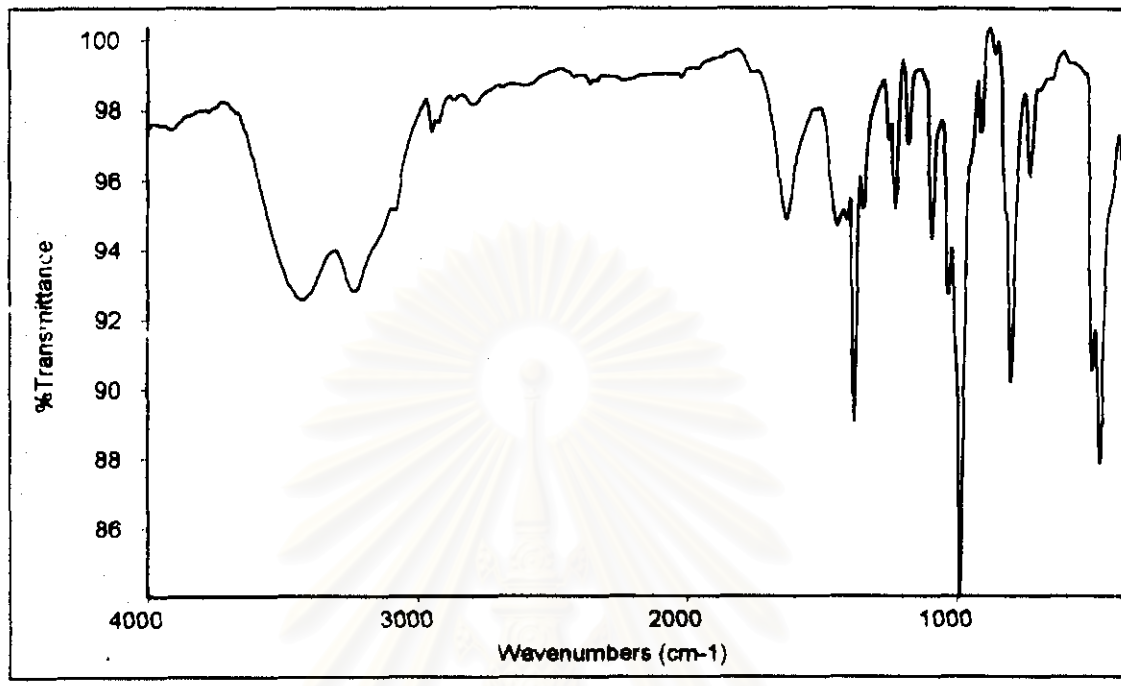


**Figure 5.40** FTIR spectrum of ferrocenylmethylalcohol

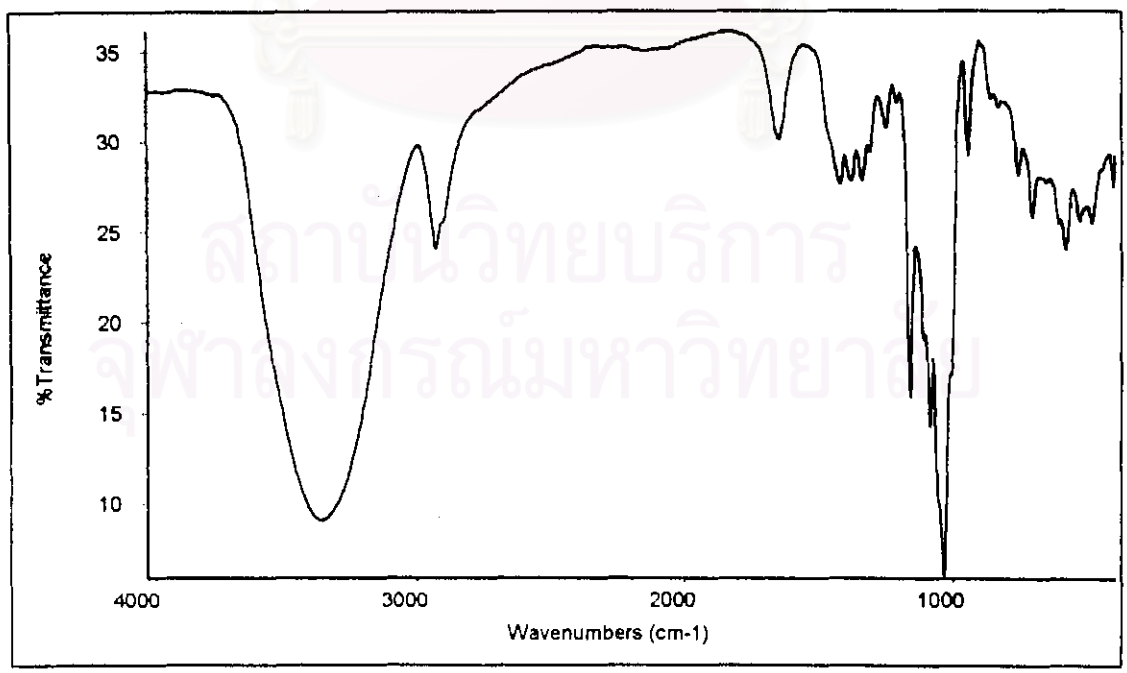


**Figure 5.41** FTIR spectrum of β-cyclodextrin-ferrocenylmethylalcohol inclusion compound

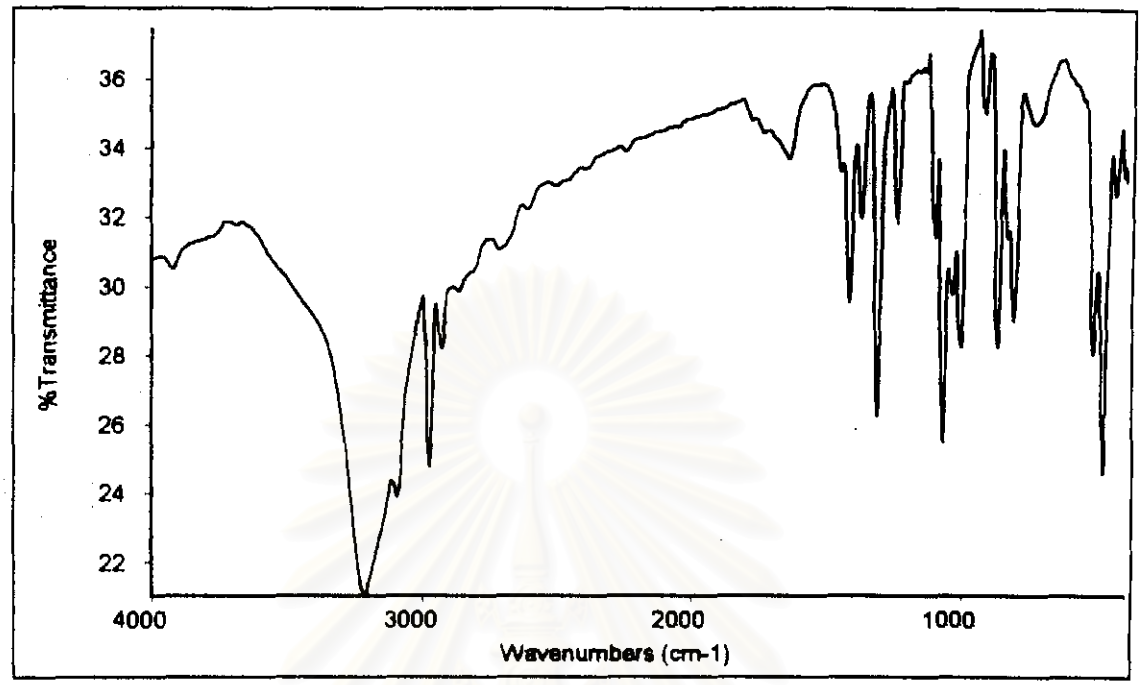


**Figure 5.42** FTIR spectrum of α-hydroxyethylferrocene

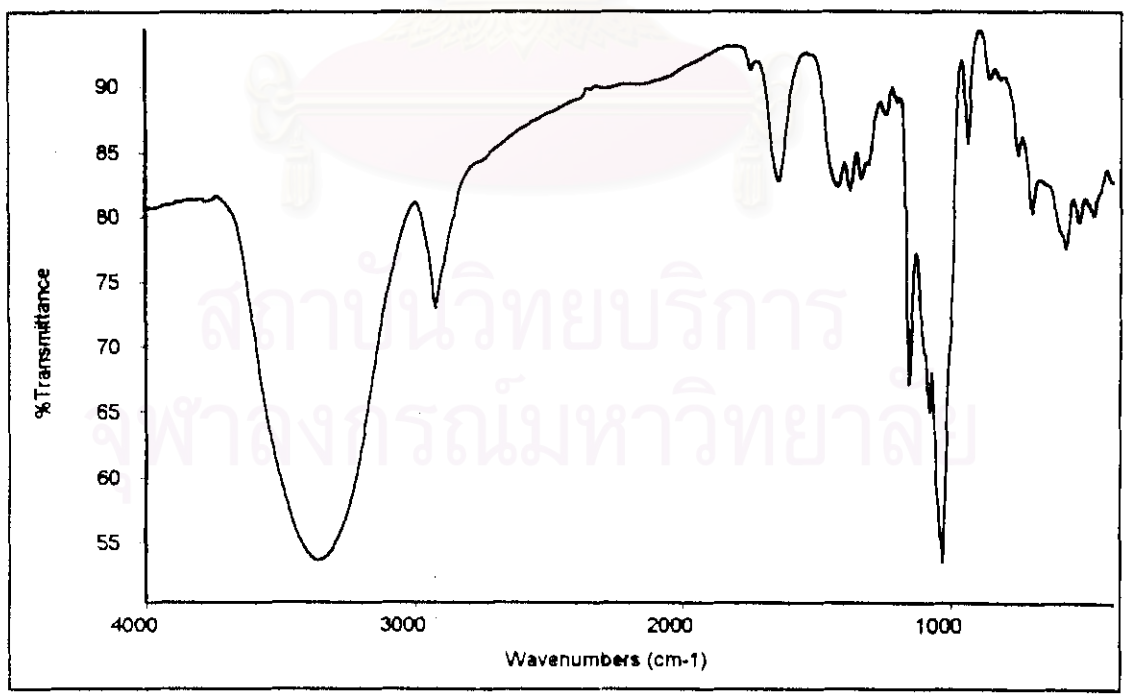


**Figure 5.43** FTIR spectrum of β-cyclodextrin-α-hydroxyethylferrocene inclusion compound

## 5.8 Characterization of Inclusion Compounds by X-Ray Powder Diffraction

In order to confirm the inclusion phenomenon, X-ray powder diffraction technique was used. A comparison of the diffractrograms of the mixture (guest + cyclodextrin) with inclusion compound was made. The diffractrograms are different.

For example, a mixture of *N, N*-dimethylaminomethylferrocene methiodide and β-cyclodextrin showed a diffraction pattern which is the superposition of patterns from guest and host. On the contrary, diffractrogram of the inclusion compound showed new peaks and there were some peaks disappeared as shown in Figure 5.44

X-ray diffraction patterns of other ferrocenylamines were shown in Figures 45-47

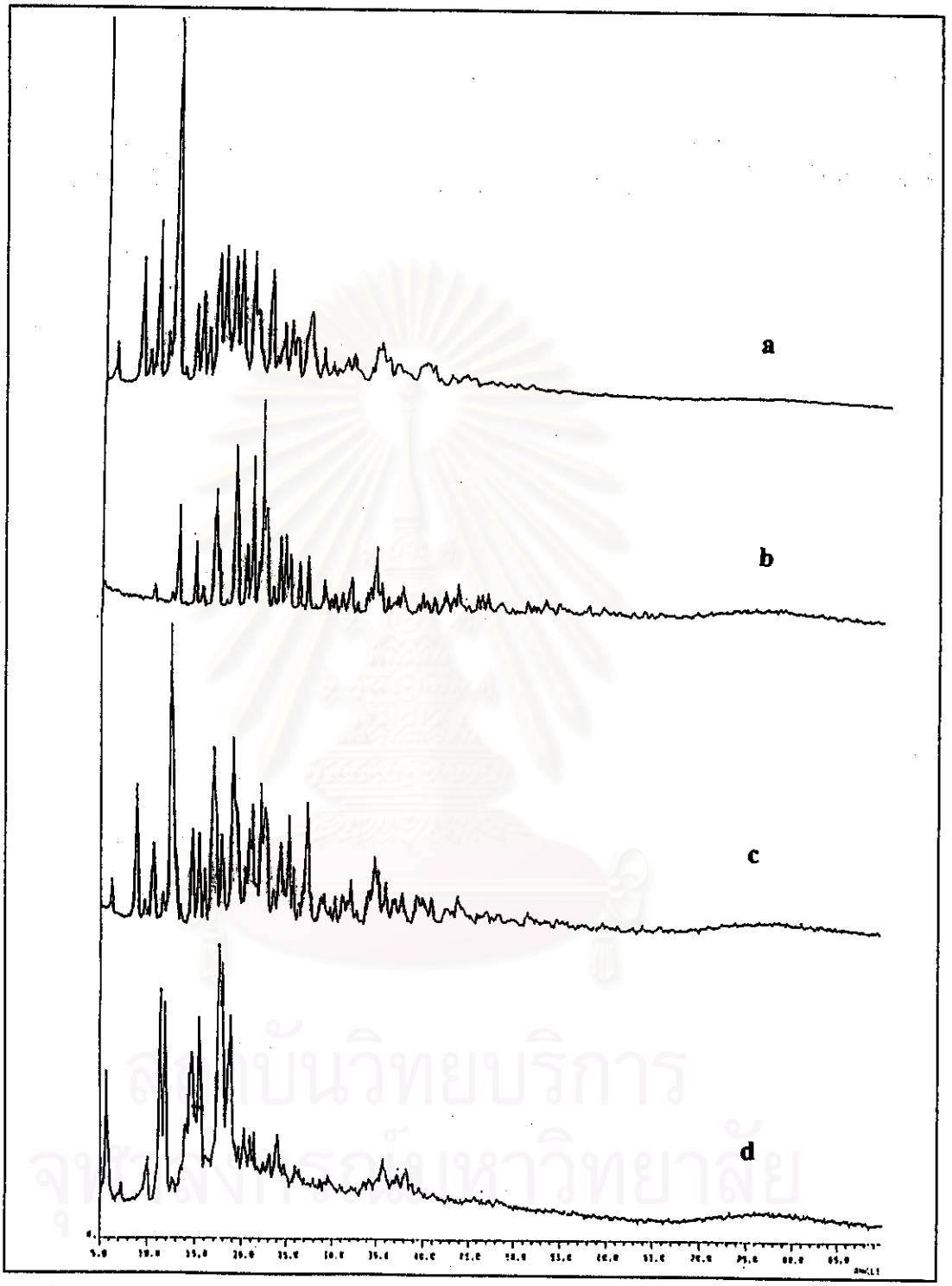


**Figure 5.44** X-ray diffraction patterns of

a) β-cyclodextrin

b) *N, N*-dimehylaminomethylferrocene methiodide

c) mixture

d) inclusion compound

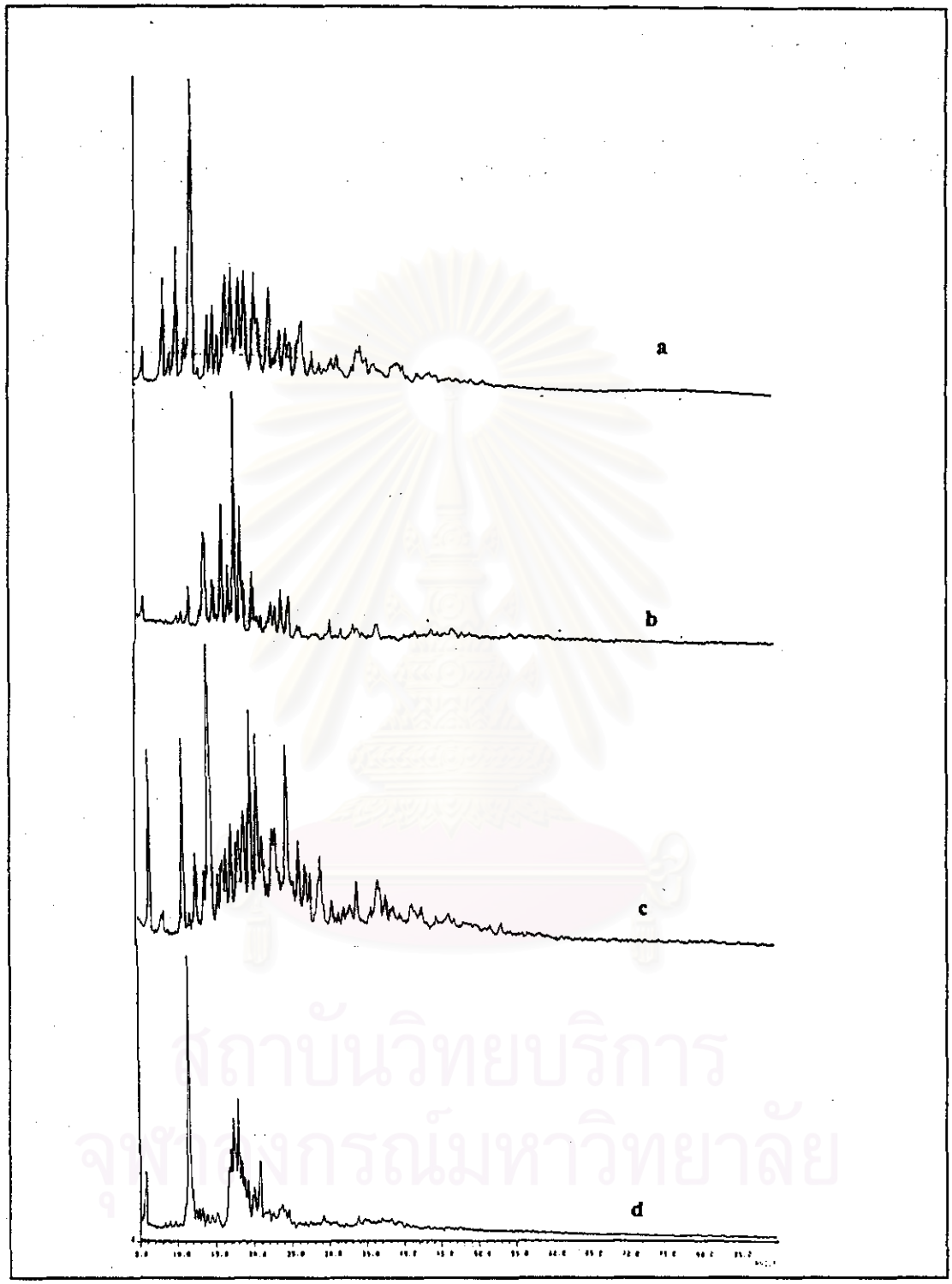


**Figure 5.45** X-ray diffraction patterns of

a) β-cyclodextrin

b) α-methylferrocenylmethylamine

c) mixture

d) inclusion compound

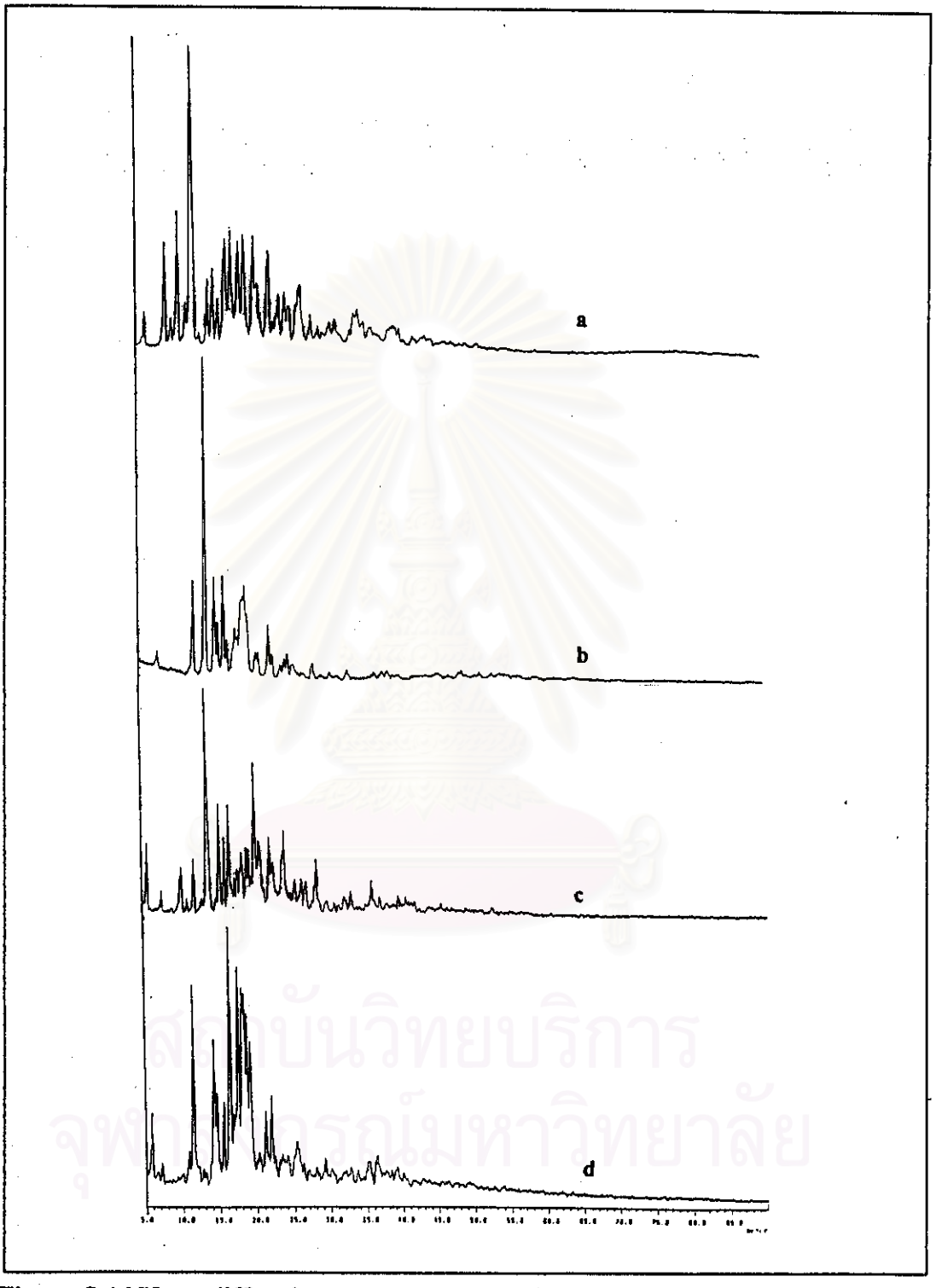


**Figure 5.46** X-ray diffraction patterns of

a) β-cyclodextrin

b) Shiff base derivative

c) mixture

d) inclusion compound

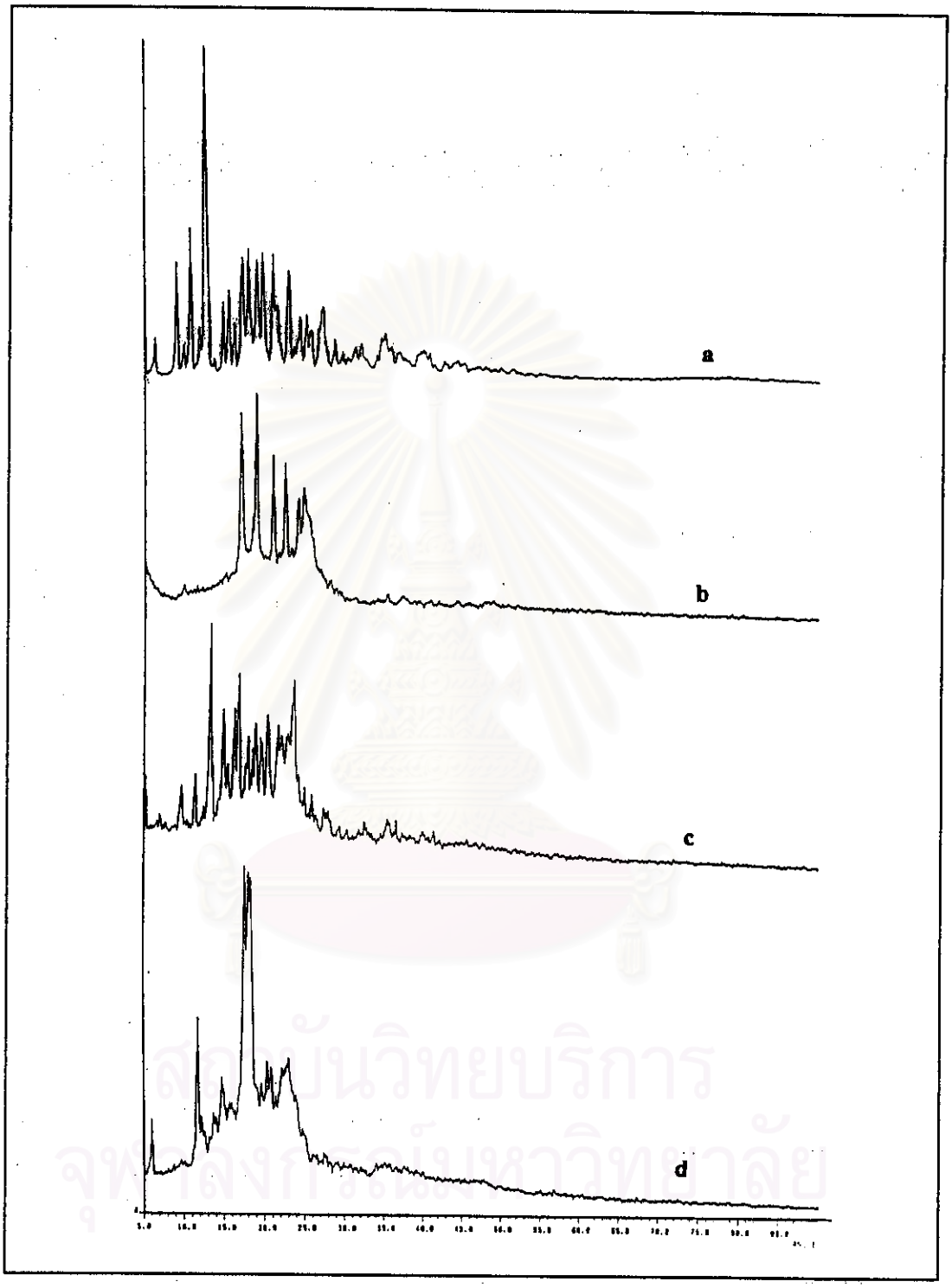


**Figure 5.47** X-ray diffraction patterns of

a) β-cyclodextrin

b) reduced Shiff base derivative

c) mixture

d) inclusion compound

## 5.9 Ultraviolet -Visible Absorption Spectroscopy

Ferrocene can absorb visible light at 443 nm, resultings from electron transition of d orbital ($n \rightarrow \pi^*$). Ferrocene derivatives absorb UV-visible light at different wavelength. To record the absorption spectrum, the dimethyl sulfoxide solution at concentration of $10^{-3}$ M (ferrocenyl derivative or inclusion compound) was prepared.

From the spectra in Appendix B (Figures 1b to 9b), most of inclusion compounds absorb visible light at the same wavelength as that of their ferrocenyl derivatives (ferrocenylamine, ferrocenylalcohol, acylferrocene) but the molar absorptivity is different. The molar absorptivity decreased (hypochromic shift) in the inclusion compound,[21] except the inclusion compound of Schiff base derivative, which showed hyperchromic shift.

## 5.10 Alkylation of Benzaldehyde with Diethylzinc

The addition of diethylzinc to aldehyde can be accelerated by a wide range of catalysts affording asymmetric secondary alcohol. Benzaldehyde has been most extensively studied. Some common factors such as the choice of solvent, reaction temperature, mole ratio etc. were examined.

In this work some β-cyclodextrin-ferrocenyl derivatives were used as catalysts. Percent yield of alkylation product and the effect of the catalyst structure upon enantioselectivity of product were studied. The chiral product of the ethylation of benzaldehyde was 1-phenyl-1-propanol as shown in Scheme 5.9.

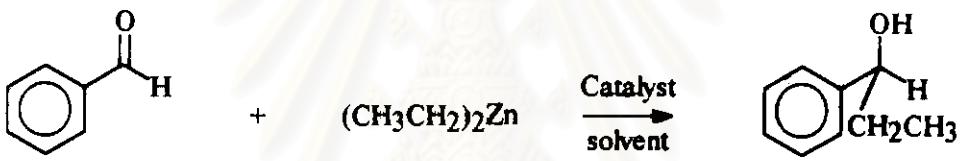


**Scheme 5.9** Ethylation of benzaldehyde

Percent yield was determined by gas chromatography. Chromatogram (Figure 5.48) showed retention time of 1-phenyl-1-propanol at 3.74 min. The occurrence of benzyl alcohol[44] at 2.58 might be from the reaction proposed in Scheme 5.10

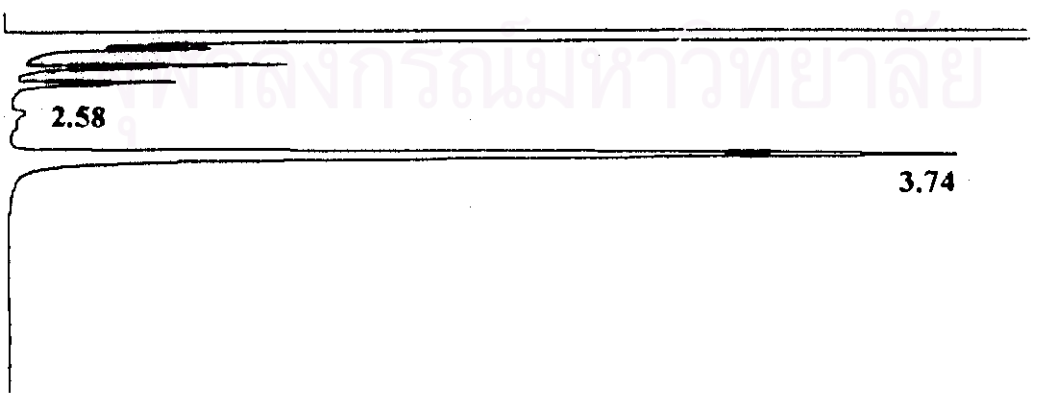


**Figure 5.48** Chromatogram of product from ethylation

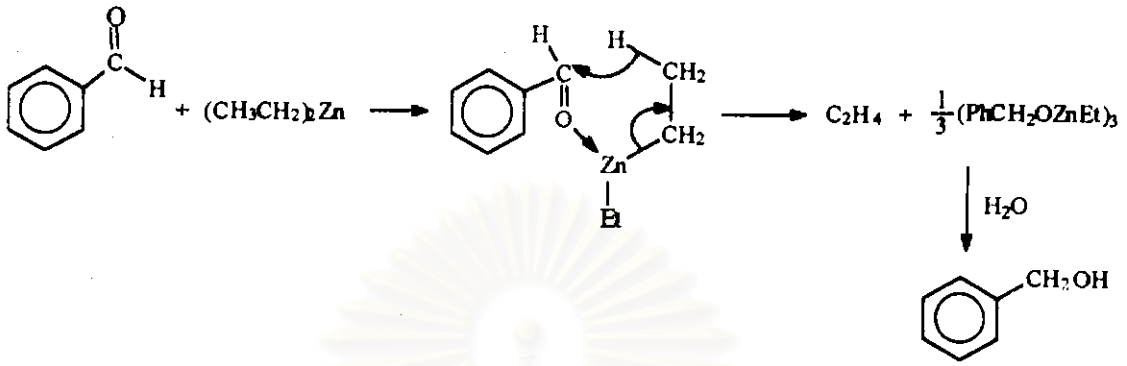

**Scheme 5.10** Benzyl alcohol formation

Since diethylzinc is very sensitive to moisture and oxygen, the alkylation reaction of benzaldehyde needs to be done in inert atmosphere. In the presence of oxygen at room temperature, soluble peroxide $CH_3CH_2ZnOOCH_2CH_3$ (hydrolyzed to $CH_3CH_3$ + $CH_3CH_2$-O-OH) was first formed but after a few minutes there is a white precipitate of insoluble $CH_3CH_2$-O-Zn-$OCH_2CH_3$. If the absorption of oxygen is controlled so that the process takes several weeks, then insoluble solids are formed but these consist for the most part of zinc alkoxides $Zn(OCH_2CH_3)_2$ since they are hydrolysed mainly to $CH_3CH_2OH$ with the formation of little peroxide[45] as shown in Scheme 5.11

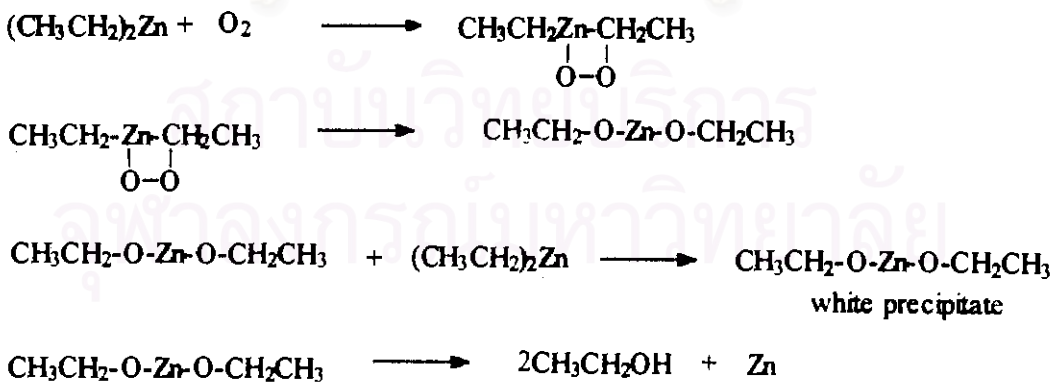

**Scheme 5.11** Reaction of diethylzinc with oxygen

## 5.11 Determination of % Yield

### 5.11.1 Alkylation Product Yield

The products of alkylation of benzaldehyde with diethylzinc were 1-phenyl-1-propanol and benzyl alcohol (by-product). Determination of % yield for each run was done duplicate, using internal standard. The measured data were corrected using correction factor.

### 5.11.2 Correction Factor

Correction factor was determined by gas chromatography. The gas chromatogram shown in Figure 5.49 displayed retention time at 3.82, 2.44 and 1.43 belonging to 1-phenyl-1-propanol, benzyl alcohol and cyclohexanol (internal standard) respectively.

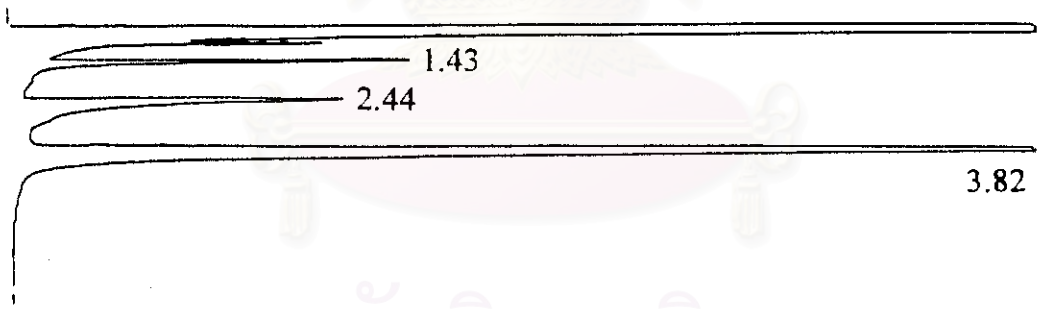


**Figure 5.49** Gas chromatogram of alkylation product and internal standard

| | Retention time | Peak area | Mmol (Calculated from amount prepared) |
|---|---|---|---|
| Cyclohexanol | 1.43 | 64797 | 0.0948 |
| 1-Phenyl-1-propanol | 3.82 | 568804 | 0.0729 |
| Benzyl alcohol | 2.44 | 141575 | 0.0193 |

From gas chromatogram, mole of 1-phenyl-1-propanol and benzyl alcohol can be calculated as following: 0.0948 mmol cyclohexanol (internal standard) possessed peak area 64799, therefore peak area 568804 of 1-phenyl-1-propanol corresponded to 0.0832 mmol and peak area 141575 of benzyl alcohol corresponded to 0.0207 mmol. The correction factor was calculated as shown below.

$$\text{Correction factor of 1-phenyl-1-propanol} = \frac{\text{Mole of 1-phenyl-1-propanol from GC}}{\text{Mole of 1-phenyl-1-propanol from preparation}}$$

$$= \frac{0.0729}{0.0832}$$

$$= 0.88$$

$$\text{Correction factor of benzyl alcohol} = \frac{\text{Mole of benzyl alcohol from GC}}{\text{Mole of benzyl alcohol from preparation}}$$

$$= \frac{0.0193}{0.0207}$$

$$= 0.93$$

Correction factor of 1-phenyl-1-propanol and benzyl alcohol was 0.88 and 0.93 respectively. % Yield of product (corrected) can be obtained by multiply % yield of product (from peak area) with correction factor.

## 5.12 Some Effects on % Yield of Alkylation Reaction

### 5.12.1 Mole Ratio of Benzaldehyde:Diethylzinc

The result shown in Table 5.37 demonstrated that the mole ratio of benzaldehyde to diethylzinc affected % yield. Without catalyst, hexane as solvent, 24 hr reaction time, 1:2 and 1:3 ratios gave similar yields, so 1:2 ratio was chosen for all reactions.

**Table 5.37** Effect of mole ratio of benzaldehyde to diethylzinc on % yield

| Mole ratio (Benzaldehyde : Diethylzinc) | % GC Yield |
|---|---|
| 1:1 | 28 |
| 1:2 | 34 |
| 1:3 | 35 |

Uncatalyzed reaction, 1-phenyl-1-propanol came from reaction between benzaldehyde and diethylzinc made from self catalytic reaction[12] as shown in Scheme 5.12.

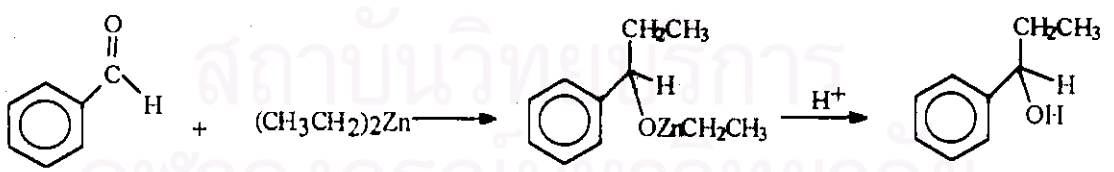


**Scheme 5.12** Self catalytic reaction of benzaldehyde to 1-phenyl-1-propanol

### 5.12.2 Solvent, Temperature and Time

Fc-$CH_2N(CH_3)_2$ and its inclusion were chosen to study the effect of solvent, temperature and time on alkylation.

**Effect of Solvent**

Ferrocenyl derivatives can dissolve in hexane and toluene while the inclusion compounds cannot. The results of alkylation at room temperature, 4 hr reaction time, as shown in Table 5.38 showed hexane was better solvent than toluene.

**Table 5.38** Effect of solvent on % yield

| Catalysts | % GC Yield | |
|---|---|---|
| | Hexane | Toluene |
| None | 24 | 13 |
| Fc-$CH_2$-$N(CH_3)_2$ | 42 | 36 |
| Fc-$CH_2$-$N(CH_3)_2$-CD | 18 | 15 |

**Effect of Temperature**

Table 5.39 shows the alkylation yield at 0 °C, room temperature (30 °C) and 60 °C, using hexane as solvent, 4 hr reaction time. From the result, it can be explained that high temperature increases yield. However, at high temperature, more formation of the reduction product, benzyl alcohol, was observed in Table 5.40, so room temperature was chosen for studying all alkylation reactions.

**Table 5.39** Effect of temperature on % yield

| Catalyst | % GC Yield | | |
|---|---|---|---|
| | 0 °C | RT | 60 °C |
| Fc-$CH_2N(CH_3)_2$ | 25 | 42 | 58 |
| Fc-$CH_2N(CH_3)_2$-CD | 10 | 15 | 38 |

**Table 5.40** Benzyl alcohol formation with temperature

| Catalyst | % Benzyl alcohol | | |
|---|---|---|---|
| | 0 °C | RT | 60 °C |
| Fc-$CH_2N(CH_3)_2$ | 1 | 1 | 10 |
| Fc-$CH_2N(CH_3)_2$-CD | 1 | 3 | 25 |

**Effect of Time**

Alkylation reaction was done at room temperature on various time, using 2 mol % of catalyst and hexane as solvent. The effect of time on % yield is shown in Table 5.41. The results indicated that % yield increased with time and reaction was completed after 24 hr.

**Table 5.41** Effect of time on % yield

| Catalyst | % GC Yield | | | | |
|---|---|---|---|---|---|
| | 4 hr | 10 hr | 24 hr | 36 hr | 72 hr |
| Fc-$CH_2N(CH_3)_2$ | 42 | 63 | 70 | 73 | 73 |
| Fc-$CH_2N(CH_3)_2$-CD | 15 | 24 | 30 | 32 | 33 |

### 5.12.3 Mol % of Catalyst

$Fc\text{-}CH_2N(CH_3)_2$, cyclodextrin and its inclusion were chosen to study effect of mol % of catalyst . The alkylation was done at room temperature, 24 hr reaction time. The results in Table 5.42 showed that 5 mol % of catalyst gave higher yield.

**Table 5.42** Effect of mol % of catalyst on % yield

| Catalyst | % GC Yield | | |
|---|---|---|---|
| | 2% | 5% | 10% |
| $Fc\text{-}CH_2\text{-}N(CH_3)_2$ | 70 | 85 | 30 |
| CD | 30 | 25 | 15 |
| $Fc\text{-}CH_2\text{-}N(CH_3)_2\text{-}CD$ | 30 | 41 | 21 |

In addition, % yield for each % mol of catalyst (2, 5 and 10 mol %) monitored with time was studied, the results are displayed with graph in Figures 5.50-5.52.

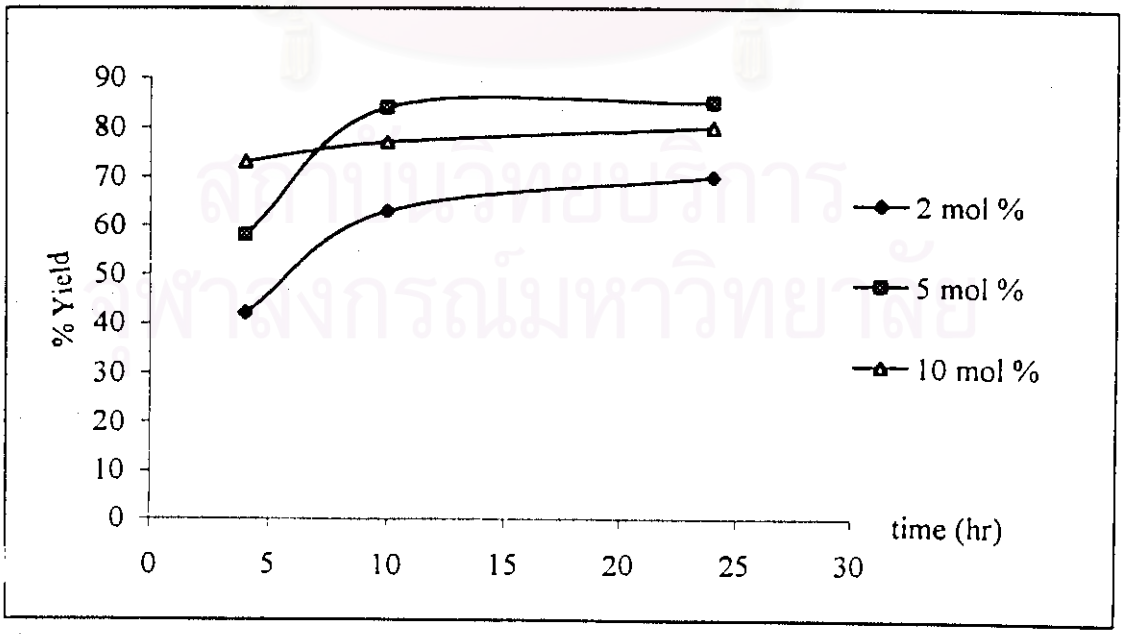


**Figure 5.50** Graph plotted between % yield and time of *N, N*-dimethylaminomethyl ferrocene

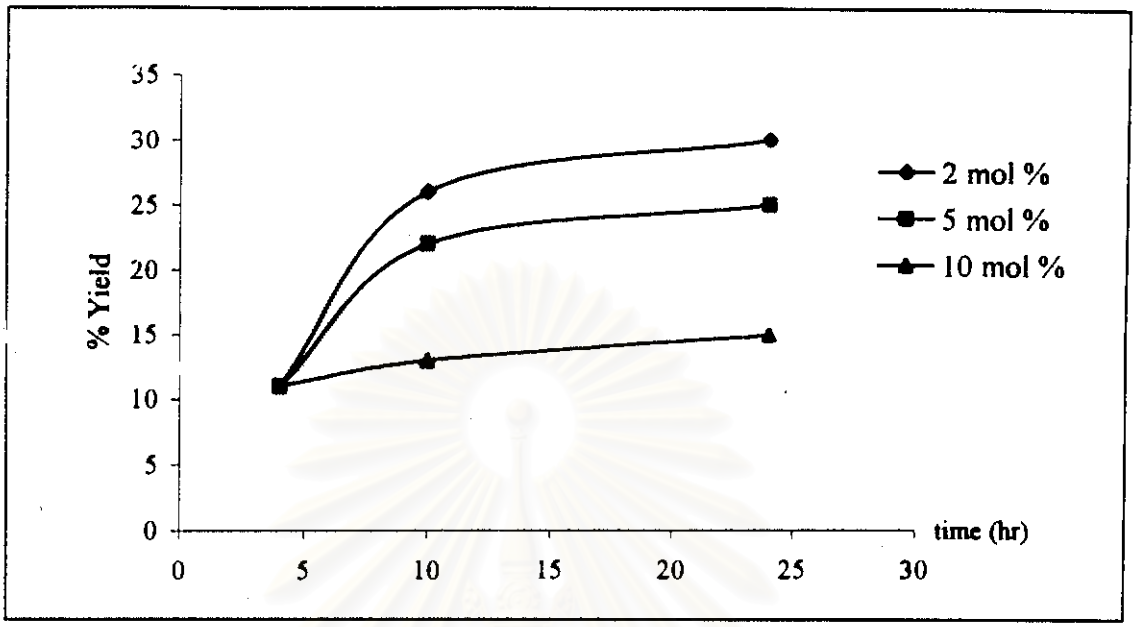


**Figure 5.51** Graph plotted between % yield and time of β-cyclodextrin

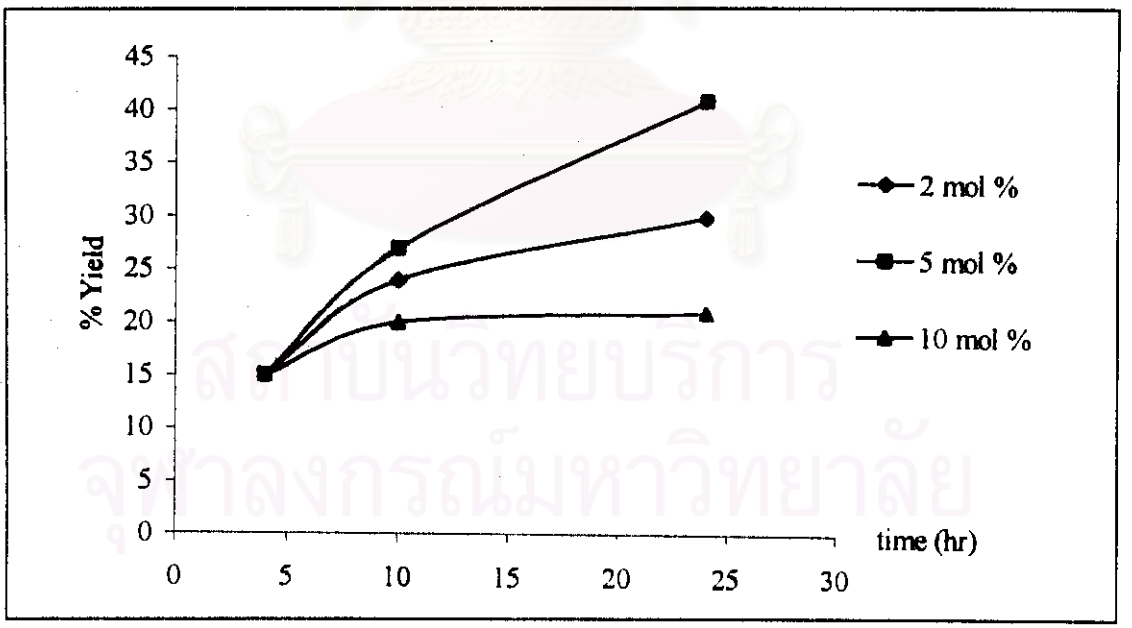


**Figure 5.52** Graph plotted between % yield and time of β-cyclodextrin-*N, N*-dimethyl aminomethylferrocene

### 5.12.4 Types of Catalysts

**Ferrocenylamine Derivatives**

Percent yields of alkylation with diethylzinc using ferrocenylamine derivatives and its inclusion as catalyst are shown in Table 5.43.

**Table 5.43** Effect of ferrocenylamine derivative catalysts on % yield

| Catalyst | % GC Yield |
|---|---|
| None | 34 |
| $Fc\text{-}CH_2\text{-}N(CH_3)_2$ | 70 |
| $Fc\text{-}CH_2\text{-}N(CH_3)_2$-CD | 30 |
| $Fc\text{-}CH_2NHCH_3$ | 70 |
| $Fc\text{-}CH_2NHCH_3$-CD | 54 |
| $Fc\text{-}CH_2N(CH_3)_3I$ | 25 |
| $Fc\text{-}CH_2N(CH_3)_3I$-CD | 16 |
| $Fc\text{-}CH_2\text{-}CH_2\text{-}NH_2$ | 73 |
| $Fc\text{-}CH_2\text{-}CH_2\text{-}NH_2$-CD | 40 |
| $Fc\text{-}CH{=}N\text{-}(CH_2)_2\text{-}N{=}CH\text{-}Fc$ | 96 |
| CD-$Fc\text{-}CH{=}N\text{-}(CH_2)_2\text{-}N{=}CH\text{-}Fc$-CD | 37 |
| $Fc\text{-}CH_2\text{-}NH\text{-}(CH_2)2\text{-}NH\text{-}CH_2\text{-}Fc$ | 45 |
| CD-$Fc\text{-}CH_2\text{-}NH\text{-}(CH_2)_2\text{-}NH\text{-}CH_2\text{-}Fc$-CD | 25 |
| $Fc\text{-}CH_2\text{-}NPh_2$ | 45 |
| $Fc\text{-}C_6H_4N\text{-}C_6H_4N$ | 65 |
| $Fc\text{-}CH_2N(CH_3)_2$<br>$C\text{-}OH\text{-}Ph_2$ | 76 |

Ferrocenylamine derivatives gave high yield of 1-phenyl-1-propanol compared to its inclusion with β-cyclodextrin. The activity trend of ferrocenylamine catalysts corresponded to the trend in basicity of amino group as shown in Table 5.44.

**Table 5.44** $pK_b$ of ferrocenylamine derivatives

| Ferocenylamine Derivative | $pK_b$ |
|---|---|
| $Fc\text{-}CH_2NHCH_3$ | 4.65 |
| $Fc\text{-}CH_2CH_2NH_2$ | 4.95 |
| $Fc\text{-}CH_2N(CH_3)_2$ | 5.17 |
| $Fc\text{-}CH_2NPh_2$ | >9 |

Amino group in ferrocenylamine derivative was donor to coordinate with Zn atom. The more basicity, is the more reactivity of the catalyst. The increase in basicity of $Fc\text{-}CH_2NHCH_3$ is due to the stabilization of the positive charge of the cation by the $-CH_3$. Substitution with a second alkyl group further increases the basicity. The tertiary alkyl amines are not continuing this trend. The reason for this is that the tertiary amine is more hindered and the cation is less stabilized by solvation.

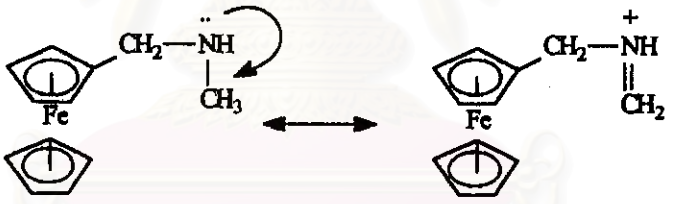


**Scheme 5.13** Resonance stabilization of amine

From the result in Table 5.43, inclusion compounds gave lower yield than free complexes. One explanation might be diethylzinc was more reactive to hydroxyl group of cyclodextrin than carbonyl group of benzaldehyde so it bound with hydroxyl group of cyclodextrin (Figure 5.53).

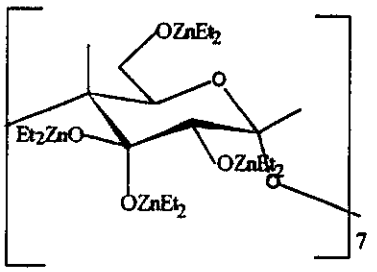


**Figure 5.53** Binding of diethylzinc to hydroxyl group

**Ferrocenylalcohol Derivatives**

Ferrocenylalcohol derivatives did not act as a catalyst. They gave lower yields compared to uncatalyzed reaction (Table 5.45). Their inclusion compounds gave similar results. It can be explained that diethylzinc favorably formed zinc alkoxide with hydroxyl group of alcohol more than coordinated with carbonyl group of benzaldehyde.

**Table 5.45** Effect of ferrocenylalcohol catalysts on % yield

| Catalyst | % GC Yield |
|---|---|
| None | 34 |
| Fc-$CH_2$-OH | 12 |
| Fc-$CH_2$-OH-CD | 15 |
| Fc-CH(-$CH_3$)-OH | 18 |
| Fc-CH(-$CH_3$)-OH-CD | 20 |

**Carbonylferrocene Derivatives**

The results in Table 5.46, can be explained that ferrocenylaldehyde and acetylferrocene did not act as a catalyst because of the inertness of carbonyl group to diethylzinc. The inclusion compounds gave lower yield compared to free complexes.

**Table 5.46** Effect of carbonylferrocene catalysts on % yield

| Catalyst | % GC Yield |
|---|---|
| None | 34 |
| Fc-COH | 30 |
| Fc-COH-CD | 26 |
| $Fc\text{-}COCH_3$ | 32 |
| $Fc\text{-}COCH_3$-CD | 24 |

## 5.13 Enantioselectivity

To study enantioselective addition of dialkylzinc to aldehyde, the reaction was carried out in the presence of various ferrocenylamine derivatives and their inclusion compounds with β-cyclodextrin.

### 5.13.1 Determination of Enantioselectivity by Gas Chromatography

1-Phenyl-1-propanol was reacted with R(-)MTPA-Cl to give diastereomer of MTPA-ester as shown in Scheme 5.14

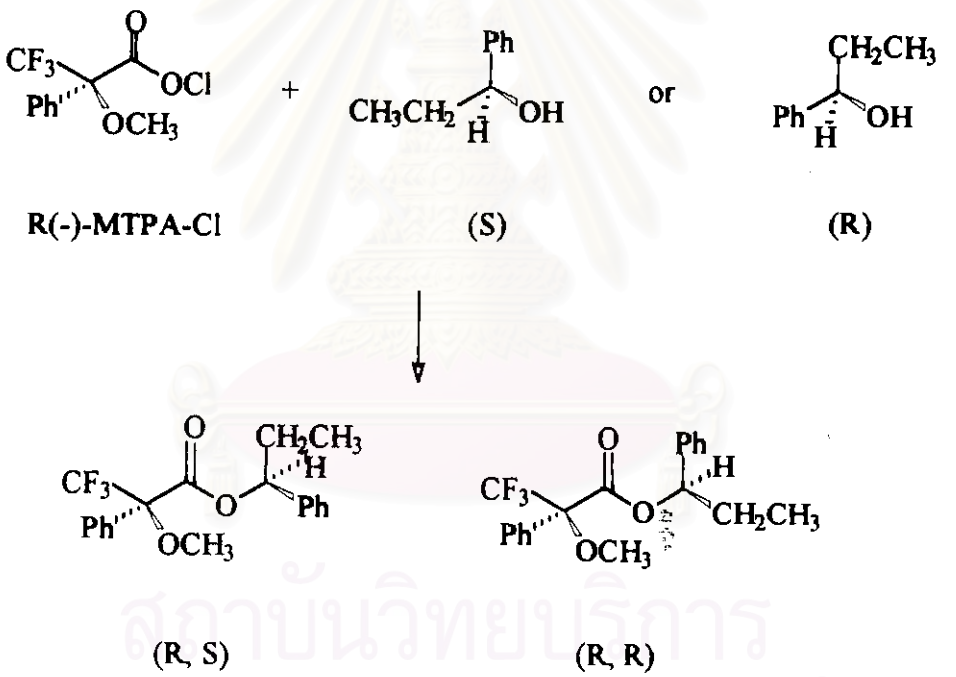


**Scheme 5.14** Two diastereomers of MTPA-ester

Standard racemic of 1-phenyl-1-propanol was derivatized with R(-)MTPA-Cl and % enantiomeric excess was determined with gas chromatography. The two diastereomers showed peaks in chromatogram at retention times at 14.80 and 15.18 as shown in Figure 5.54. The ratio of R to S isomer was determined by the ratio of peak area. The result showed that standard racemic 1-phenyl-1-propanol was 54:46 (R:S)

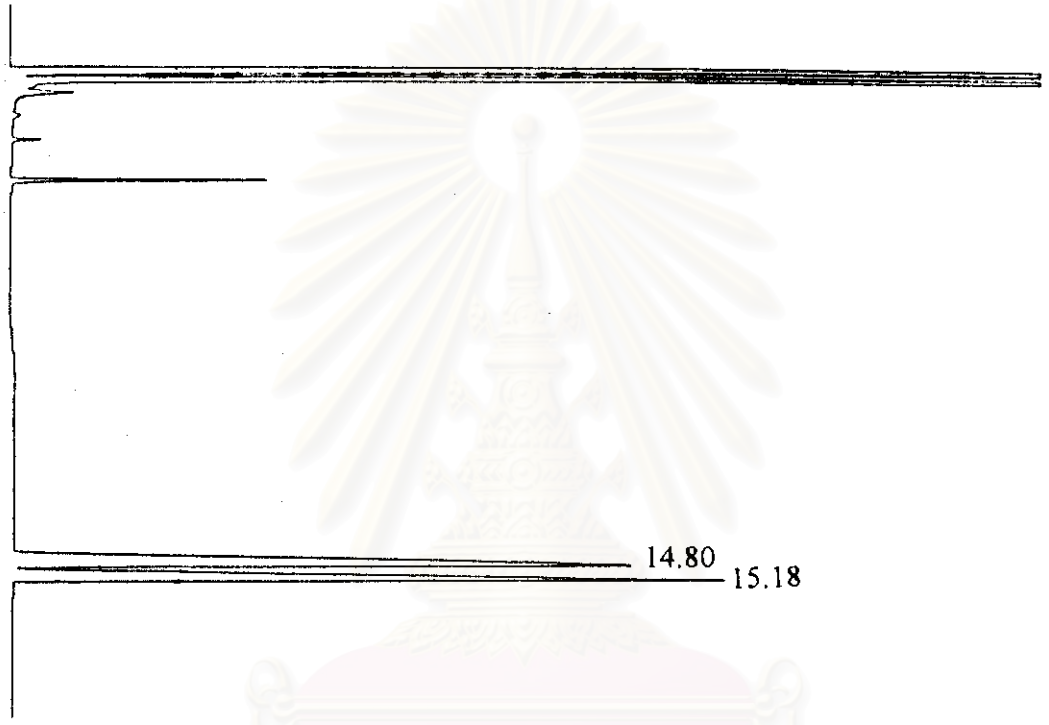


**Figure 5.54** Gas chromatogram of R and S products of alkylation after derivatized with R(-)MTPA-Cl

The structures of two diastereomers of MTPA-ester were determined by mass spectrometry. Mass spectrum of two diastereomers was shown in Figure 5.55

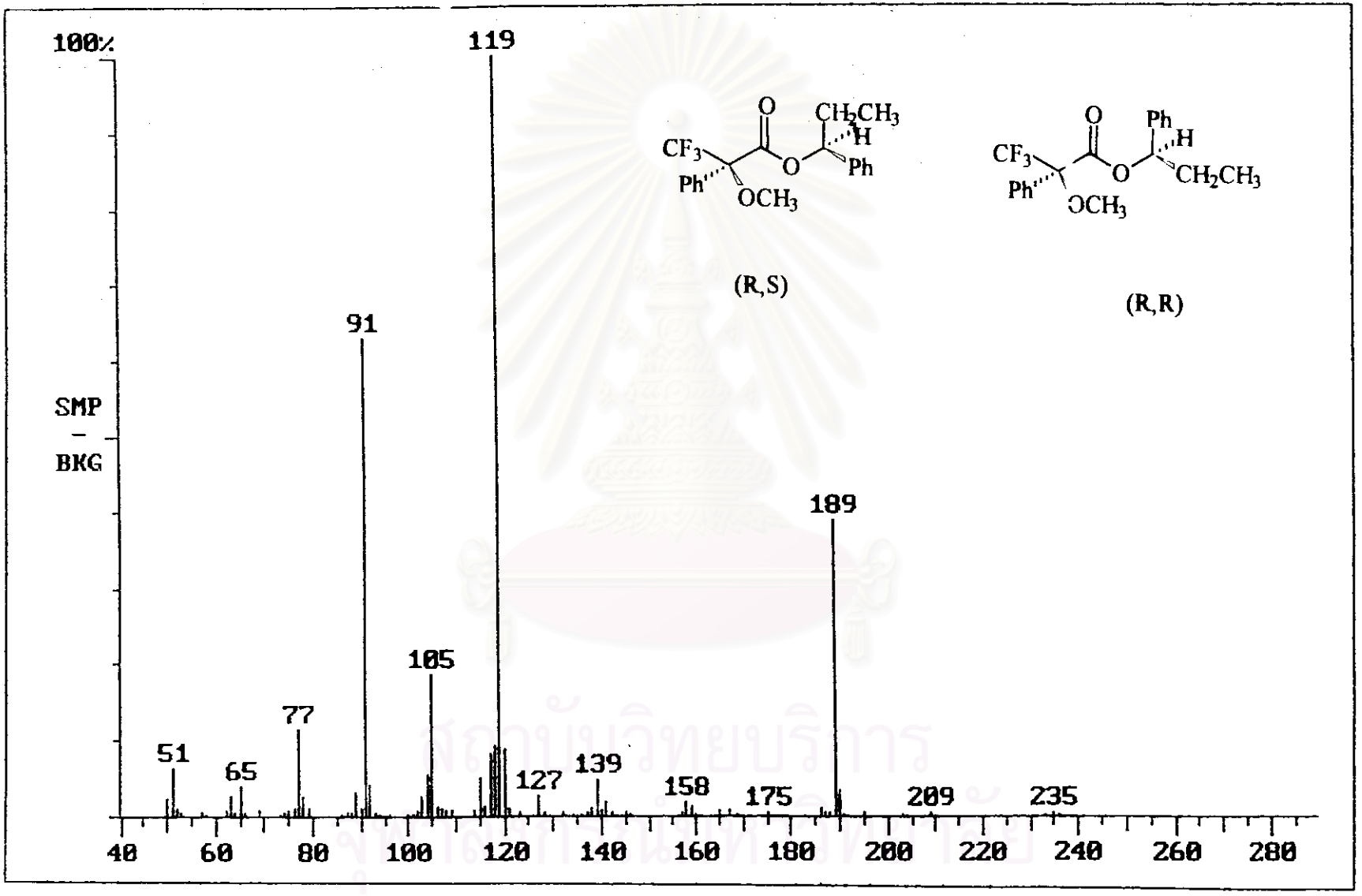


**Figure 5.55** Mass spectrum of MTPA-ester

MTPA-ester showed diagnostic peak at 119 m/z, resulted from the elimination of alkyl moiety. Peak at 235 m/z was resulted from the cleavage of ester involving the shift of two hydrogen atoms (McLafferty rearrangement) as shown in Scheme 5.15.

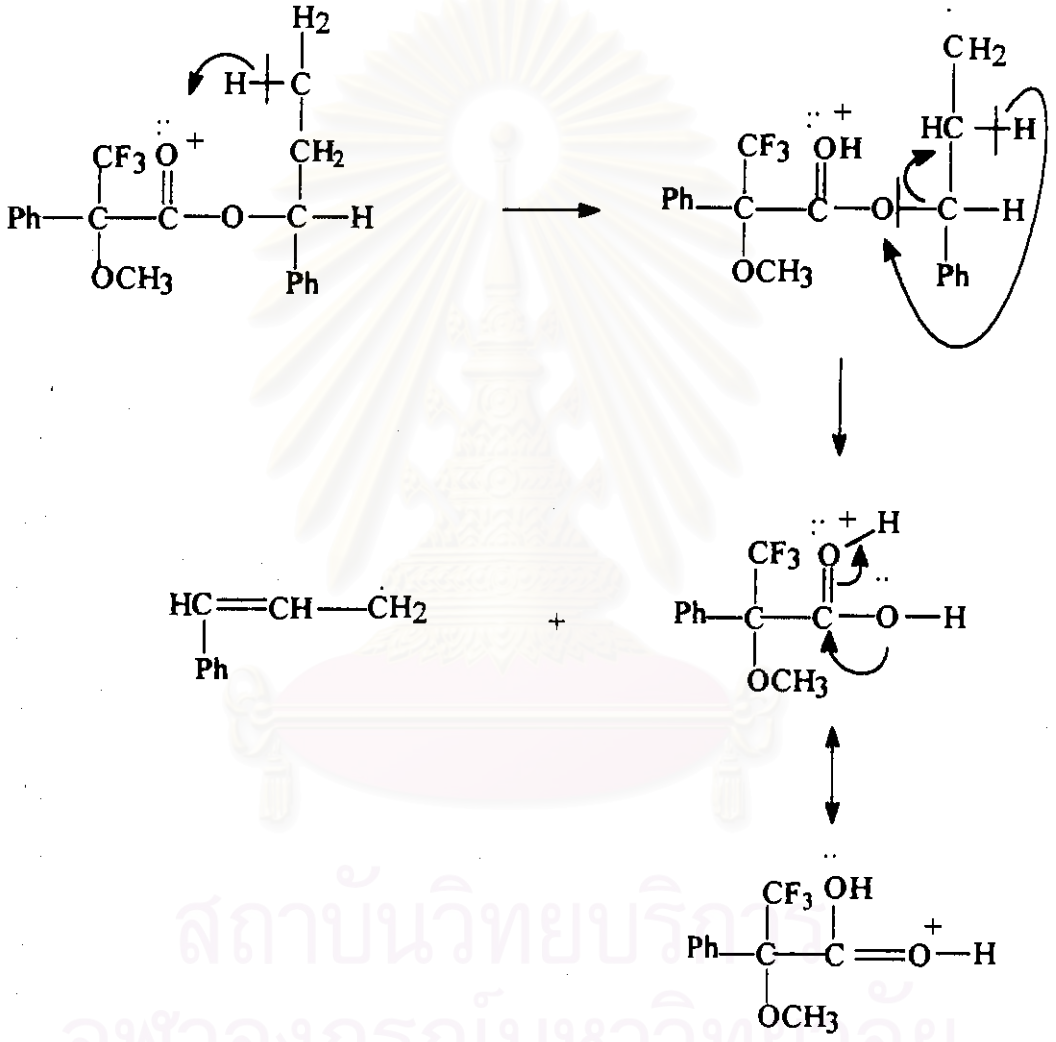

**Scheme 5.15** Fragments of MTPA-ester

In some derivatization reactions, the gas chromatogram showed some peaks at retention times of 8.74 and 15.47 as shown in Figure 5.56.

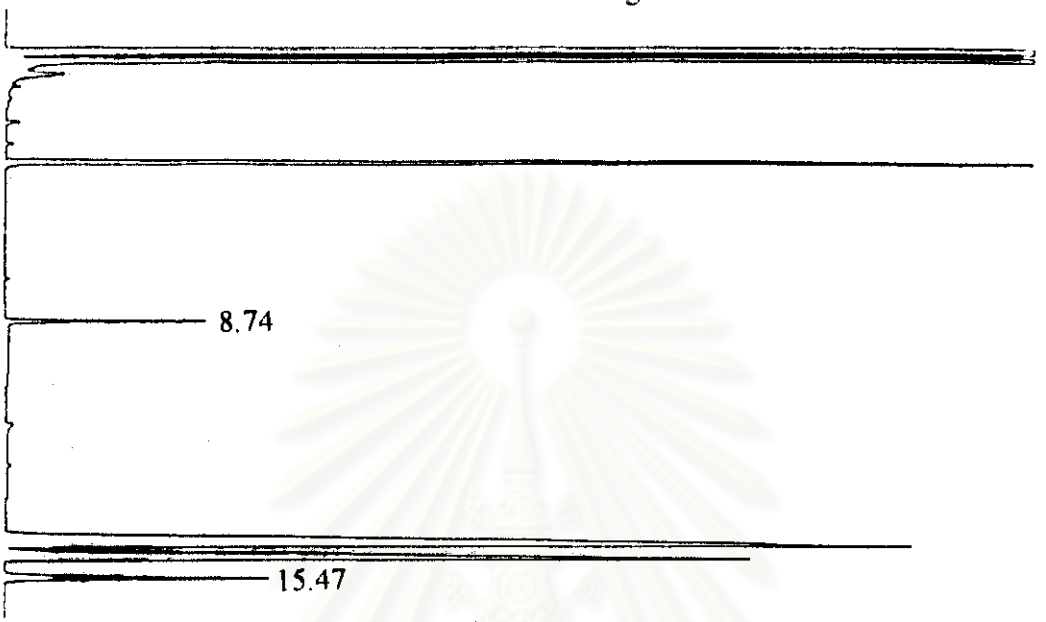


**Figure 5.56** Gas chromatogram of derivatization showing peaks

The occurrence of strange peaks might be from the reaction as shown in Scheme 5.16. When there was moisture, R(-)MTPA-Cl can change to S(-)MTPA and react with R(-)MTPA-Cl to form MTPA anhydride.

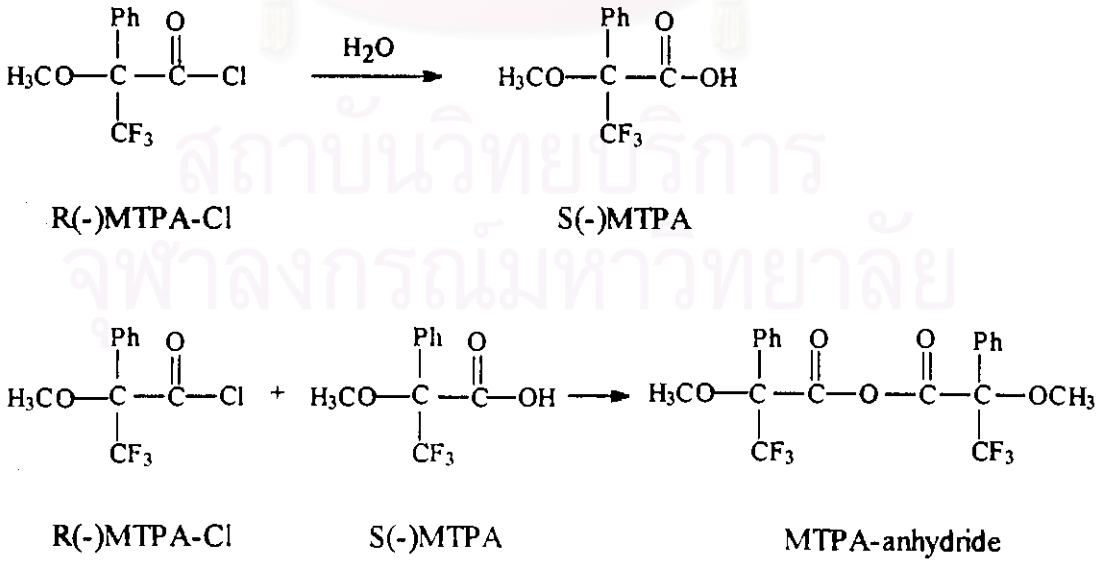


**Scheme 5.16** MTPA-anhydride formation

Some ferrocenylamine derivative catalysts and its inclusion compounds were tested for enantioselectivity. The results are shown in Table 5.47.

**Table 5.47** Enantioselectivity of catalysts by gas chromatography

| Catalyst | Enantiomeric ratio S:R | % e. e. |
|---|---|---|
| None | 54:46 | 8 |
| CD | 63:37 | 26 |
| Fc-$CH_2$-N($CH_3$)$_2$ | 57:43 | 14 |
| Fc-$CH_2$-N($CH_3$)$_2$-CD | 65:35 | 30 |
| Fc-$CH_2NHCH_3$-CD | 64:36 | 28 |

The results indicate that inclusion compounds of ferrocenylamine gave % enantiomeric excess higher than free complexes.

The proposed mechanism of alkylation with inclusion catalyst is shown in Scheme 5.17. Zinc monoalkoxide on cyclodextrin reacted with dialkylzinc to form intermediates. The coordination geometry of the zinc atom is tetrahedral with the coordination of the oxygen or the nitrogen atom of ferrocenyl derivative, and the nucleophilicity of the alkyl group of the diethylzinc is increased. The aldehyde is attacked at the si face *via* a six-center transition state to afford chiral alkylzinc alkoxide with S isomer.[12]

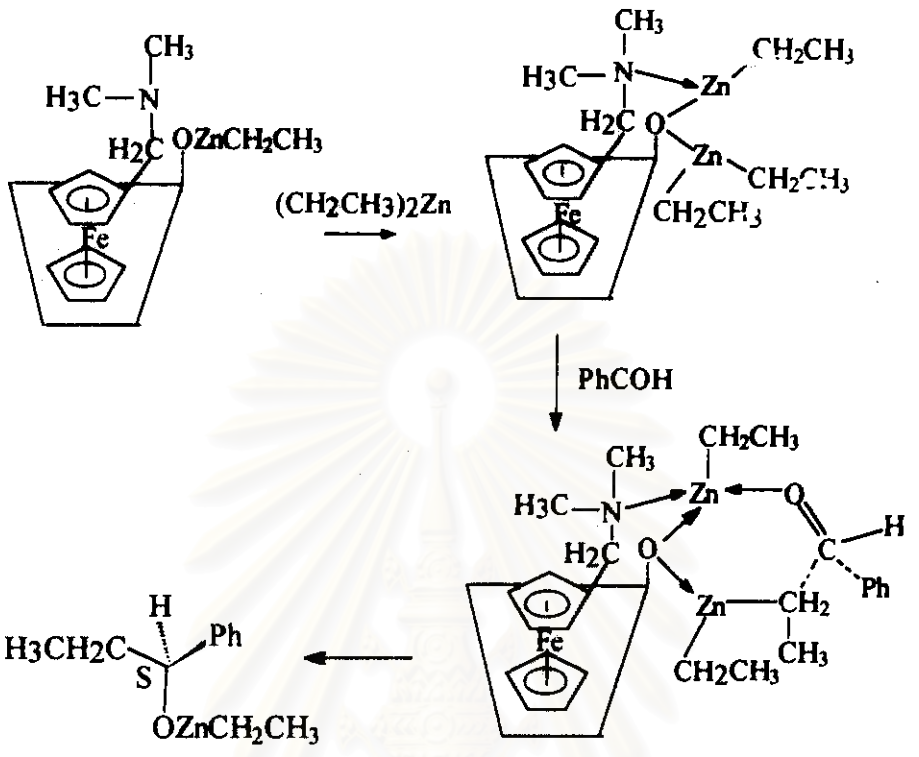


**Scheme 5.17** Proposed mechanism of alkylation with *N, N*-dimethylaminomethyl ferrocene inclusion compound catalyst

### 5.13.2 Determination of Enantioselectivity by $^1$H NMR Technique

$^1$H NMR technique was used to determine % enantiomeric excess. The NMR data of diastereomers were collected in Table 5.48 and $^1$H NMR spectrum was shown in Figure 5.54.

**Table 5.48** $^1$H NMR chemical shifts of diastereomeric ester

| Chemical shift | Multiplicity | Assignment |
|---|---|---|
| 7.13-7.35 | multiplet | $-C_6H_5$ |
| 5.75 and 5.83 | doublets of doublet | -H |
| 3.38 and 3.47 | doublet | $-OCH_3$ |
| 1.77 and 1.92 | multiplet | $-CH_2$ |
| 0.76 and 0.86 | triplet | $-CH_3$ |

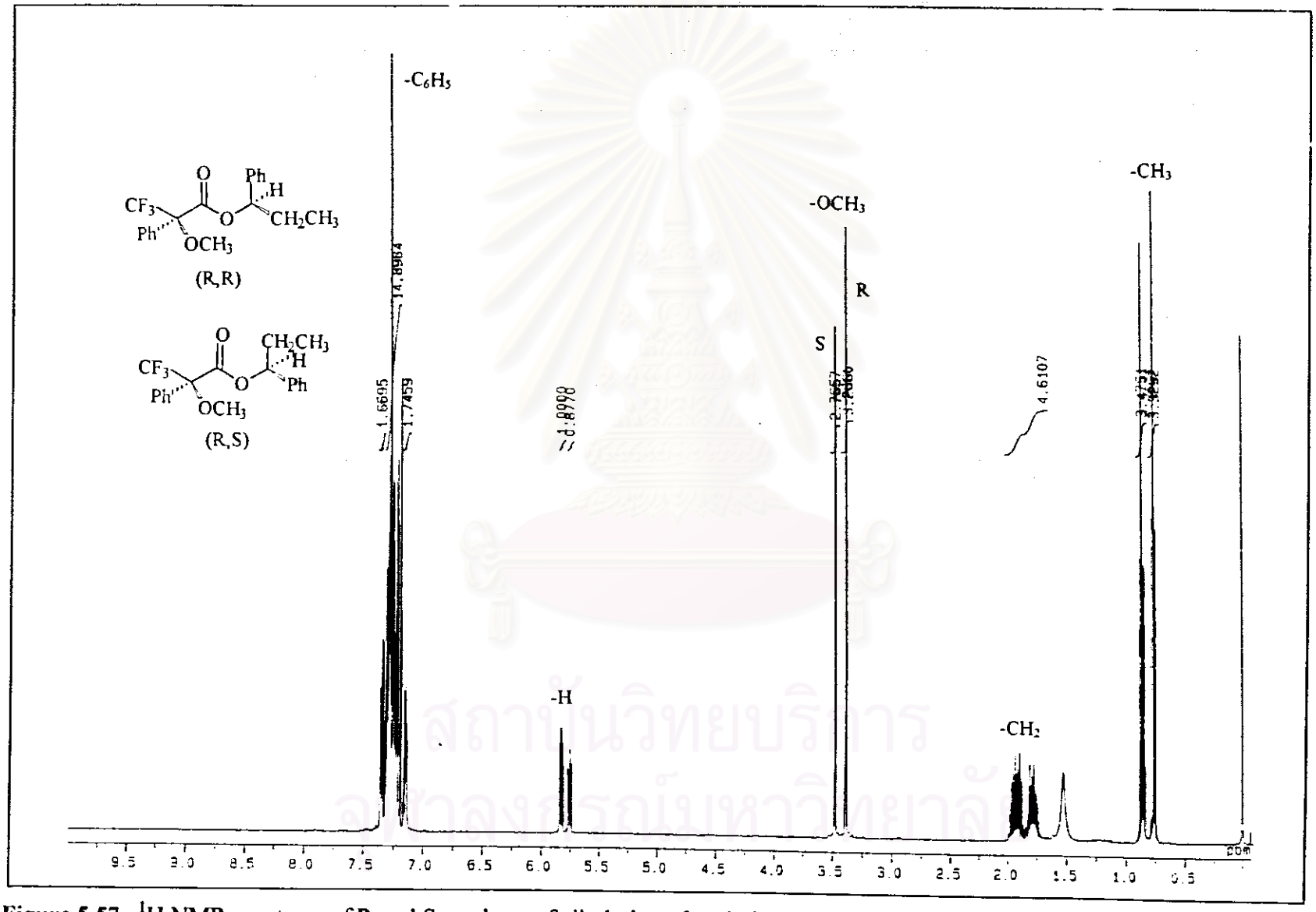


**Figure 5.57** $^{1}$H NMR spectrum of R and S products of alkylation after derivatized with R(-)MTPA-Cl

The $^1H$ NMR spectrum of MTPA-ester showed chemical shifts of two diastereomers at different positions. In the case of R, S diastereomer, the orientation of $-CH_2CH_3$ group was near the phenyl ring so its chemical shift was shielded by anisotropic effect. In the case of R, R diastereomer, chemical shifts of $-CH_2CH_3$ and $-OCH_3$ were shielded by phenyl ring.

These observations taken together crucial different interaction of the anisotropic α-phenyl substituent on the chiral acid moiety with the alkyl substituents were explained in Scheme 5.18.


(R, S) shielding on $CH_2CH_3$


(R, R) shielding on $OCH_3$ and $CH_2CH_3$

**Scheme 5.18** The influence of the phenyl ring on $^1H$ NMR signals of two diastereomeric esters of R(-)MTPA-Cl

Shielding in $-OCH_3$ group was found in only R, R diastereomer. Integration data indicated 54:46 ratio of R:S isomer of standard racemic 1-phenyl-1-propanol that was in good agreement with the result obtained from gas chromatographic technique.

**ต้นฉบับไม่มีหน้านี้**

**NO THIS PAGE IN ORIGINAL**